

Aus der Klinik und Poliklinik für Nuklearmedizin

Klinik der Universität München

Kommissarischer Direktor: Prof. Dr. Matthias Brendel

**In-vivo-Quantifizierung neuronaler Netzwerk-Veränderungen mittels
metabolischer Konnektivität in Mausmodellen neurodegenerativer
Erkrankungen**

Dissertation

zum Erwerb des Doktorgrades der Medizin

an der Medizinischen Fakultät der

Ludwig-Maximilians-Universität zu München

vorgelegt von

François Michel Richard Ruch

aus

Köln

Jahr

2024

Mit Genehmigung der Medizinischen Fakultät
der Universität München

Berichterstatter: Prof. Dr. Matthias Brendel
Mitberichterstatter: PD Dr. Janusch Peter Blautzik
Prof. Dr. Jonas Neher

Mitbetreuung durch den
promovierten Mitarbeiter: Dr. Florian Eckenweber

Dekan: Prof. Dr. med. Thomas Gudermann

Tag der mündlichen Prüfung: 17.10.2024

I Eidesstattliche Versicherung



Eidesstattliche Versicherung

Ruch, François

Name, Vorname

Ich erkläre hiermit an Eides statt, dass ich die vorliegende Dissertation mit dem Titel:

**In-vivo-Quantifizierung neuronaler Netzwerk-Veränderungen mittels metabolischer
Konnektivität in Mausmodellen neurodegenerativer Erkrankungen**

selbständig verfasst, mich außer der angegebenen, keiner weiteren Hilfsmittel bedient und alle Erkenntnisse, die aus dem Schrifttum ganz oder annähernd übernommen sind, als solche kenntlich gemacht und nach ihrer Herkunft unter Bezeichnung der Fundstelle einzeln nachgewiesen habe.

Ich erkläre des Weiteren, dass die hier vorgelegte Dissertation nicht in gleicher oder in ähnlicher Form bei einer anderen Stelle zur Erlangung eines akademischen Grades eingereicht wurde.

München, den 29.10.2024

Francois Ruch

Ort, Datum

Unterschrift Doktorand

Kumulative Dissertation gemäß § 4a der Promotionsordnung

II Inhaltsverzeichnis

I	Eidesstattliche Versicherung	2
II	Inhaltsverzeichnis	3
III	Abkürzungsverzeichnis	4
IV	Publikationen der kumulativen Dissertation	6
1.	Einführung	8
1.1	Pathophysiologie der Alzheimer-Erkrankung.....	9
1.2	Mausmodelle der Alzheimer-Krankheit	11
1.3	Alzheimer als Netzwerk-Erkrankung	13
1.4	PET-Bildgebung von Glukosestoffwechsel und Neuroinflammation beim Morbus Alzheimer.....	14
1.5	PET-Studien zur metabolischen Konnektivität am Menschen und Kleintieren	16
1.6	Abgeleitete Fragestellung	18
2.	Inhalt der Promotionsarbeit.....	19
2.1	Validität und Wert der metabolischen Konnektivität in Mausmodellen für β -Amyloid und Tauopathie.....	19
2.2	Die Mikroglia-Aktivität wird durch das Geschlecht in Amyloid Mausmodellen, nicht jedoch in Tau-Mausmodellen beeinflusst.	29
3.	Zusammenfassung	33
4.	Summary	36
V	Literaturverzeichnis	39
VI	Abbildungsverzeichnis	43
VII	Paper I	45
VIII	Paper II	55
IX	Danksagung	65

III Abkürzungsverzeichnis

A β	β -Amyloid, Amyloid Beta Peptid
AD	Alzheimer Demenz
APP	Amyloid Vorläuferprotein
FAD	Familiäre Alzheimer Krankheit
¹⁸ F	Fluor-Radioisotop; Massenzahl 18
DMN	Ruhezustandsnetzwerk (engl. Default Mode Network)
MAPT	Mikrotubuli-assoziiertes Protein Tau
ICC	Interkorrelationskoeffizienten
M	Monate
MRT	Magnetresonanztomographie
MWM	Morris-Wasserlabyrinth
SUV	Standard-Aufnahmewert
SUVR	Relative Standardaufnahmewerte (engl. Standardized-Uptake-Value-Ratio)
RMSE	Quadratwurzel des mittleren quadratischen Fehlers (engl. Root Mean Squared Error)
TG	Transgen
TSPO	18-kDa-Translokator-Protein
WT	Wildtyp
μ PET	Kleintier Positronen-Emissions-Tomographie
MCI	Leichte kognitive Störung (engl. Mild cognitive Impairment)
MC	Metabolische Konnektivität (engl. Metabolic Connectivity)
VOI	Volumen von Interesse (engl. Volume-of-interest)
CTX	Kortex
HIP	Hippocampus

AMY

Amygdala

PCC

Posteriorer Cingulärer Kortex

IV Publikationen der kumulativen Dissertation

Die vorliegende kumulative Dissertation umfasst zwei bereits publizierte Manuskripte:

Ruch, F., Gnörich, J., Wind, K., Köhler, M., Zatcepin, A., Wiedemann, T., Gildehaus, F. J., Lindner, S., Boening, G., von Ungern-Sternberg, B., Beyer, L., Herms, J., Bartenstein, P., Brendel, M., & Eckenweber, F. (2024). Validity and value of metabolic connectivity in mouse models of β -amyloid and tauopathy. *NeuroImage*, 286, 120513. <https://doi-org.emedien.ub.uni-muenchen.de/10.1016/j.neuroimage.2024.120513>

Biechele, G., Franzmeier, N., Blume, T., Ewers, M., Luque, J. M., Eckenweber, F., Sacher, C., Beyer, L., **Ruch-Rubinstein, F.**, Lindner, S., Gildehaus, F. J., von Ungern-Sternberg, B., Cumming, P., Bartenstein, P., Rominger, A., Höglinger, G. U., Herms, J., & Brendel, M. (2020). Glial activation is moderated by sex in response to amyloidosis but not to tau pathology in mouse models of neurodegenerative diseases. *Journal of neuroinflammation*, 17(1), 374. <https://doi-org.emedien.ub.uni-muenchen.de/10.1186/s12974-020-02046-2>

Beschreibung des Eigenanteils an der Publikation:

„Validity and value of metabolic connectivity in mouse models of β -amyloid and tauopathy.“

Entwicklung des Forschungskonzepts in Zusammenarbeit mit dem Betreuer, Durchführung von Kleintier-PET-Scans und kognitiven Verhaltenstests für verschiedene Kohorten. Teilnahme an der Betreuung, Fütterung und regelmäßigen Überwachung des Wohlbefindens der Versuchsmäuse. Nach Abschluss des praktischen Teils der Studie eigenständige Auswertung und Interpretation der PET-Scan-Daten sowie statistische Analyse in kontinuierlicher Abstimmung mit dem

Betreuer. Durchführung der abschließenden Perfusionsverfahren an den Tieren. Eigenständige Verfassung des ersten Manuskriptentwurfs für das veröffentlichte Paper. Anpassung und Ergänzung weiterer Analysen entsprechend den Anmerkungen der Gutachter nach erfolgter Revision. Nachfolgende Überarbeitung des Entwurfs bis zur endgültigen Version in Zusammenarbeit mit dem Betreuer.

„Glial activation is moderated by sex in response to amyloidosis but not to tau pathology in mouse models of neurodegenerative diseases.“

Durchführung der Kleintier-PET-Scans und Perfusionsverfahren an den Versuchstieren. Mitarbeit bei der Datenanalyse und -auswertung. Kritische Prüfung des Manuskriptentwurfs, Beurteilung und Anpassung des Entwurfs.

1. Einführung

Die weltweite Anzahl der Demenz-Patienten wurde 2015 auf 46,8 Millionen geschätzt und wird sich nach Prognosen alle 20 Jahre fast verdoppeln [1]. Insbesondere einkommensschwache Länder sind von diesem Anstieg stark betroffen. Aber auch in Industrienationen, wie in den Ländern der Europäischen Union, beträgt die Prävalenz an Demenzpatienten in der Bevölkerung über 60 Jahre ca. 7 % und ab 90 Jahre steigt dieser Anteil auf fast 40 % an [2]. Durch eine steigende Lebenserwartung und die zunehmend alternde Bevölkerung ist in den kommenden Jahrzehnten mit einer starken Zunahme dieser Prävalenz zu rechnen. Die daraus resultierende Kostenbelastung des Gesundheitssystems in Europa lag 2019 bereits bei etwa 439 Milliarden US-Dollar, was einem durchschnittlichen Kostenaufwand von etwa 27.815 Euro pro Patient entspricht und damit dem durchschnittlichen Brutto-Inlandsprodukt pro Kopf in Europa (ca. 31.000 Euro) nahe kommt [3]. Ca. 50 % dieser Kosten entfallen auf die Pflege durch Angehörige [4]. Ab dem 60. Lebensjahr gehört Demenz zu den zehn häufigsten Ursachen für einen Verlust an gesunden Lebensjahren, die durch eine Behinderung verloren gehen [5] und etwa 2/3 der Fälle sind auf eine Alzheimer-Erkrankung zurückzuführen [4]. Es ist von essenzieller Bedeutung, diesem Trend einerseits durch eine sichere und frühzeitige Diagnosestellung und andererseits durch die Entwicklung kausaler Therapien und Präventionsstrategien entgegenzuwirken. Neben nicht-medikamentösen Maßnahmen, wie Physio- und Ergotherapie, wird in der klinischen Praxis medikamentös lediglich eine symptomatische Therapie mit Acetylcholinesterase-Inhibitoren und NMDA-Rezeptor-Antagonisten angewandt [6]. Seit 2023 ermöglichen die kürzlichen Zulassungen spezifischer Antikörpertherapien gegen β -Amyloid-Aggregate mit Aducanumab und Lecanemab in den Vereinigten Staaten erstmals auch eine verlaufsmodifizierende Therapie in den frühen Krankheitsstadien [7, 8]. Dies betont die Bedeutung krankheitsspezifischer Biomarker,

die zu einer frühen Diagnosestellung beitragen können. Durch die Entwicklung nicht-invasiver und möglichst sensitiver Biomarker wie der PET-Bildgebung können bereits frühzeitig Muster eines erhöhten Risikos, an einer Alzheimer-Demenz zu erkranken, erkannt werden [9]. Aktuell dauert es bis zur Diagnose einer Alzheimer-Erkrankung bei Patienten unter 65 Jahren, die von einer verlaufsmodifizierenden Therapie profitieren könnten, durchschnittlich 5,5 Jahre [10]. Solche Biomarker tragen nicht nur zu einer verbesserten Diagnose bei, sondern auch zu einem tieferen ätiologischen Verständnis der Erkrankung und geben Aufschluss über individuelle Verläufe sowie die Wirksamkeit neuer kausaler Therapieansätze.

1.1 Pathophysiologie der Alzheimer-Erkrankung

Die Akkumulation von extrazellulären β -Amyloid-Plaques, intrazellulären Neurofibrillen bestehend aus hyperphosphoryliertem Tau-Protein sowie die Initiierung neuroinflammatorischer Mechanismen werden als etablierte pathophysiologische Charakteristika der Alzheimer-Erkrankung betrachtet [11-14]. Die genaue Kausalität, sowie zeitliche und räumliche Abfolge der neuropathologischen Prozesse, die zum Verlust der Synapsen und Nervenzellen führen, sind nicht abschließend geklärt [15, 16]. Der Schaden an Synapsen und deren Untergang scheint am stärksten mit der kognitiven Beeinträchtigung bei Alzheimer Demenz (AD) zu korrelieren [17] und dem Verlust von Nervenzellen voranzugehen [18, 19].

Durch die pathologische Spaltung des transmembranen Amyloid-Vorläuferproteins (APP) durch β - und γ -Sekretasen [20, 21] kommt es zu einem Ungleichgewicht an Produktion und Ausscheidung verschiedener Isoformen von β -Amyloid [22]. Die progressive Akkumulation von β -Amyloid führt zur Bildung neurotoxischer A β -

Oligomere und Fibrillen als Hauptbestandteile extrazellulärer Plaques [23, 24], welche bereits Jahrzehnte vor klinischen Symptomen auftreten können [25, 26].

Intrazelluläre Neurofibrillen werden durch Aggregate des Mikrotubuli-assoziierten Proteins Tau (MAPT) gebildet [27], welches unter anderem den intrazellulären Vesikel-Transport gewährleistet [28, 29].

In hyperphosphoryliertem Zustand verliert Tau seine biologische Aktivität und Bindefähigkeit an Tubulin, wodurch die Organisation der Mikrotubuli beeinträchtigt wird [28]. Als Ursache dafür werden abnormale posttranslationale Modifikationen vermutet [30, 31]. Durch die Bindung normaler Tau-Proteine und weiterer Mikrotubuli-assoziiierter Proteine (MAP 1 und 2) wird die Bildung und Stabilität der Mikrotubuli weiter gestört [32]. Dieser neurotoxische Effekt zeigt sich jedoch durch die Dephosphorylierung des hyperphosphorylierten Tau-Proteins reversibel [33]. Die Tau-Pathologie breitet sich Prionen-ähnlich über neuronale Schaltkreise entlang eines stereotypen Musters im menschlichen Gehirn aus [11, 34] und trägt dadurch zum progressiven Absterben von Neuronen bei [35].

Der Neuroinflammation werden über den Abbau der A β -Ablagerungen durch die Aktivierung von Mikroglia sowohl positive Effekte auf die neuronale Dysfunktion zugesprochen als auch negative Effekte durch die vermehrte Ausschüttung zytotoxischer Substanzen [36]. Die Mikroglia-Aktivierung führt zu einer Phagozytose der Synapsen, kann die Ausbreitung der Tau-Pathologie verstärken [37] und zur Aktivierung neurotoxischer Astrozyten führen [38].

1.2 Mausmodelle der Alzheimer-Krankheit

Transgene (Tg) Mausmodelle haben seit den 1990er-Jahren maßgeblich zur weiteren Aufklärung der pathophysiologischen Prozesse bei der Alzheimer-Erkrankung und Identifizierung therapeutischer Ziele beigetragen [39]. Die ersten Generationen dieser Modelle basierten größtenteils auf Mutationen, die zur Ausbildung der autosomal-dominant vererbten familiären Alzheimer Demenz (FAD) führen. Wesentliche Gene sind dabei das β -Amyloid Precursor Protein (APP)-Gen [40] und die für die Untereinheit der γ -Sekretase kodierenden Presenilin-1- und -2-Gene [41]. Im Verlauf folgte die Entwicklung von Tauopathie-Mausmodellen mit Mutationen im MAPT-Gen. Die JNPL3-Linie mit Expression der P301L-Mutation war das erste Tg-Mausmodell der Tauopathie [42].

Die transgene Mauslinie B6.PS2APP koexprimiert homozygot Mutationen im humanen APP-Gen und im Presenilin-2 (PS2)-Gen [43]. Erste A β Plaques sind im Alter von 6 Monaten im frontolateralen Kortex sowie im Hippocampus festzustellen, bevor sie sich über den Großteil des Neokortex sowie des Thalamus und im Bereich der Ponskerne ausbreiten [44]. Im Alter von 8 Monaten werden erste kognitive Defizite erkennbar [45].

Das APPPS1-Mausmodell exprimiert ebenfalls eine Doppelmutation im APP-Gen und im Presenilin-1 (PS1)-Gen [46]. Erste A β -Ablagerungen treten in der 6. bis 8. Woche auf [46], reichlich ausgeprägt im Hippocampus und Kortex im Alter von 9 Monaten [44], und kognitive Defizite ab einem Alter von 7 Monaten [39].

Als ein weiteres β -Amyloid-Mausmodell, welches auf einer APP-Gen-Mutation basiert, ist das App^{NL-G-F}-Mausmodell ein Knock-in-Mausmodell bestehend aus drei integrierten Mutationen im APP-Gen [44]. Dadurch kommt es nach 2 Monaten im

Cortex zu einer gesteigerten A β 42-Produktion, zu vermehrter Amyloid-Plaque-Bildung und zu vermehrter Plaque-Akkumulation [47]. Defizite im räumlichen Lernen und Gedächtnis treten im Alter von 6 Monaten auf [44].

Das Tau-Mausmodell P301S exprimiert durch eine homozygote Mutation im MAPT-Gen eine menschliche Isoform von hyperphosphoryliertem Tau (0N4R), welches sich im Alter von 5 bis 6 Monaten im Kortex, Hippocampus und besonders ausgeprägt im Hirnstamm und Rückenmark nachweisen lässt [48]. Schwere motorische Defizite und eine Paraparese treten ab 5 Monaten und kognitive Defizite im räumlichen Lernen bereits ab 2,5 Monaten auf [49].

1.3 Alzheimer als Netzwerk-Erkrankung

In den letzten Jahren hat sich das Verständnis der Alzheimer-Erkrankung zunehmend in Richtung einer cerebralen Netzwerk-Erkrankung entwickelt. Die genauen kausalen Zusammenhänge, die zu den Veränderungen interregionaler Hirnnetzwerke und den kognitiven Defiziten führen, sind jedoch noch nicht vollständig geklärt. Es wird vermutet, dass eine Störung der Synchronität spezifischer Netzwerke der Gedächtniskodierung, sowohl durch Aktivierungs- als auch Deaktivierungsdefizite als Ursache in Frage kommt und dass diese Veränderungen bereits Jahrzehnte vor dem Auftreten der Symptome einer Alzheimer-Demenz auftreten können. [50, 51].

Ein charakteristisches und frühzeitiges Muster der Alzheimer-Erkrankung besteht in der Atrophie und einem reproduzierbaren Hypometabolismus im posterioren cingulären Kortex (PCC) und im parieto-temporalen Kortex [52, 53]. Der PCC ist gemeinsam mit dem medialen präfrontalen Kortex und dem unterem Parietallappen Teil des „Default Mode Network“ (DMN), einem funktionellen Netzwerk, das bei gesunden Probanden im ruhenden, aufgabenfreien Zustand aktiviert ist [53, 54]. Es wurde festgestellt, dass eine hippocampale Aktivierung während bestimmter Aufgaben, ohne angemessene Deaktivierung des DMN, mit einer beeinträchtigten Gedächtnisbildung bei gesunden Probanden assoziiert ist [50]. Bei Patienten mit einer Alzheimer-Erkrankung wurden ein Verlust der Verbindungen zwischen dem PCC und anderen temporalen, parietalen und präfrontalen Knoten des DMN [55] sowie eine beeinträchtigte Deaktivierung des DMN während des Lernens festgestellt [56].

Eine gestörte Deaktivierung von Komponenten des DMN zeigt enge Verbindungen zu Amyloid-Ablagerungen bei Patienten mit und ohne Alzheimer-Pathologie [57]. Kognitiv normale ältere Erwachsene mit Anzeichen von Amyloid-Ablagerungen weisen im Vergleich zu Menschen ohne solche Ablagerungen eine reduzierte funktionelle Verbindung im DMN auf [58] und ein linearer Zusammenhang zwischen der Amyloid-

Belastung und der Beeinträchtigung der funktionellen Konnektivität konnte nachgewiesen werden [59]. Im Prodromalstadium der Alzheimer-Erkrankung ist die Amyloid-Akkumulation im postero-medialen Kortex, inklusive PCC, mit einer Hypoaktivität im DMN assoziiert [60] und im Endstadium besteht eine erhebliche topographische Übereinstimmung zwischen den Gehirnregionen des DMN und den Amyloid-Ablagerungen [61].

Aber auch die Tau-Pathologie zeigt einen engen Zusammenhang mit Veränderungen der funktionellen Konnektivität, da Regionen, die stark funktionell mit Gebieten hoher Tau-Belastung verbunden sind, selbst auch einen hohen Gehalt an hyperphosphorylierten Tau-Aggregaten aufweisen [62]. Es besteht eine bessere Übereinstimmung der Tau-Kovarianzmuster in AD, gemessen mit [¹⁸F]Flortaucipir-PET mit funktionellen Netzwerken junger gesunder Erwachsenen, was die Annahme stützt, dass sich die Tau-Pathologie über umschriebene Gehirnetzwerke ausbreitet [63, 64]. Eine erhöhte Signalaufnahme im Tau-PET hängt mit einer Hypokonnektivität im DMN im Frühstadium der typischen amnestischen AD zusammen [65, 66]. Im Gegensatz zu der identischen Verteilung der β -Amyloid-Pathologie in allen AD-Subtypen (wie der posterioren kortikalen Atrophie, der logopenische Variante der primär progressiven Aphasie oder der dysexekutiven Variante der AD) [67], korrelieren die Muster der Tau-Akkumulation besser mit der heterogenen klinischen Symptomatik und Topologie der Neurodegeneration, die es im phänotypischen Spektrum der Alzheimer-Erkrankung gibt [64]. Ebenso zeigte sich eine bei Patienten mit atypischer AD im MCI-Stadium sowie bei der typischen amnestischen Erscheinungsform ein Verlust der funktionellen Konnektivität zwischen Temporal- und Parietalknoten [68].

1.4 PET-Bildgebung von Glukosestoffwechsel und Neuroinflammation beim Morbus Alzheimer

Das [¹⁸F]-Fluordesoxyglucose (FDG)-PET liefert als molekularer in vivo Biomarker zur Visualisierung des Glukosestoffwechsels, mit einer hohen Sensitivität (91 %) und Spezifität (86 %), wertvolle Informationen zur Diagnose, Differentialdiagnose und Beurteilung des Krankheitsverlaufs der Alzheimer-Erkrankung [69, 70] und übertrifft in der prodromalen Phase sogar Liquor-basierte Biomarker in der Vorhersage des Krankheitsverlaufs [71].

Durch Veränderungen des cerebralen Glucosestoffwechsels, der im Wesentlichen die synaptische glutamaterge Aktivität widerspiegelt [72, 73], können Rückschlüsse auf die Gehirnaktivität gemacht werden. Ein synaptischer Funktionsverlust führt zu einer Abnahme des neuronalen Energiebedarfs, was zu einem verminderten Glucosestoffwechsel führt. Es lässt sich daher annehmen, dass der Hypometabolismus bei der Alzheimer-Erkrankung den Verlust der synaptischen Aktivität und Dichte widerspiegelt [74].

Regionale Unterschiede im Hypometabolismus erlauben eine Trennung zwischen einer Alzheimer-Demenz, einem MCI-AD, anderen neurodegenerativen Erkrankungen und einem Hypometabolismus durch physiologisches Altern [9, 75].

Zur Bildgebung der Neuroinflammation ist das mitochondriale 18kDa-Translokatorprotein (TSPO) das am häufigsten verwendete Ziel angewandter Tracer. Es handelt sich dabei um ein in der äußeren Mitochondrienmembran exprimiertes Protein steroid-synthetisierender Zellen des zentralen Nervensystems, zu denen unter anderem Mikrogliazellen und Astrozyten gehören [76]. Als Tracer der dritten Generation bietet [¹⁸F]GE-180 den Vorteil einer bessern Durchlässigkeit der Blut-Hirn-Schranke und eines optimierten Kontrastverhältnisses von Signal zu Hintergrund [77].

In Patienten mit AD sowie in AD-Tiermodellen wurde eine vermehrte Expression von TSPO in aktivierten Mikrogliazellen festgestellt [78] sowie eine hohe Korrelation mit Tau und Amyloid [79].

1.5 PET-Studien zur metabolischen Konnektivität am Menschen und Kleintieren

Die Gehirnfunktion ist durch ein Zusammenspiel aus biochemischen und physiologischen Prozessen innerhalb neuronaler Netzwerke gekennzeichnet. Es ist von großem Interesse, krankheitsspezifische zeitliche und räumliche Veränderungen betroffener Netzwerke auf neuronaler Ebene, statt allein auf der Ebene von Veränderungen einzelner Gehirnregionen, besser zu verstehen. Gehirnetzwerke können als funktionelle Konnektivität mithilfe elektrophysiologischer und bildgebender Verfahren erfasst werden [80].

Unter den bildgebenden Modalitäten ermöglicht FDG-PET neben der Darstellung regionaler Glukoseaufnahme auch die Untersuchung der metabolischen Konnektivität (MC) durch Berücksichtigung des gesamten Bildmusters [53]. Die metabolische Konnektivität impliziert eine Wechselwirkung zwischen unterschiedlichen Gehirnregionen [81]. Durch die Korrelation der neuronalen Aktivität an mehreren Standorten, gemessen an der FDG-Aufnahme als Parameter für den Energieverbrauch, kann der Grad der Synchronität zwischen neuronalen Populationen bestimmt werden [50].

In einer klinischen Studie, konnte gezeigt werden, dass ein Verlust der metabolischen Konnektivität, insbesondere des posterioren cingulären Kortex (PCC), dem dortigen Hypometabolismus als Zeichen synaptischer Degeneration vorausgeht [53]. Ein

Verlust der Konnektivität zwischen dem PCC und dem Hippocampus erwies sich als Gemeinsamkeit bei allen AD-Subtypen, was auf ein charakteristisches Merkmal der Alzheimer-Erkrankung schließen lässt [82]. Regionale Unterschiede in den Netzwerkveränderungen zwischen den AD-Subtypen sind allerdings auch erkennbar [82]. Ebenso konnten stadienabhängig signifikante Veränderungen der metabolischen Konnektivität in depressionsassoziierten Netzwerken des dopaminergen mesocortico- limbischen Signalwegs bei Alzheimererkrankten festgestellt werden [83].

Bei Patienten mit Lewy-Body-Demenz, die einen fortgeschrittenen Dopaminverlust und mittlere bis schwere Nigrostriatale-Degeneration aufweisen, wurde ein Verlust der metabolischen Konnektivität im limbischen System und den Basalganglien im Vergleich zu gesunden Kontrollen beobachtet, was die Verbindung zwischen Dopaminverlust und dem Gehirnstoffwechsel unterstützt [84].

Präklinische Studien an β -Amyloid- und Tau-Mausmodellen ermöglichen spezifischere Analysen einzelner pathologischer Merkmale von AD, wie beispielsweise die der Auswirkung der Mikroglia-Aktivität auf die metabolische Konnektivität [85] oder um den metabolischen Beitrag von Astrozyten im Rattengehirn zu veranschaulichen [86]. Allerdings wurde MC bisher noch nicht in großem Umfang für die Untersuchung der Neurodegeneration in transgenen Mausmodellen neurodegenerativer Erkrankungen eingesetzt.

1.6 Abgeleitete Fragestellung

Die klinische Interpretation der FDG-PET-Bildgebung hat durch ihre hohe Sensitivität bei Verdacht auf eine Alzheimer-Erkrankung weiterhin einen hohen diagnostischen Wert [87]. Insbesondere zur Früherkennung ist ein Alzheimer-typischer Hypometabolismus im Vergleich zu anderen diagnostischen Modalitäten (MRT, Liquor) meist früher erkennbar [69, 71].

In den letzten Jahren ist das Interesse an der Erforschung der Auswirkungen der Alzheimer-Erkrankung auf zerebrale Netzwerke zunehmend, nicht zuletzt aufgrund des potenziellen Nutzens der funktionellen Konnektivität als Biomarker für Krankheitsstadium, -risiko und -prognose [88]. Die molekulare Bildgebung mittels [¹⁸F]FDG-PET ist dabei ein vielversprechendes Werkzeug, da sie die Nutzung der Daten zur Bestimmung der metabolischen Konnektivität ermöglicht [80]. Zur weiteren Anwendung und Bewertung der Methode muss diese auf ihre Validität und Reproduzierbarkeit untersucht werden. Zur präklinischen Anwendung an spezifischen Mausmodellen mit neurodegenerativer Erkrankung existieren dazu jedoch nur wenige Studien.

In dieser Arbeit wurde daher die Anwendbarkeit und das Verfahren der metabolischen Konnektivität an Mausmodellen mit und ohne β -Amyloid- bzw. Tau-Pathologie untersucht und mit Ergebnissen der kognitiven Verhaltenstestung verglichen. Das Verfahren wurde hinsichtlich optimaler Auswertung, Einfluss des Anästhetikums und Inter-Scanner-Reproduzierbarkeit untersucht.

Darüber hinaus wurde der Einfluss des Geschlechts auf die Mikrogliaentzündung in den verwendeten β -Amyloid- und Tau-Mausmodellen analysiert.

2. Inhalt der Promotionsarbeit

2.1 Validität und Wert der metabolischen Konnektivität in Mausmodellen für β -Amyloid und Tauopathie

Obwohl die Methodik der metabolischen Konnektivität bereits bei verschiedenen Fragestellungen am Menschen [83, 84] sowie an verschiedenen Nagetiermodellen [86, 89] angewendet wurde, richtete diese Studie ihren Fokus darauf, erstmals eine methodische Grundlage dieser Technik am Mausmodell zu etablieren. Durch Validierungsanalysen sollte die Anwendbarkeit dieser Methode an Mausmodellen, die mit β -Amyloid und Tau assoziiert sind, nachgewiesen werden. Alle in dieser Studie präsentierten Daten wurden unter Verwendung bereits etablierter Untersuchungsmethoden an unserem Institut gewonnen, die in zahlreichen Studien mit transgenen Mausmodellen erfolgreich angewendet wurden [90].

Es erfolgte die Analyse von [^{18}F]FDG- μ PET-Daten an zwei Mausmodellen mit β -Amyloid (PS2APP und APPPS1), einem Mausmodell mit Tau-Pathologie (P301S) und altersgleichen Wildtypen. Die Aufnahmen wurden an $n = 24$ weiblichen PS2APP-Mäusen, $n = 16$ altersgleichen weiblichen Wildtypen, $n = 16$ weiblichen APPPS1-Mäusen und $n = 25$ altersgleichen weiblichen Wildtypen durchgeführt. Zur Überprüfung der Inter-Scanner-Vergleichbarkeit wurden an einer kleineren Kohorte von $n = 12$ APPPS1-Mäusen und altersgleichen $n = 17$ Wildtypen-Aufnahmen im FDG- μ PET/MR generiert. Als Tau-Mausmodell wurden $n = 32$ weibliche P301S-Mäuse und $n = 32$ altersgleiche Wildtypen untersucht. An allen Modellen wurde eine kognitive Verhaltenstestung mittels des Morris-Wasserlabyrinths durchgeführt. Zusätzlich wurde der Einfluss der Anästhesie auf die metabolische Konnektivität durch einen direkten

Vergleich an n= 11 weiblichen Wildtyp-Mäusen untersucht, die jeweils einen Scan im Wachzustand und unter Isofluran-Narkose erhielten.

Zur Berechnung der interregionalen metabolischen Konnektivität wurde auf funktionelle Einheiten und Gehirnnetzwerke in der Maus basierend, ein Set aus verschiedenen dreidimensionalen Zielvolumina erstellt, um das [¹⁸F]FDG-μPET-Signal und die metabolische Aktivität zu messen (**Abb. 1**). Alle Hirnregionen wurden gemäß dem Allen Maus Hirn Atlas definiert.

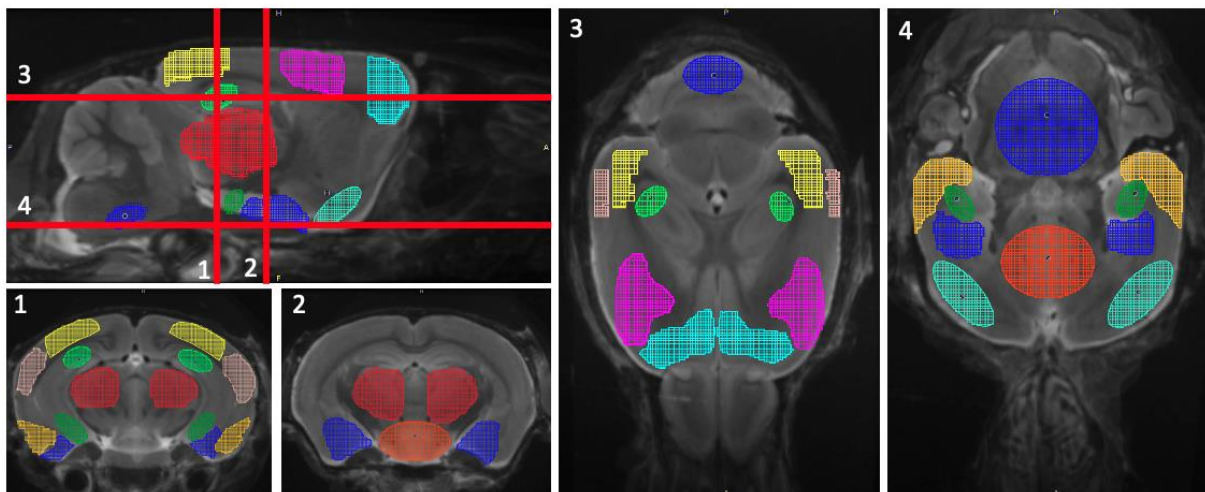


Abbildung 2.1-1: μPET-Zielregionen

Die definierten Zielregionen im Mausgehirn umfassen bilateral das Ammonshorn mit den Abschnitten 1 (CA1) (hellgrün) und 3 (CA3) (dunkelgrün), den Thalamus (rot), die Amygdala (blau), den entorhinalen Cortex (hellorange), den piriformen Cortex (türkis), den visuellen (gelb), auditiven (pink), motorischen (hellblau), und somatosensorischen (lila) Cortexbereich sowie den Hypothalamus (orange), das Kleinhirn (blau) und den Hirnstamm (blau).

Zur Auswahl der Skalierung unserer Daten wurden herkömmliche Standard-Aufnahmewerte ($SUV = x \frac{\text{Gewicht}}{\text{injizierte Aktivität}}$) und relative Standard-Aufnahmewerte zur Referenzregion des globalen Mittelwertes ($SUVR = \frac{VOI}{\text{Globaler Mittelwert}}$) gewonnen. Die

Simulationsanalyse zur Bestimmung der Quadratwurzel des mittleren quadratischen Fehlers ($RMSE = \sqrt{\frac{\sum(ICC_{P301S} - ICC_{WT})^2}{n_{ICC}}}$) mit abnehmender Kohortengröße ergab einen vergleichbaren Fehler zwischen beiden Skalierungsmethoden ab einer Kohortengröße von 12 Mäusen (**Abb. 2A**). Die SUVR-Skalierung weist in den intra-neokortikalen Verbindungen allerdings höhere Effektgrößen der Interkorrelationskoeffizienten zwischen P301S-Mäusen und Wildtyp-Mäusen auf (**Abb. 2B**). Daraus lässt sich ableiten, dass SUVR eine empfindlichere Anzeige für Unterschiede der metabolischen Konnektivität zwischen P301S-Mäusen und WT darstellt.

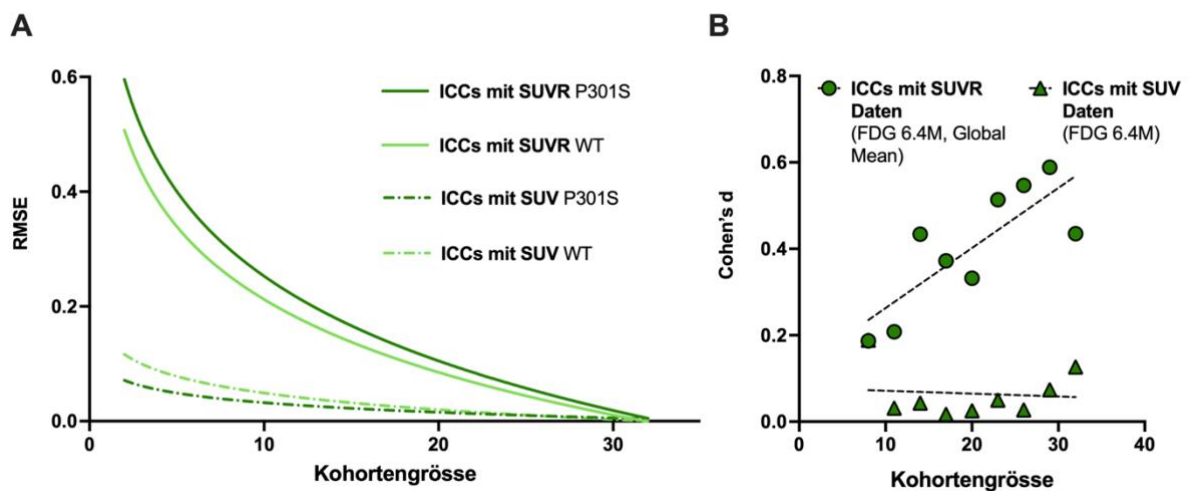


Abbildung 2.1-2: Simulationsanalyse zur Read-out-Bestimmung

A Quadratwurzel des mittleren quadratischen Fehlers (RMSE) der Summe der Interkorrelationskoeffizienten (ICCs) basierend auf SUV- und SUVR-Werten und in Abhängigkeit der Stichprobengröße bei P301S- und Wildtyp-Mäusen. **B** Effektgrößen (Cohen's d) der ICCs in den intraneokortikalen Verbindungen zwischen P301S- und Wildtyp-Mäusen in Abhängigkeit der Stichprobengröße, abgeleitet aus SUV- und SUVR-Werten.

Bei der Gegenüberstellung von $[^{18}\text{F}]\text{FDG}$ - μPET -Scans von Wildtyp-Mäusen nach erfolgter Tracer-Injektion, jeweils im Wach- und Anästhesiezustand, zeigten sich in den meisten untersuchten Volumes-of-Interest (VOIs) vergleichbare SUVR-Werte. Lediglich im piriformen Kortex wurde eine signifikant reduzierte $[^{18}\text{F}]\text{FDG}$ -Aufnahme

unter Isofluran festgestellt. Im Gegensatz dazu war die $[^{18}\text{F}]\text{FDG}$ -Aufnahme im Hypothalamus und in der Amygdala erhöht unter Isofluran (**Abb. 3A**). Die Netzwerkstruktur in den Korrelationsmatrizen waren vergleichbar, quantifizierbar an einer starken Gesamtkorrelation zwischen den ICCs der beiden Matrizen (**Abb. 3B-C**).

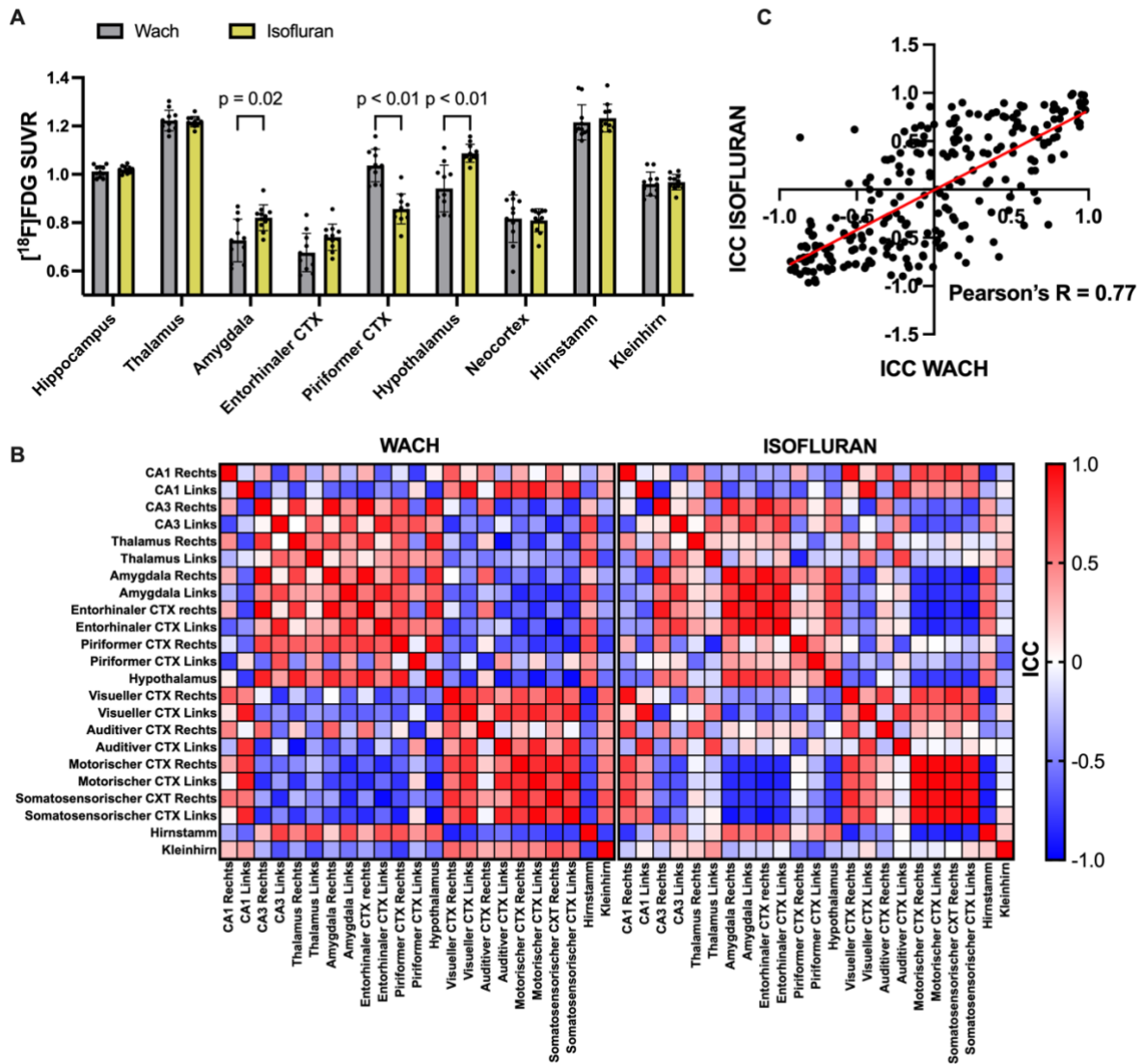


Abbildung 2.1-3: Vergleich zwischen Tracer-Injektion im Wach- und Anästhesiezustand

A $[^{18}\text{F}]\text{FDG}$ -SUVR-Werte. **B** Korrelationsmatrix mit ICCs für alle 23 analysierten Hirnregionen. **C** Korrelationen zwischen ICCs für alle 23 analysierten Hirnregionen

Ein direkter quantitativer Vergleich zwischen beiden Zuständen zeigte ebenso keinen signifikanten Unterschied in den durchschnittlichen ICCs, sowohl in den kortikalen als auch in den subkortikalen Verbindungen (**Abb.4**).

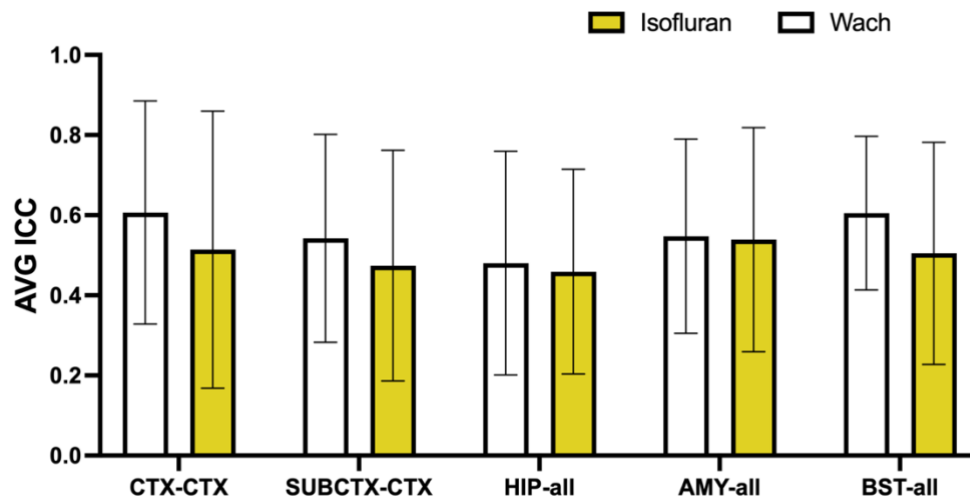


Abbildung 2.1-4: Vergleich der durchschnittlichen ICCs (AVG ICC) in kortikalen und subkortikalen Verbindungen zwischen Untergruppen von Mäusen mit Tracer-Injektion im Wachzustand und unter Isofluran-Narkose.

In einem Inter-Scanner-Vergleich zur Überprüfung der Reproduzierbarkeit wiesen die ICCs im APPPS1 β -Amyloid-Mausmodell und in den altersentsprechenden Wildtypen eine starke Korrelation auf, sowohl bei der Betrachtung aller Verbindungen als auch für intraneokortikale Verbindungen allein (**Abb. 6A-B**). Auch die durchschnittlichen ICCs der intraneokortikalen Verbindungen ergaben keinen signifikanten Unterschied zwischen μ PET- und μ PET/MR-Scanner (**Abb. 6C**). Insgesamt zeigen die Ergebnisse eine robuste Reproduzierbarkeit zwischen beiden Scannern.

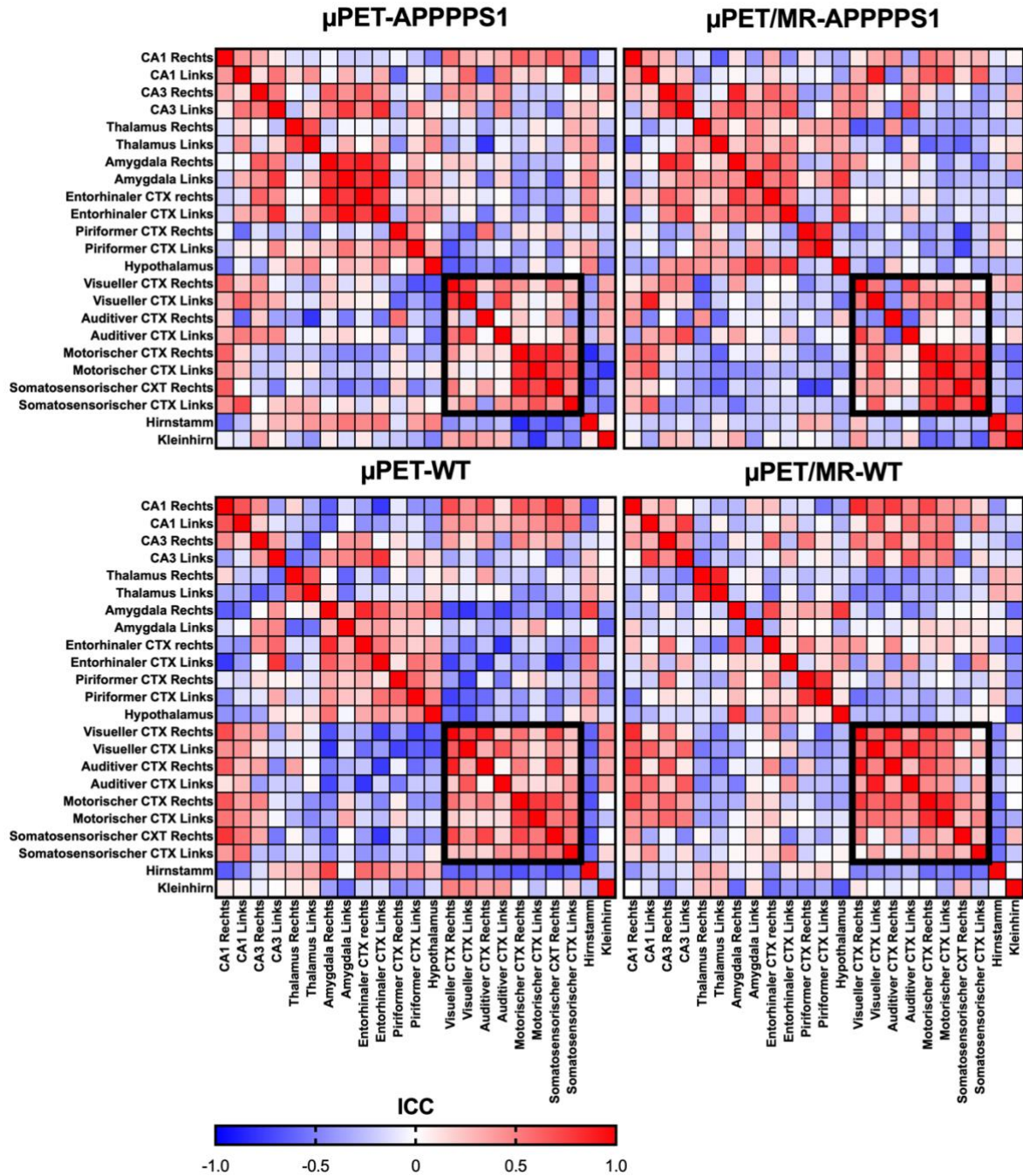


Abbildung 2.1-5: Korrelationsmatrix der ICCs für alle 23 VOIs und intra-neokortikale Verbindungen (schwarzer Rahmen).

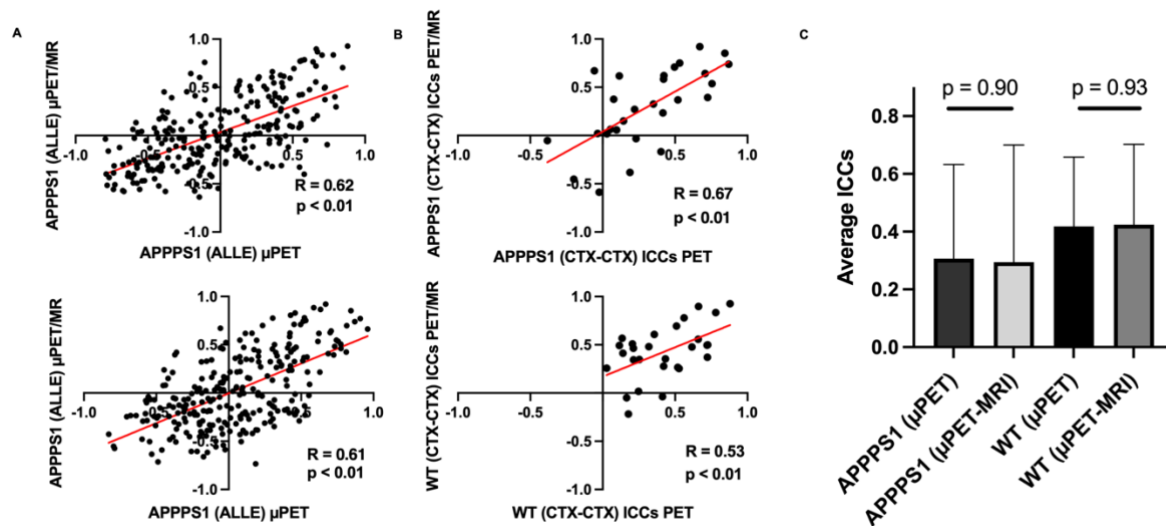


Abbildung 2.1-6: Reproduzierbarkeitsanalyse der metabolischen Konnektivität zwischen μ PET- und μ PET/MR-Scannern für APPPS1- und Wildtyp-Mäuse.

A Korrelation der ICCs für alle 23 VOI-Regionen. **B** Korrelation der intraneokortikalen ICCs. **C** Vergleich der durchschnittlichen intraneokortikalen ICCs (Average ICCs).

In der regionalen Konnektivitätsanalyse ergaben sich in beiden β -Amyloid-Mausmodellen PS2APP und APPPS1 keine signifikanten Unterschiede der metabolischen Konnektivität im Vergleich zu den altersgleichen Wildtypen in den intraneokortikalen Verbindungen. In PS2APP-Mäusen ließ sich jedoch ein signifikanter Verlust in den Verbindungen zum Hippocampus und zur Amygdala feststellen. Im APPPS1-Modell konnte nur in den Verbindungen zwischen Kortex und Subkortex ein signifikanter Verlust gemessen werden (**Abb. 7**)

Im Vergleich zu altersgleichen Wildtypen zeigte das P301S Tau-Mausmodell in allen regionalen Netzwerkeinheiten einen signifikanten Verlust der Konnektivität. Am ausgeprägtesten jedoch in den intraneokortikalen Verbindungen und in den Verbindungen zum Hirnstamm, aber auch in den Netzwerkverbindungen des räumlichen Lernens (**Abb. 7**).

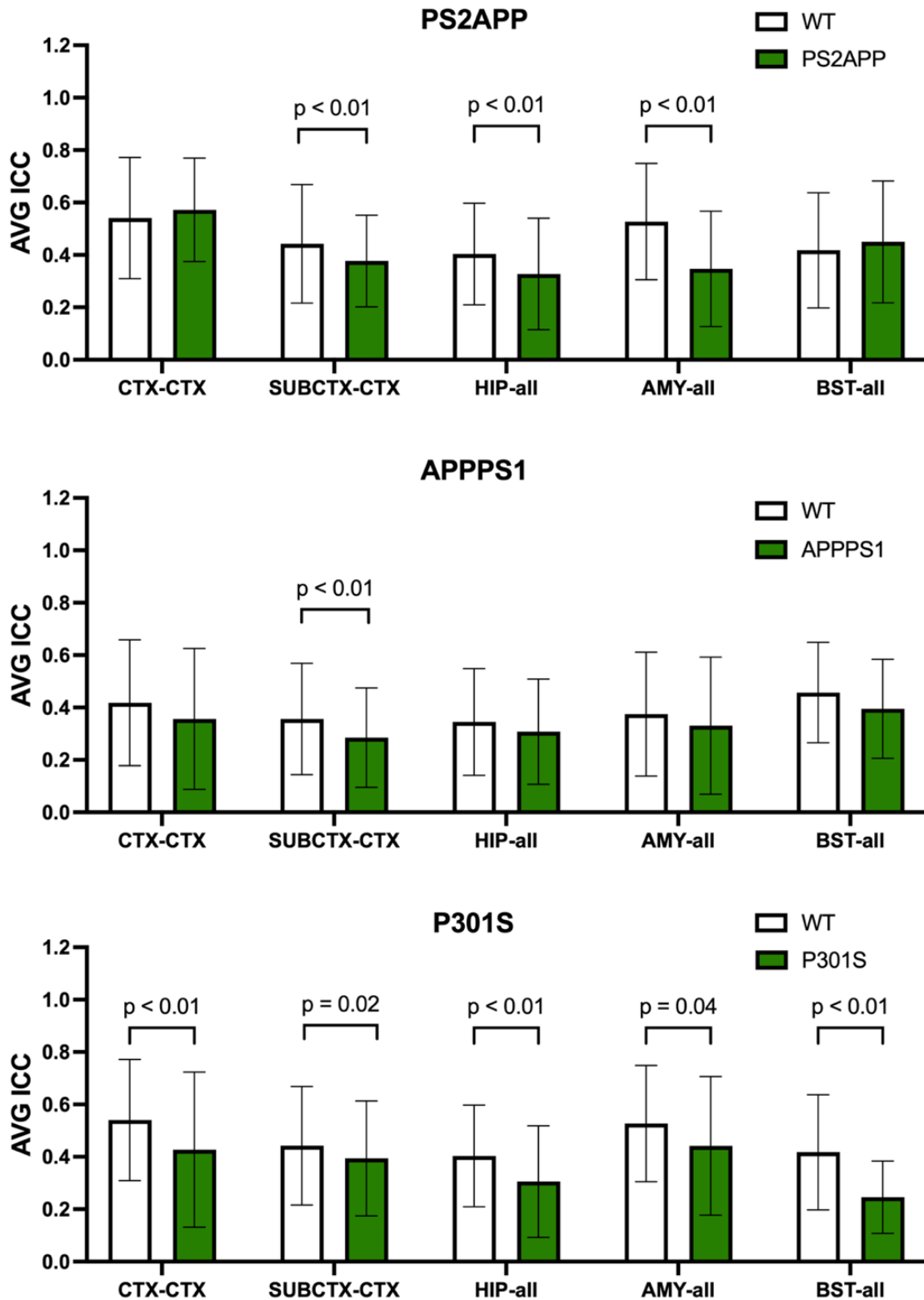


Abbildung 2.1-7: Vergleich des durchschnittlichen ICC (AVG ICC) von μ PET-SUVR-Daten zwischen verschiedenen transgenen (TG) Mausmodellen und entsprechenden Wildtyp (WT)-Kontrollen

Die qualitative Validierung der Ergebnisse aus der MC-Analyse bezogen auf motorische Funktionen und Funktionen des räumlichen Lernens mit denen der konventionellen VOI-basierten SUVR-Werte und den Ergebnissen der Verhaltenstestung im MWM wurde in einer Übersichtstabelle veranschaulicht (**Abb. 8**). In beiden Mausmodellen der Amyloidose wurden keine signifikanten Veränderungen des motorischen Netzwerks beobachtet. Damit übereinstimmend konnte in PS2APP- und APPPS1-Mäusen ebenso keine signifikante Geschwindigkeitsreduzierung in der Verhaltenstestung festgestellt werden. Die VOI-basierten SUVR-Werte zeigten sich allerdings mit einem ausgeprägten Hypermetabolismus der Regionen des Motorkortex in beiden β -Amyloid-Mausmodellen dazu abweichend. Im P301S-Mausmodell wurde ein signifikanter Verlust der motorischen Funktion beobachtet entsprechend ein Konnektivitätsverlust zwischen motorischen und verbleibenden kortikalen VOIs in diesem Tau-Modell, während die konventionellen SUVR-Analysen keinen signifikanten Unterschied erkennen.

Die konventionelle VOI-basierte Analyse zeigte ebenso keinen signifikanten Unterschied zwischen den transgenen Mausmodellen PS2APP- und P301S-Mäusen und entsprechenden Wildtypen in Gehirnregionen, die mit räumlichem Lernen verbunden sind. In den intrasubkortikalen Verbindungen, die an räumlichen Lernprozessen beteiligt sind, konnte durch die MC-Analyse ein signifikanter Konnektivitätsverlust im PS2APP-Modell sowie im P301S-Modell nachgewiesen werden, womit sich die MC in Übereinstimmung mit den Ergebnissen der Verhaltenstestung zeigt. Beide transgenen Mausmodelle schnitten bei den räumlichen Lernfunktionen schlechter ab als die entsprechenden Wildtypen, gemessen an der Fluchtlatenz. In den APPPS1-Mäusen konnte in der ICC-Analyse ein geringfügiger, jedoch nicht signifikanter Verlust der Netzwerkverbindungen zum Hippocampus

beobachtet werden, während die VOI-basierten SUVR-Daten einen signifikanten Hypermetabolismus in den Hippocampusregionen aufwiesen. Die Ergebnisse der Verhaltenstestung ergaben einen signifikanten Verlust räumlicher Lernfunktionen. Somit zeigte sich auch in diesem Mausmodell eine bessere Übereinstimmung der MC mit den Ergebnissen der Verhaltensanalyse, was vermuten lässt, dass MC im Gegensatz zur konventionellen VOI-basierten Methode weniger anfällig für durch Mikroglia-Entzündungen bedingte Veränderungen der [¹⁸F]FDG-Aufnahme ist.

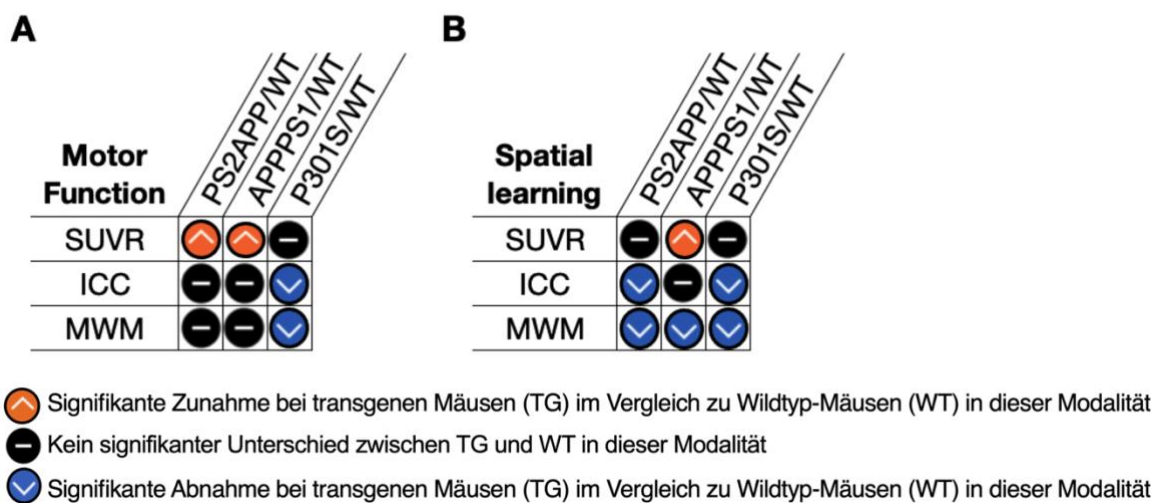


Abbildung 2.1-8: Zusammenfassung der signifikanten Unterschiede ($p > 0,05$) zwischen verschiedenen transgenen (TG) Mausmodellen und entsprechenden Wildtypen (WT).

Gegenüberstellung der Analyse von [¹⁸F]FDG- μ PET SUVR, metabolischer Konnektivität (MC) und Verhalten (MWM). **A** Motorische Funktionen (SUVR = [¹⁸F]FDG- μ PET-Aufnahme in motorischen Cortex-VOIs; MC = durchschnittlicher ICC in Verbindungen des motorischen Cortex; MWM = Durchschnittliche Geschwindigkeit). **B** Räumliches Lernen (SUVR = [¹⁸F]FDG- μ PET-Aufnahme in hippocampalen VOIs; MC = durchschnittlicher ICC in intra-subkortikalen Verbindungen; MWM = durchschnittliche Fluchtlatenz).

2.2 Die Mikroglia-Aktivität wird durch das Geschlecht in Amyloid Mausmodellen, nicht jedoch in Tau-Mausmodellen beeinflusst.

In meiner Koautorschaft war das Ziel, den Einfluss des Geschlechts auf die Mikroglia-Aktivierung an Mausmodellen mit neurodegenerativer Erkrankung zu untersuchen. Hierfür wurde eine erneute Verarbeitung der Rohdaten interner Studien zur Mikrogliaentzündung mittels Positronenemissionstomographie des 18-kDa Translokator-Protein-Liganden [¹⁸F]-GE-180 (TSPO-PET) durchgeführt. Die Studie umfasste Scans von C57BL/6 Wildtypen im Alter von 2 bis 13 Monaten, APP^{NL-G-F}-Mäusen im Alter von 2,5; 5,0; 7,5 und 10 Monaten als β -Amyloid-Modell, sowie P301S-Mäusen im Alter von 2, 4, 6 und 8 Monaten als Tau-Pathologie-Mausmodell. Die Ergebnisse von [¹⁸F]-GE-180- μ PET wurden durch eine unabhängige immunhistochemische in vitro Analyse mittels Mikroglia (Iba-1, CD68), Astrozyten (GFAP) und Tau (AT8)-Markern bestätigt.

Mit zunehmendem Alter zeigten Wildtyp-Mäuse einen Anstieg an TSPO- μ PET-SUVR im Kortex, wobei eine signifikante Interaktion zwischen Alter und Geschlecht festgestellt wurde. Der TSPO- μ PET-SUVR Anstieg erwies sich als ausgeprägter bei weiblichen Wildtyp-Mäusen ab einem Alter von 6 bis 7 Monaten im Vergleich zu männlichen Wildtypen (**Abb. 1A**). Die immunhistochemische Analyse bestätigte analog dazu eine höhere Mikroglia-Aktivität in weiblichen Wildtyp-Mäusen (**Abb. 2A**).

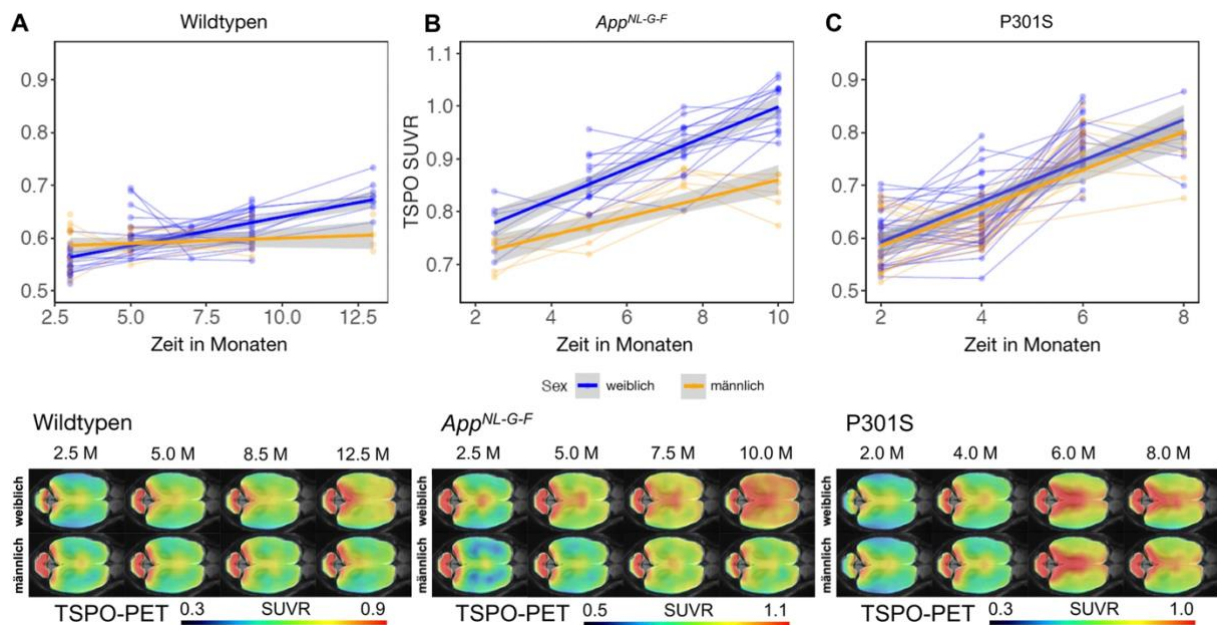


Abbildung 2.2-1: Geschlechtsspezifische Analyse des TSPO-PET-Signals in verschiedenen Mausmodellen.

Obere Reihe: Gemischte lineare Modelle des TSPO-PET-Signal bei männlichen (gelb) und weiblichen (blau) **A** Wildtyp-Mäusen, **B** APP^{NL-G-F} -Mäusen und **C** P301S-Mäusen. **Untere Reihe:** $[^{18}F]$ -GE-180 TSPO-PET-Gruppenschnittbilder in verschiedenen Altersstufen, auf einer MRI-Standardvorlage in horizontaler Ebene.

Bei Vorliegen einer β -Amyloid-Pathologie wie im APP^{NL-G-F} -Mäusen gab es ebenfalls einen signifikanteren TSPO- μ PET-SUVR-Anstieg mit zunehmendem Alter und eine signifikante Geschlecht-Alter-Interaktion mit stärkerem Anstieg in weiblichen Mäusen (**Abb. 1B**). Unter $[^{18}F]$ -Florbetaben-PET-SUVR zeigte sich eine vergleichbare Zunahme der fibrillären β -Amyloid-Aggregation im Kortex zwischen männlichen und weiblichen APP^{NL-G-F} -Mäusen, was darauf schließen lässt, dass Geschlechtsunterschiede bei TSPO-PET-SUVR nicht auf Unterschiede in der fibrillären β -Amyloid-Belastung zurückzuführen sind (**Abb. 3A**). Damit übereinstimmend konnte in der Immunhistochemie eine höhere Expression aktiver Mikroglia-Marker bei weiblichen Mäusen (**Abb. 2B**) und nur ein geringfügig höherer β -Amyloid-Spiegel zum Endzeitpunkt festgestellt werden (**Abb. 3B**).

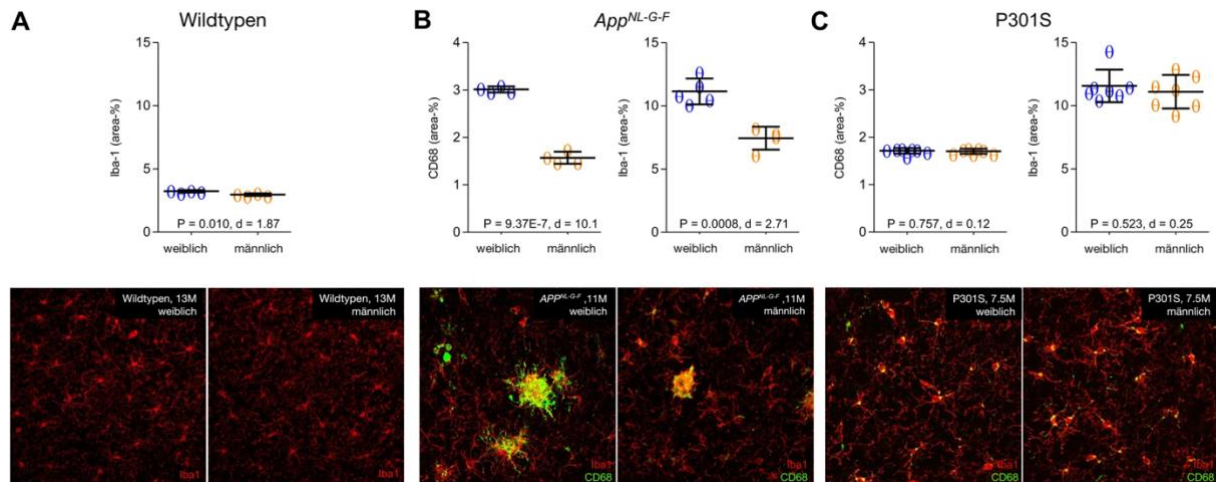


Abbildung 2.2-2: Streudiagramme und repräsentative Bilder der Iba-1- und CD68-Mikroglia-Marker nach Geschlecht in verschiedenen Mausmodellen.

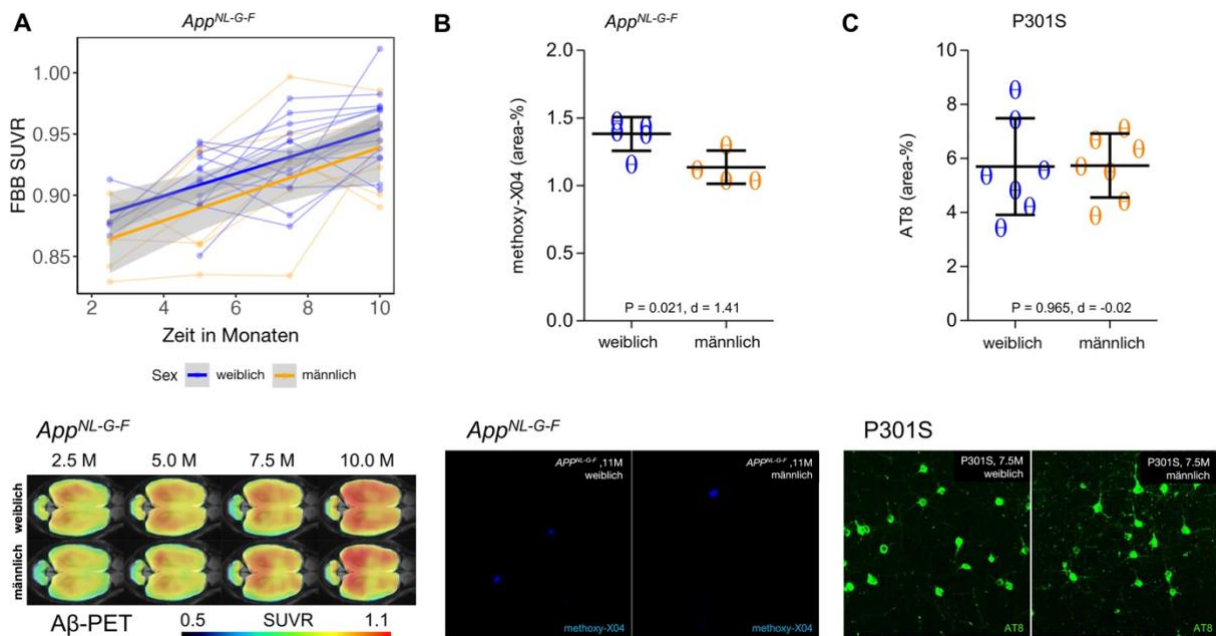


Abbildung 2.2-3: Geschlechtsspezifische Effekte auf A β - und Tau-Überexpression in APP^{NL-G-F}- und P301S-Mäusen.

A Gemischte lineare Modelle zur [¹⁸F]-Florbetaben-A β -PET als Funktion des Alters für weibliche (blau) und männliche (gelb) APP^{NL-G-F}-Mäuse und Gruppenschichtbilder in verschiedenen Altersstufen in einer horizontalen Ebene (n = 6–15). **B** Streudiagramm und repräsentative Bilder zur terminalen Methoxy-X04 A β -Färbung bei männlichen und weiblichen APP^{NL-G-F}-Mäusen im Alter von 11 Monaten **C** Streudiagramm und repräsentative Bilder zur terminalen AT8-Tau-Färbung bei männlichen und weiblichen P301S-Mäusen im Alter von 7–8 Monaten.

Ebenso ergab die GFAP-Immunhistochemie eine etwas ausgeprägtere Reaktivität der Astrozyten in APP^{NL-GF}-Weibchen zum Endzeitpunkt von 11 Monaten (**Abb. 4**)

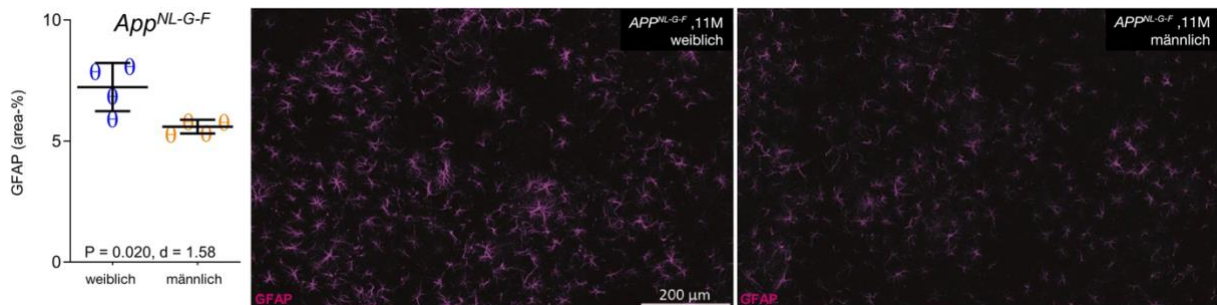


Abbildung 2.2-4: Streudiagramme und repräsentative Bilder der GFAP-Immunfärbung zur Darstellung der reaktiven Astrozyten bei männlichen und weiblichen APP^{NL-GF}-Mäusen.

Auch im P301S-Mausmodell zeigte sich mit zunehmendem Alter ein Anstieg des TSPO- μ PET-Signals, allerdings ohne signifikanten Unterschied zwischen männlichen und weiblichen P301S-Mäusen (**Abb. 1C**). Dies wurde in vitro in der terminalen immunhistochemischen Analyse der P301S-Mäuse im Alter von 7-8 Monaten bestätigt (**Abb. 2C**).

3. Zusammenfassung

Die metabolische Konnektivität bietet als bildgebendes Verfahren die Möglichkeit, funktionelle Interaktionen zwischen verschiedenen Hirnregionen auf der Grundlage von PET-Aufnahmen mit dem Glukoseanalogon [¹⁸F]-Fluordesoxyglukose ([¹⁸F]FDG) zu identifizieren und krankheitsspezifische Netzwerkveränderungen zu beschreiben. Mausmodelle ermöglichen es, dazu durch genetische Manipulationen spezifische biologische Prozesse der Krankheit zu untersuchen und darauf basierende Krankheitsmodelle zu entwickeln und durch Verhaltensstudien zu validieren.

Ziel dieser Arbeit war es daher, eine methodische Grundlage zu schaffen und die Validität sowie Aussagekraft der metabolischen Konnektivität an Mausmodellen neurodegenerativer Erkrankungen zu untersuchen. [¹⁸F]FDG-PET-Scans an Wildtyp- und transgenen Mausmodellen mit β -Amyloid- bzw. Tau-Pathologie wurden dazu im Alter von 6 bis 12 Monaten analysiert. In einer vergleichenden Simulationsanalyse erwiesen sich relative Standardaufnahmewerte (SUVR) auf den globalen Mittelwert skaliert durch höhere Effektgröße in den intraneokortikalen Verbindungen (+85%; $p < 0,0001$) als sensitiveres Read-Out zur Erkennung modellspezifischer Veränderungen der metabolischen Konnektivität verglichen mit Standardaufnahmewerten (SUV). Der qualitative und quantitative Vergleich metabolischer Konnektivitätsanalysen ergab bei einer hohen Gesamtkorrelation der Konnektivitätsmatrizen ($R = 0,77$) keinen signifikanten Unterschied zwischen einer Tracer-Injektion im Wachzustand oder unter Isofluran-Narkose, was die Validität der angewandten Methodik bestätigt. In einem unabhängigen Inter-Scanner-Vergleich konnten keine signifikanten Unterschiede bei den Interkorrelationskoeffizienten (ICC) festgestellt werden, sowohl für APPPS1-Mäuse ($p = 0,90$) als auch für Wildtypen ($p = 0,93$). Für beide Mausmodelle konnten die Ergebnisse hoher Korrelation zwischen den Scannern reproduziert werden (APPPS1-Mäuse: $R = 0,61$, $p < 0,0001$; Wildtypen: $R = 0,62$, $p < 0,0001$). Im

modellspezifischen Vergleich mit altersgleichen Wildtypen ließ sich bei allen transgenen Mausmodellen ein signifikanter Verlust der Konnektivität in den Netzwerkregionen des räumlichen Lernens feststellen, erkennbar in den Verbindungen zwischen Kortex und Subkortex, sowie im PS2APP-Modell an den Verbindungen zum Hippocampus und zur Amygdala. Anders als in den β -Amyloid-Pathologie-Mausmodellen zeigte das Tau-Pathologie-Mausmodell P301S ebenso einen Verlust in den Verbindungen zum Hirnstamm (-41 %; $p = 0,002$) und in den intraneokortikalen Verbindungen (-21 %; $p = 0,001$). Dieser Verlust zeigte sich gegenüber Wildtypen auch in den Verbindungen zum Motorkortex ausgeprägter (-36 %; $p = 0,04$), womit sich die MC als besserer Prädiktor für motorische Defizite in der Verhaltenstestung erweist. Auch die Befunde der abschließenden kognitiven Verhaltenstestung mittels Morris-Wasserlabyrinth bezüglich der Funktionen des räumlichen Lernens erwiesen sich in besserer Übereinstimmung mit den Ergebnissen der Netzwerkanalyse als mit denen der herkömmlichen VOI-basierten regionalen [^{18}F]FDG-Aufnahmen, was die Validität und Aussagekraft der metabolischen Konnektivität an Mausmodellen neurodegenerativer Erkrankungen weiter bestätigt.

Die zweite Arbeit befasste sich mit dem Einfluss des Geschlechts auf die Mikroglia-Aktivität in Wildtypen und in transgenen Mausmodellen neurodegenerativer Erkrankungen. Dazu erfolgten in einem longitudinalem Studiendesign an C57Bl/6 Wildtyp-Mäusen, am APP^{NL-G-F} β -Amyloid-Mausmodell und dem Tau-Pathologie-Mausmodell P301S, TSPO- μ PET-Scans in der Altersspanne von 2-13 Monaten. PET-Ergebnisse wurde in vitro immunhistochemisch bestätigt. In allen Mausmodellen zeigte sich mit zunehmendem Alter ein Anstieg des TSPO- μ PET-Signals, als Maß für die Mikroglia-Inflammation. Ein signifikant stärkerer Anstieg war sowohl in weiblichen Wildtyp-Mäusen ($T = -4,171$, $b/SE = -0,009/0,002$, $p < 0,001$) als auch in weiblichen APP^{NL-G-F} β -Amyloid-Mäusen ($T = -2,953$, $b/SE = -0,011/0,004$, $p = 0,0048$)

festzustellen. Ein Störeffekt durch das Fortschreiten der fibrillären A β -Pathologie ließ sich in vivo nicht als Ursache der Geschlechtsunterschiede nachweisen. Im P301S-Tau-Mausmodell konnten keine signifikanten Unterschiede im TSPO- μ PET-SUVR-Anstieg zwischen männlichen und weiblichen Mäusen beobachtet werden ($T = -0,671$, $b/SE = -0,003/0,005$, $p = 0,504$). Die fehlenden Geschlechtsunterschiede in den μ PET-Befunde werden in vitro in der Iba-1- und CD68-Immunhistochemie und durch die gleichen Mengen an hyperphosphoryliertem AT8-positivem Tau bei weiblichen und männlichen P301S-Mäusen im Alter von 7 Monaten gestützt. Zusammenfassend liefern die Ergebnisse damit einen Hinweis auf einen geschlechtsspezifischen Effekt auf die Mikroglia-Entzündung bei alternden Wildtypen und im Zusammenhang mit der β -Amyloid-Akkumulation bei transgenen Mäusen, ohne dass allerdings ein Zusammenhang mit der Tau-Pathologie im Mausmodell nachgewiesen werden konnte.

4. Summary

Metabolic connectivity, as an imaging technique, allows the identification of functional interactions between different brain regions based on PET scans using the glucose analog [¹⁸F]fluorodeoxyglucose ([¹⁸F]FDG) and describing disease-specific network changes. Mouse models, through genetic manipulations, enable the investigation of specific biological processes of neurodegenerative diseases, the development of disease models, and validation through behavioral studies.

The objective of this study was to lay down a methodological framework and assess the reliability and validity of metabolic connectivity in mouse models of neurodegenerative diseases. [¹⁸F]FDG- μ PET scans were analyzed in wild-type and transgenic mouse models with β -amyloid or tau pathology at 6 to 12 months of age. In a comparative simulation analysis, relative standardized uptake value ratios (SUVR) scaled to the global mean proved to be a better-suited read-out for detecting model-specific changes in metabolic connectivity by a higher effect size compared to standardized uptake values (SUV) (+85%; $p < 0,0001$).

The qualitative and quantitative comparison of metabolic connectivity analyses showed no significant differences between awake and isoflurane-anesthetized conditions and a high correlation between connectivity matrices ($R = 0.77$), confirming the validity of the applied methodology. Results were reproducible in an independent inter-scanner comparison without significant differences in intercorrelation coefficients (ICC), both for APPPS1-mice ($p = 0.90$) and wild-types ($p = 0.93$). For both mouse-models, the results demonstrated a high correlation between the scanners (APPPS1 mice: $R = 0.61$, $p < 0.0001$; wild-types: $R = 0.62$, $p < 0.0001$).

In model-specific comparisons with age-matched wild-types, all transgenic mouse-models exhibited a significant loss of connectivity in network regions related to spatial learning. This loss was evident in connections between the cortex and subcortex, and

in the PS2APP-model, also in connections to the hippocampus and amygdala. Unlike in β -amyloid-pathology-mouse-models, the tau-pathology-mouse-model P301S also showed a loss in connections to the brainstem (-41 %; $p = 0.002$) and intra-neocortical connections (-21 %; $p = 0.001$). This loss was pronounced in connections to the motor cortex (-36 %; $p = 0.04$), making metabolic connectivity a better predictor for motor deficits in behavioral testing. Regarding spatial learning functions, test results from the Morris Water Maze also proved to be in better agreement with the results of the network analysis than with those of conventional VOI-based regional [^{18}F]FDG recordings, affirming the credibility and informative nature of metabolic connectivity in mouse models of neurodegenerative diseases. The second study examined how sex influences microglial activity in both wild-type and transgenic mouse models of neurodegenerative diseases. TSPO- μ PET-scans were performed in a longitudinal study design in C57Bl/6 wild-type mice, the β -amyloid-mouse-model APP^{NL-G-F}, and the tau-pathology-mouse-model P301S in the age range of 2-13 months. PET results were confirmed in vitro by immunohistochemistry. All mouse models showed an increase in TSPO- μ PET-signal as a measure of microglial inflammation with increasing age. A significant interaction between age and sex with a more pronounced increase in female mice was observed both in wild-type mice ($T = - 4.171$, $b/SE = - 0, 009/0.002$, $p < 0.001$), as well as in the APP^{NL-G-F} β -amyloid mice ($T = - 2.953$, $b/SE = - 0.011/0.004$, $p = 0.0048$). A confounding effect due to the progression of fibrillar A β pathology could not be detected in vivo as a cause of the sex differences. No significant differences in TSPO- μ PET-SUVr increase were detected between male and female P301S tau mice ($T = - 0.671$, $b/SE = - 0.003/0.005$, $p = 0.504$). This absence of significant sex differences is supported in vitro by immunohistochemistry. Overall, the findings offer support for a sex-specific impact on microglial inflammation in aging wild-

type mice and in relation to β -amyloid accumulation in transgenic mice, without a confirmed correlation with tau pathology in the mouse model.

V Literaturverzeichnis

1. Prince, M., Wimo, A., Guerchet, M., Ali, G.C., Wu, Y.T., Prina, M. *World Alzheimer Report 2015, The Global Impact of Dementia, An analysis of prevalence, incidence, cost and trends*. 2015; Available from: <https://www.alzint.org/u/WorldAlzheimerReport2015.pdf>.
2. OECD. *Health at a Glance: Europe 2018, State of Health in the EU Cycle*. 2018.
3. Jonsson, L., *The personal economic burden of dementia in Europe*. *Lancet Reg Health Eur*, 2022. **20**: p. 100472.
4. WHO. *Dementia*. 2023; Available from: <https://www.who.int/news-room/fact-sheets/detail/dementia>.
5. WHO. *Global status report on the public health response to dementia*. 2021; Available from: <https://www.who.int/publications/i/item/9789240033245>.
6. Grossberg, G.T., et al., *Present Algorithms and Future Treatments for Alzheimer's Disease*. *J Alzheimers Dis*, 2019. **67**(4): p. 1157-1171.
7. Verger, A., et al., *FDA approval of lecanemab: the real start of widespread amyloid PET use? - the EANM Neuroimaging Committee perspective*. *Eur J Nucl Med Mol Imaging*, 2023. **50**(6): p. 1553-1555.
8. van Dyck, C.H., et al., *Lecanemab in Early Alzheimer's Disease*. *N Engl J Med*, 2023. **388**(1): p. 9-21.
9. Mosconi, L., et al., *Multicenter standardized 18F-FDG PET diagnosis of mild cognitive impairment, Alzheimer's disease, and other dementias*. *J Nucl Med*, 2008. **49**(3): p. 390-8.
10. Kvello-Alme, M., et al., *Time to Diagnosis in Young Onset Alzheimer's Disease: A Population-Based Study from Central Norway*. *J Alzheimers Dis*, 2021. **82**(3): p. 965-974.
11. Braak, H. and E. Braak, *Neuropathological staging of Alzheimer-related changes*. *Acta Neuropathol*, 1991. **82**(4): p. 239-59.
12. De Strooper, B. and E. Karran, *The Cellular Phase of Alzheimer's Disease*. *Cell*, 2016. **164**(4): p. 603-15.
13. Scheltens, P., et al., *Alzheimer's disease*. *Lancet*, 2021. **397**(10284): p. 1577-1590.
14. Heneka, M.T., et al., *Neuroinflammation in Alzheimer's disease*. *Lancet Neurol*, 2015. **14**(4): p. 388-405.
15. Hampel, H., et al., *The Amyloid-beta Pathway in Alzheimer's Disease*. *Mol Psychiatry*, 2021. **26**(10): p. 5481-5503.
16. Moya-Alvarado, G., et al., *Neurodegeneration and Alzheimer's disease (AD). What Can Proteomics Tell Us About the Alzheimer's Brain?* *Mol Cell Proteomics*, 2016. **15**(2): p. 409-25.
17. Terry, R.D., et al., *Physical basis of cognitive alterations in Alzheimer's disease: synapse loss is the major correlate of cognitive impairment*. *Ann Neurol*, 1991. **30**(4): p. 572-80.
18. Overk, C.R. and E. Masliah, *Pathogenesis of synaptic degeneration in Alzheimer's disease and Lewy body disease*. *Biochem Pharmacol*, 2014. **88**(4): p. 508-16.
19. Forner, S., et al., *Synaptic Impairment in Alzheimer's Disease: A Dysregulated Symphony*. *Trends Neurosci*, 2017. **40**(6): p. 347-357.
20. Citron, M., et al., *Mutation of the beta-amyloid precursor protein in familial Alzheimer's disease increases beta-protein production*. *Nature*, 1992. **360**(6405): p. 672-4.

21. Rogaev, E.I., et al., *Familial Alzheimer's disease in kindreds with missense mutations in a gene on chromosome 1 related to the Alzheimer's disease type 3 gene*. Nature, 1995. **376**(6543): p. 775-8.
22. Mawuenyega, K.G., et al., *Decreased clearance of CNS beta-amyloid in Alzheimer's disease*. Science, 2010. **330**(6012): p. 1774.
23. Selkoe, D.J., *Translating cell biology into therapeutic advances in Alzheimer's disease*. Nature, 1999. **399**(6738 Suppl): p. A23-31.
24. Crews, L. and E. Masliah, *Molecular mechanisms of neurodegeneration in Alzheimer's disease*. Hum Mol Genet, 2010. **19**(R1): p. R12-20.
25. Jansen, W.J., et al., *Prevalence of cerebral amyloid pathology in persons without dementia: a meta-analysis*. JAMA, 2015. **313**(19): p. 1924-38.
26. Hardy, J. and D.J. Selkoe, *The amyloid hypothesis of Alzheimer's disease: progress and problems on the road to therapeutics*. Science, 2002. **297**(5580): p. 353-6.
27. Delacourte, A. and A. Defossez, *Alzheimer's disease: Tau proteins, the promoting factors of microtubule assembly, are major components of paired helical filaments*. J Neurol Sci, 1986. **76**(2-3): p. 173-86.
28. Kolarova, M., et al., *Structure and pathology of tau protein in Alzheimer disease*. Int J Alzheimers Dis, 2012. **2012**: p. 731526.
29. Tapia-Rojas, C., et al., *It's all about tau*. Prog Neurobiol, 2019. **175**: p. 54-76.
30. Tarutani, A., et al., *Distinct tau folds initiate templated seeding and alter the post-translational modification profile*. Brain, 2023. **146**(12): p. 4988-4999.
31. Gotz, J., G. Halliday, and R.M. Nisbet, *Molecular Pathogenesis of the Tauopathies*. Annu Rev Pathol, 2019. **14**: p. 239-261.
32. Li, B., et al., *Disruption of microtubule network by Alzheimer abnormally hyperphosphorylated tau*. Acta Neuropathol, 2007. **113**(5): p. 501-11.
33. Alonso, A.D., et al., *Abnormal phosphorylation of tau and the mechanism of Alzheimer neurofibrillary degeneration: sequestration of microtubule-associated proteins 1 and 2 and the disassembly of microtubules by the abnormal tau*. Proc Natl Acad Sci U S A, 1997. **94**(1): p. 298-303.
34. Dujardin, S. and B.T. Hyman, *Tau Prion-Like Propagation: State of the Art and Current Challenges*. Adv Exp Med Biol, 2019. **1184**: p. 305-325.
35. Gomez-Isla, T., et al., *Neuronal loss correlates with but exceeds neurofibrillary tangles in Alzheimer's disease*. Ann Neurol, 1997. **41**(1): p. 17-24.
36. Ahmad, M.H., M. Fatima, and A.C. Mondal, *Influence of microglia and astrocyte activation in the neuroinflammatory pathogenesis of Alzheimer's disease: Rational insights for the therapeutic approaches*. J Clin Neurosci, 2019. **59**: p. 6-11.
37. Leyns, C.E.G. and D.M. Holtzman, *Glial contributions to neurodegeneration in tauopathies*. Mol Neurodegener, 2017. **12**(1): p. 50.
38. Hansen, D.V., J.E. Hanson, and M. Sheng, *Microglia in Alzheimer's disease*. J Cell Biol, 2018. **217**(2): p. 459-472.
39. Sanchez-Varo, R., et al., *Transgenic Mouse Models of Alzheimer's Disease: An Integrative Analysis*. Int J Mol Sci, 2022. **23**(10).
40. Sasaguri, H., et al., *APP mouse models for Alzheimer's disease preclinical studies*. EMBO J, 2017. **36**(17): p. 2473-2487.
41. Elder, G.A., et al., *Presenilin transgenic mice as models of Alzheimer's disease*. Brain Struct Funct, 2010. **214**(2-3): p. 127-43.

42. Lewis, J., et al., *Neurofibrillary tangles, amyotrophy and progressive motor disturbance in mice expressing mutant (P301L) tau protein*. Nat Genet, 2000. **25**(4): p. 402-5.
43. Weidensteiner, C., et al., *Cortical hypoperfusion in the B6.PS2APP mouse model for Alzheimer's disease: comprehensive phenotyping of vascular and tissular parameters by MRI*. Magn Reson Med, 2009. **62**(1): p. 35-45.
44. Yokoyama, M., et al., *Mouse Models of Alzheimer's Disease*. Front Mol Neurosci, 2022. **15**: p. 912995.
45. Ozmen, L., et al., *Expression of transgenic APP mRNA is the key determinant for beta-amyloid deposition in PS2APP transgenic mice*. Neurodegener Dis, 2009. **6**(1-2): p. 29-36.
46. Radde, R., et al., *Abeta42-driven cerebral amyloidosis in transgenic mice reveals early and robust pathology*. EMBO Rep, 2006. **7**(9): p. 940-6.
47. Saito, T., et al., *Single App knock-in mouse models of Alzheimer's disease*. Nat Neurosci, 2014. **17**(5): p. 661-3.
48. Allen, B., et al., *Abundant tau filaments and nonapoptotic neurodegeneration in transgenic mice expressing human P301S tau protein*. J Neurosci, 2002. **22**(21): p. 9340-51.
49. Xu, H., et al., *Memory deficits correlate with tau and spine pathology in P301S MAPT transgenic mice*. Neuropathol Appl Neurobiol, 2014. **40**(7): p. 833-43.
50. Palop, J.J. and L. Mucke, *Network abnormalities and interneuron dysfunction in Alzheimer disease*. Nat Rev Neurosci, 2016. **17**(12): p. 777-792.
51. Mondadori, C.R., et al., *Enhanced brain activity may precede the diagnosis of Alzheimer's disease by 30 years*. Brain, 2006. **129**(Pt 11): p. 2908-22.
52. Mosconi, L., *Brain glucose metabolism in the early and specific diagnosis of Alzheimer's disease. FDG-PET studies in MCI and AD*. Eur J Nucl Med Mol Imaging, 2005. **32**(4): p. 486-510.
53. Morbelli, S., et al., *Resting metabolic connectivity in prodromal Alzheimer's disease. A European Alzheimer Disease Consortium (EADC) project*. Neurobiol Aging, 2012. **33**(11): p. 2533-50.
54. Smallwood, J., et al., *The default mode network in cognition: a topographical perspective*. Nat Rev Neurosci, 2021. **22**(8): p. 503-513.
55. Antoine, N., et al., *Anosognosia and default mode subnetwork dysfunction in Alzheimer's disease*. Hum Brain Mapp, 2019. **40**(18): p. 5330-5340.
56. Anticevic, A., et al., *The role of default network deactivation in cognition and disease*. Trends Cogn Sci, 2012. **16**(12): p. 584-92.
57. Sperling, R.A., et al., *Functional alterations in memory networks in early Alzheimer's disease*. Neuromolecular Med, 2010. **12**(1): p. 27-43.
58. Sheline, Y.I., et al., *Amyloid plaques disrupt resting state default mode network connectivity in cognitively normal elderly*. Biol Psychiatry, 2010. **67**(6): p. 584-7.
59. Hedden, T., et al., *Disruption of functional connectivity in clinically normal older adults harboring amyloid burden*. J Neurosci, 2009. **29**(40): p. 12686-94.
60. Myers, N., et al., *Within-patient correspondence of amyloid-beta and intrinsic network connectivity in Alzheimer's disease*. Brain, 2014. **137**(Pt 7): p. 2052-64.
61. Buckner, R.L., et al., *Molecular, structural, and functional characterization of Alzheimer's disease: evidence for a relationship between default activity, amyloid, and memory*. J Neurosci, 2005. **25**(34): p. 7709-17.

62. Franzmeier, N., et al., *Functional connectivity associated with tau levels in ageing, Alzheimer's, and small vessel disease*. *Brain*, 2019. **142**(4): p. 1093-1107.
63. Jack, C.R., Jr., et al., *NIA-AA Research Framework: Toward a biological definition of Alzheimer's disease*. *Alzheimers Dement*, 2018. **14**(4): p. 535-562.
64. Ossenkoppele, R., et al., *Tau covariance patterns in Alzheimer's disease patients match intrinsic connectivity networks in the healthy brain*. *Neuroimage Clin*, 2019. **23**: p. 101848.
65. Yokoi, T., et al., *Involvement of the Precuneus/Posterior Cingulate Cortex Is Significant for the Development of Alzheimer's Disease: A PET (THK5351, PiB) and Resting fMRI Study*. *Front Aging Neurosci*, 2018. **10**: p. 304.
66. Schumacher, J., et al., *Dementia with Lewy bodies: association of Alzheimer pathology with functional connectivity networks*. *Brain*, 2021. **144**(10): p. 3212-3225.
67. Lehmann, M., et al., *Diverging patterns of amyloid deposition and hypometabolism in clinical variants of probable Alzheimer's disease*. *Brain*, 2013. **136**(Pt 3): p. 844-58.
68. Putcha, D., et al., *Tau and the fractionated default mode network in atypical Alzheimer's disease*. *Brain Commun*, 2022. **4**(2): p. fcac055.
69. Chetelat, G., et al., *Amyloid-PET and (18)F-FDG-PET in the diagnostic investigation of Alzheimer's disease and other dementias*. *Lancet Neurol*, 2020. **19**(11): p. 951-962.
70. Marcus, C., E. Mena, and R.M. Subramaniam, *Brain PET in the diagnosis of Alzheimer's disease*. *Clin Nucl Med*, 2014. **39**(10): p. e413-22; quiz e423-6.
71. Caminiti, S.P., et al., *FDG-PET and CSF biomarker accuracy in prediction of conversion to different dementias in a large multicentre MCI cohort*. *Neuroimage Clin*, 2018. **18**: p. 167-177.
72. Sestini, S., A. Castagnoli, and L. Mansi, *The new FDG brain revolution: the neurovascular unit and the default network*. *Eur J Nucl Med Mol Imaging*, 2010. **37**(5): p. 913-6.
73. Magistretti, P.J. and L. Pellerin, *Cellular mechanisms of brain energy metabolism and their relevance to functional brain imaging*. *Philos Trans R Soc Lond B Biol Sci*, 1999. **354**(1387): p. 1155-63.
74. Herholz, K., *PET studies in dementia*. *Ann Nucl Med*, 2003. **17**(2): p. 79-89.
75. Kato, T., et al., *Brain fluorodeoxyglucose (FDG) PET in dementia*. *Ageing Res Rev*, 2016. **30**: p. 73-84.
76. Zhou, R., et al., *PET Imaging of Neuroinflammation in Alzheimer's Disease*. *Front Immunol*, 2021. **12**: p. 739130.
77. Vivash, L. and T.J. O'Brien, *Imaging Microglial Activation with TSPO PET: Lighting Up Neurologic Diseases?* *J Nucl Med*, 2016. **57**(2): p. 165-8.
78. Gui, Y., et al., *Characterization of the 18 kDa translocator protein (TSPO) expression in post-mortem normal and Alzheimer's disease brains*. *Brain Pathol*, 2020. **30**(1): p. 151-164.
79. Dani, M., et al., *Microglial activation correlates in vivo with both tau and amyloid in Alzheimer's disease*. *Brain*, 2018. **141**(9): p. 2740-2754.
80. Sala, A., et al., *Brain connectomics: time for a molecular imaging perspective?* *Trends Cogn Sci*, 2023. **27**(4): p. 353-366.
81. Yakushev, I., A. Drzezga, and C. Habeck, *Metabolic connectivity: methods and applications*. *Curr Opin Neurol*, 2017. **30**(6): p. 677-685.
82. Herholz, K., et al., *Metabolic regional and network changes in Alzheimer's disease subtypes*. *J Cereb Blood Flow Metab*, 2018. **38**(10): p. 1796-1806.

83. Iaccarino, L., et al., *In vivo MRI Structural and PET Metabolic Connectivity Study of Dopamine Pathways in Alzheimer's Disease*. J Alzheimers Dis, 2020. **75**(3): p. 1003-1016.
84. Huber, M., et al., *Metabolic Correlates of Dopaminergic Loss in Dementia with Lewy Bodies*. Mov Disord, 2020. **35**(4): p. 595-605.
85. Gnorich, J., et al., *Depletion and activation of microglia impact metabolic connectivity of the mouse brain*. J Neuroinflammation, 2023. **20**(1): p. 47.
86. Zimmer, E.R., et al., *[(18)F]FDG PET signal is driven by astroglial glutamate transport*. Nat Neurosci, 2017. **20**(3): p. 393-395.
87. Morbelli, S., et al., *A Cochrane review on brain [(1)(8)F]FDG PET in dementia: limitations and future perspectives*. Eur J Nucl Med Mol Imaging, 2015. **42**(10): p. 1487-91.
88. Brier, M.R., J.B. Thomas, and B.M. Ances, *Network dysfunction in Alzheimer's disease: refining the disconnection hypothesis*. Brain Connect, 2014. **4**(5): p. 299-311.
89. Grosch, M., et al., *Dynamic whole-brain metabolic connectivity during vestibular compensation in the rat*. Neuroimage, 2021. **226**: p. 117588.
90. Brendel, M., et al., *Time Courses of Cortical Glucose Metabolism and Microglial Activity Across the Life Span of Wild-Type Mice: A PET Study*. J Nucl Med, 2017. **58**(12): p. 1984-1990.

VI Abbildungsverzeichnis

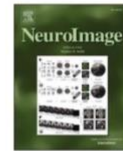
Abbildung 2.1-1: μ PET-Zielregionen	20
Abbildung 2.1-2: Simulationsanalyse zur Read-out-Bestimmung	21
Abbildung 2.1-3: Vergleich zwischen Tracer-Injektion im Wach- und Anästhesiezustand	22
Abbildung 2.1-4: Vergleich der durchschnittlichen ICCs (AVG ICC) in kortikalen und subkortikalen Verbindungen zwischen Untergruppen von Mäusen mit Tracer- Injektion im Wachzustand und unter Isofluran-Narkose.....	23
Abbildung 2.1-5: Korrelationsmatrix der ICCs für alle 23 VOIs und intra-neokortikale Verbindungen (schwarzer Rahmen).....	24
Abbildung 2.1-6: Reproduzierbarkeitsanalyse der metabolischen Konnektivität zwischen μ PET- und μ PET/MR-Scannern für APPPS1- und Wildtyp-Mäuse.....	25
Abbildung 2.1-7: Vergleich des durchschnittlichen ICC (AVG ICC) von μ PET-SUVR- Daten zwischen verschiedenen transgenen (TG) Mausmodellen und entsprechenden Wildtyp (WT)-Kontrollen.....	26
Abbildung 2.1-8: Zusammenfassung der signifikanten Unterschiede ($p > 0,05$) zwischen verschiedenen transgenen (TG) Mausmodellen und entsprechenden Wildtypen (WT).....	28

Abbildung 2.2-1: Geschlechtsspezifische Analyse des TSPO-PET-Signals in verschiedenen Mausmodellen.	30
Abbildung 2.2-2: Streudiagramme und repräsentative Bilder der Iba-1- und CD68- Mikroglia-Marker nach Geschlecht in verschiedenen Mausmodellen.	31



Contents lists available at ScienceDirect

NeuroImage

journal homepage: www.elsevier.com/locate/ynimg

Validity and value of metabolic connectivity in mouse models of β -amyloid and tauopathy

François Ruch^a, Johannes Gnörich^{a,b}, Karin Wind^{a,b}, Mara Köhler^a, Artem Zatcepin^{a,b}, Thomas Wiedemann^a, Franz-Joseph Gildehaus^a, Simon Lindner^a, Guido Boening^a, Barbara von Ungern-Sternberg^a, Leonie Beyer^a, Jochen Herms^{b,c,d}, Peter Bartenstein^{a,b}, Matthias Brendel^{a,b,c,*}, Florian Eckenweber^a

^a Department of Nuclear Medicine, University Hospital of Munich, LMU Munich, Munich, Germany

^b German Center for Neurodegenerative Diseases (DZNE), Munich, Germany

^c Munich Cluster for Systems Neurology (SyNergy), Munich, Germany

^d Center of Neuropathology and Prion Research, University of Munich, Munich, Germany

ARTICLE INFO

Keywords:
Alzheimer's disease
Metabolic connectivity
Amyloidosis
Tauopathy
Small animal PET
Morris water maze

ABSTRACT

Among functional imaging methods, metabolic connectivity (MC) is increasingly used for investigation of regional network changes to examine the pathophysiology of neurodegenerative diseases such as Alzheimer's disease (AD) or movement disorders. Hitherto, MC was mostly used in clinical studies, but only a few studies demonstrated the usefulness of MC in the rodent brain. The goal of the current work was to analyze and validate metabolic regional network alterations in three different mouse models of neurodegenerative diseases (β -amyloid and tau) by use of 2-deoxy-2-[¹⁸F]fluoro-D-glucose positron emission tomography (FDG-PET) imaging. We compared the results of FDG- μ PET MC with conventional VOI-based analysis and behavioral assessment in the Morris water maze (MWM). The impact of awake versus anesthesia conditions on MC read-outs was studied and the robustness of MC data deriving from different scanners was tested. MC proved to be an accurate and robust indicator of functional connectivity loss when sample sizes ≥ 12 were considered. MC readouts were robust across scanners and in awake/ anesthesia conditions. MC loss was observed throughout all brain regions in tauopathy mice, whereas β -amyloid indicated MC loss mainly in spatial learning areas and subcortical networks. This study established a methodological basis for the utilization of MC in different β -amyloid and tau mouse models. MC has the potential to serve as a read-out of pathological changes within neuronal networks in these models.

1. Introduction

In Alzheimer's disease (AD) the neurodegenerative process resulting in cognitive decline is characterized by structural and functional damage to the brain. Pathological alterations are characterized by regional atrophy in structural MRI (Barnes et al., 2009) and regional accumulation of pathological hallmarks such as extracellular β -amyloid and the intracellular deposition of hyperphosphorylated misfolded tau protein, which can be detected by PET imaging ligands. Several imaging modalities, including PET, can be used to visualize the neurodegenerative process in AD (Jack et al., 2016), such as hypometabolism in 2-deoxy-2-[¹⁸F]fluoro-D-glucose positron emission tomography (FDG-PET) (Smailagic et al., 2015) and reduced functional connectivity

in fMRI (Glover, 2011), as well as through a combination of those modalities (PET-MRI) (Judenhofer et al., 2008). FDG-PET allows to obtain not only single- or multi-region glucose uptake but also facilitates exploration of metabolic connectivity (MC) by consideration of the entire image pattern (Morbelli et al., 2012). Building on the clinical interpretation of FDG-PET imaging (Guedj et al., 2021), which is still considered one of the most informative biomarkers for dementia prediction in patients with mild cognitive impairment (MCI) (Morbelli et al., 2015), metabolic connectivity implies metabolic interactions of regional FDG uptake as a surrogate for cerebral energy consumption. Compared with classical FDG-PET data analysis, MC offers an additive value by capturing changes in relations between different brain regions and therefore allowing the investigation of functional metabolic

* Corresponding author at: Department of Nuclear Medicine, University Hospital of Munich, LMU Munich, Munich, Germany.

E-mail address: matthias.brendel@med.uni-muenchen.de (M. Brendel).

<https://doi.org/10.1016/j.neuroimage.2024.120513>

Received 14 April 2023; Received in revised form 25 August 2023; Accepted 5 January 2024

Available online 6 January 2024

1053-8119/© 2024 The Author(s). Published by Elsevier Inc. This is an open access article under the CC BY license (<http://creativecommons.org/licenses/by/4.0/>).

networks. For this reason, MC receives growing interest in AD research (Yakushev et al., 2017), and some studies applied the methodology also in preclinical settings (Zimmer et al., 2017; Grosch et al., 2021). However, the capability of MC to assess functional changes of inter- and intraregional network levels is still sparsely understood in mouse models of AD. Establishing MC in mouse models of neurodegenerative diseases could enable further exploration of model-specific neuronal network changes as well as serve as a valuable tool in the validation of biomarkers and therapeutics.

Therefore, this study aimed to interrogate the applicability of MC by analysis of interregion correlation coefficients (ICCs) in different β -amyloid and tau mouse models. Furthermore, we tested if MC has an additive value over a single region FDG- μ PET analysis. We tested the robustness of the methodology by comparing standardized uptake value (SUV) and SUV ratio (SUVR) approaches for the assessment of MC and we questioned the required sample sizes by simulation analysis. Reproducibility of MC read-outs was validated by data comparison between μ PET and μ PET/MRI scanners as well as between mice injected in awake and anesthesia conditions. Finally, we compared MC and classical FDG quantification against spatial learning to test which read-out better reflects behavioral changes in β -amyloid and tau mouse models.

2. Materials and methods

2.1. Study design

All experiments were performed in compliance with the National Guidelines for Animal Protection, Germany, and with the approval of the regional animal committee (Regierung Oberbayern) and were overseen by a veterinarian. All animal experiments complied with the ARRIVE guidelines and were carried out in accordance with the U.K. Animals (Scientific Procedures) Act, 1986 and associated guidelines, EU Directive 2010/63/EU for animal experiments. Animals were housed in a temperature- and humidity-controlled environment with 12 h light-dark cycle, with free access to food (Sniff, Soest, Germany) and water. FDG- μ PET data were collected from our in-house database for two different amyloid mouse models (PS2APP and APPPS1) and one tauopathy mouse model (P301S) with age- and sex-matched wild-type (WT) controls (Table 1). All data were acquired in a highly standardized setting at LMU Munich between 2015 and 2021. FDG- μ PET data were spatially co-registered to an FDG- μ PET template. SUV and SUVR data were extracted using a set of predefined volumes of interest (VOIs) (Fig. 1). For SUVR calculation, scaling to the mean brain uptake was applied. Pearson's R were calculated as the index of regional ICC for SUV and SUVR approaches using the principle of Seed-Correlation (Yakushev et al., 2017) as an indicator for the connection strength of each VOI pair. A correlation matrix with all ICCs was created for every model. Average ICCs were calculated for the composite of functional regions (e.g.: all intra-neocortical connections (CTX-CTX) are represented in the Average ICC (CTX-CTX), which corresponds to the mean of all ICCs of cortical VOIs). After scans have been performed, mice were subject to a standardized Morris water maze (MWM) for behavioral testing. For APPPS1 we used different batches of mice for the scans and for behavioral testing at the group level, which, however, originated

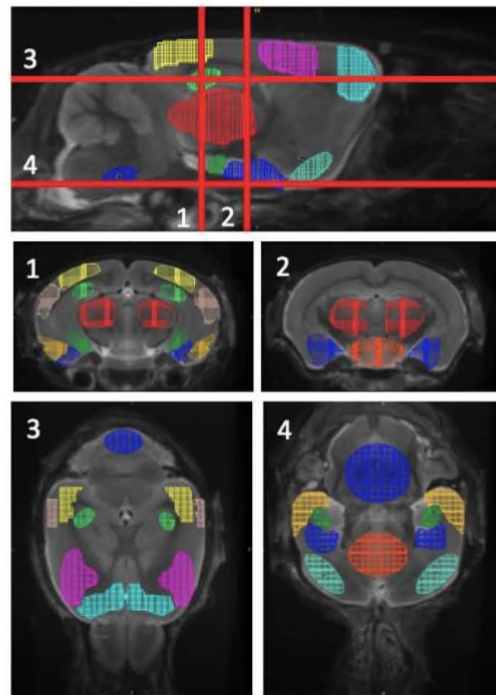


Fig. 1. Target regions used in the study projected on a mouse brain MRI atlas: bilateral cornu ammonis 1 (CA1) (light green) and 3 (CA3) (dark green), thalamus (red), amygdala (dark blue forebrain), entorhinal (light orange), piriform (turquoise), visual (yellow), auditory (pink), motor (light blue), somatosensory (purple) cortices as well as hypothalamus (orange), cerebellum (dark blue hindbrain) and brainstem (dark blue hindbrain).

from the same breeding line.

2.2. Animals

We analyzed FDG- μ PET scans of PS2APP, APPPS1, and P301S mice together with age- and sex-matched wild-type (WT) controls. To test for an impact of anesthesia on metabolic connectivity in the mouse brain, we performed a head-to-head comparison between FDG injection in the awake state and during isoflurane anesthesia (6-month-old female WT mice). Here, eleven mice received two FDG- μ PET scans with one week time gap. Awake and isoflurane conditions were switched between baseline and follow-up, starting with awake condition in 50 % of the sample.

PS2APP: The transgenic B6.PS2APP (line B6.152H) is homozygous for the human presenilin (PS) 2, N141I mutation, and the human amyloid precursor protein (APP) K670N, M671 L mutation (Weidensteiner et al., 2009). FDG- μ PET scans in PS2APP ($n = 24$) were performed at 8.6 ± 0.1 months of age, and WT ($n = 16$) mice used for comparison were imaged at 7.8 ± 1.8 months of age.

APPPS1: The transgenic mouse line APPPS1 with the double mutation in APP and PSEN1 genes (APP KM670/671NL (Swedish), PSEN1 L166P) (Radde et al., 2006) express APP in the brain, driven by Thy1.2 promoter. FDG- μ PET scans in APPPS1 ($n = 16$) and corresponding WT ($n = 25$) mice were conducted at 9.0 ± 3.0 months of age. FDG- μ PET/MR scans in different APPPS1 mice ($n = 12$) were conducted

Table 1
Overview of FDG- μ PET, μ PET/MR and behavioral testing (MWM) data.

Mouse Strain	Age (months)	PET (n)	PET/MR (n)	MWM (n)
WT (Awake)	6.0	11	–	–
WT (Isoflurane)	6.0	11	–	–
PS2APP	8.6 \pm 0.1	24	–	21
WT	7.8 \pm 1.8	16	–	14
APPPS1	9.0 \pm 3.0	16	12	8
WT	9.0 \pm 3.0	25	17	8
P301S	6.3 \pm 0.4	32	–	16
WT	6.0 \pm 0.2	32	–	14

at 8.0 ± 2.7 months of age as well as in corresponding WT mice ($n = 17$) at 10.2 ± 2.3 months of age.

P301S: Homozygous human tau P301S mice comprise a mouse line expressing the human ON4R tau isoform with the P301S mutation in exon 10 of the MAPT gene under the control of the murine thy1 promoter (Allen et al., 2002). FDG- μ PET scans in P301S mice ($n = 32$) were conducted at 6.3 ± 0.4 months of age and in corresponding WT ($n = 32$) mice at 6.0 ± 0.2 months of age. There was no significant difference in age between transgenic and corresponding WT mice at the time of scanning (Supplement Fig. 1)

2.3. Radiochemistry and μ PET recordings: data acquisition

[^{18}F]FDG was purchased commercially, and all μ PET imaging was conducted as reported previously (Brendel et al., 2017). A minimal fasting period of four hours was kept before the PET scan. Before injection of 10.1 ± 2.1 MBq [^{18}F]FDG (in 150 μ l saline), all mice were anesthetized with isoflurane (1.5 %, delivered at 3.5 L/min). Following tracer injection, animals were placed in the aperture of the Siemens Inveon DPET. Awake mice for the awake/anesthesia comparison, were placed directly in a restrainer, where tracer was rapidly injected (Supplemental Fig. 2). The uptake phase was up to 20 min in the awake state in a box. Anesthesia and placement in the μ PET scanner occurred between 20 and 30 min after tracer injection. FDG injection was defined as time $t = 0$. For anesthesia mice, isoflurane was induced at $t = -10$ min before injection and the tail vein catheter was applied $t = -5$ min before injection. Isoflurane was continuously administered until $t = +30$ min after FDG-injection.

Static [^{18}F]FDG-PET emission recordings were made in an interval of 30–60 min after tracer injection, followed by a 15 min transmission scan using a rotating [^{57}Co] point source for attenuation correction (Brendel et al., 2017). Image reconstruction was performed using 3-dimensional ordered-subset expectation-maximization (4 iterations, 12 subsets) with 3-dimensional maximum a posteriori (32 iterations) (OSEM3D/MAP), a zoom factor of 1.0, and a voxel size of $0.78 \times 0.78 \times 0.8$ mm 3 . Standard corrections for decay, scattered and random coincidences were performed.

A subset of APPPS1 mice from the same breeding line and at comparable age as well as matching WT mice were scanned with a 3T MedisoNanoScan μ PET/MR scanner (MedisoLtd, Hungary) with a single-mouse imaging chamber. A 15-minute anatomical T1 MR scan was performed 15 min after the [^{18}F]FDG injection (head receive coil, matrix size $96 \times 96 \times 22$, voxel size $0.24 \times 0.24 \times 0.8$ mm 3 , repetition time 677 ms, echo time 28.56 ms, flip angle 90°). μ PET acquisition was performed at 30–60 min post-injection. μ PET data were reconstructed using a 3D iterative algorithm (Tera-Tomo 3D, MedisoLtd, Hungary) with the following parameters: matrix size $55 \times 62 \times 187$ mm 3 , voxel size $0.3 \times 0.3 \times 0.3$ mm 3 , 8 iterations, 6 subsets. Decay, random, and attenuation correction were applied. The T1 image was used to create a body-air material map for the attenuation correction.

2.4. μ PET image analysis

Image registration was performed using PMOD Fusion tool (Version 3.5, PMOD Technologies, Basel, Switzerland) and consisted of two steps. First, individual FDG- μ PET images were manually registered to a standard mouse T1w-MRI template in Ma-Benveniste-Mirrione space (Ma et al., 2005). Second, to cope for inter-individual differences in brain size and atrophy, FDG- μ PET data were non-linearly registered to model-specific FDG- μ PET templates based on intracerebral reference regions (Overhoff et al., 2016) using the automatic SPM5 procedure implemented in PMOD (equal modality, nonlinear warping with 16 iterations, a frequency cutoff of 3, a regularization of 1.0, no thresholding). All templates were located in a harmonized space with matching brain size. In particular, transformations were saved for each individual co-registered image to obtain a connected transformation

matrix from the native to the template space for each mouse brain. The connected transformation matrix was applied to the native space μ PET data to guarantee minimal interpolation error.

As the μ PET templates had been initially aligned to a single high-resolution T1 MR template, all final fused μ PET images had the same spatial orientation and voxel dimensions, ($0.064 \times 0.064 \times 0.064$ mm 3) (Brendel et al., 2019). We conducted FDG- μ PET intensity normalization of images to standardized uptake value (SUV) by conventional SUV calculation and to the whole brain global mean (SUVR; Supplemental Fig. 3). A VOI set based on functional compartments and networks in the rodent brain (Fig. 1) was designed for the extraction of regional FDG- μ PET data. All VOIs were defined according to the Allen Mouse Brain Atlas and included: bilateral hippocampus CA1 (5 mm 3), hippocampus CA3 (7 mm 3), thalamus (26 mm 3), amygdala (12 mm 3), entorhinal cortex (10 mm 3), piriform cortex (9 mm 3), visual cortex (8 mm 3), auditory cortex (7 mm 3), motor cortex (20 mm 3) and somatosensory cortex (16 mm 3), as well as the hypothalamus (10 mm 3), cerebellum (12 mm 3) and brainstem (12 mm 3). The identical VOI set was used for all mouse models and corresponding WT.

2.5. Behavioral testing

PS2APP ($n = 21$), APPPS1 ($n = 8$), P301S ($n = 16$), and WT mice ($n = 22$) were investigated by an MWM test for spatial learning and motor deficits, which was performed according to a standard protocol (Sacher et al., 2019). On training days 1–5, each mouse had to perform four trials per day in the test basin, with the maximum time set to 70 s. The test trial was performed on day six. For analyses of escape latency and distance during MWM testing, we used the video tracking software EthoVision ® XT 13 (Noldus). The frequency and velocity of reaching the platform were then determined from the recordings.

2.6. Statistics and calculations

All Statistical analyses were performed in SPSS (Version 26, IBM Deutschland GmbH, Ehningen, Germany) and GraphPad Prism 9 (GraphPad Prism 9.3.1 (350) Serial number: GPS-2,314,993).

Interregion correlation coefficients: SUV and SUVR data were tested for normal distribution with Kolmogorov-Smirnov tests. For each VOI pair, we calculated a Pearson's R correlation coefficient as an index of ICC. The ICCs were then visualized as heat maps (i.e. Supplemental Fig. 4). For regional data analysis, VOI pairs were assigned to functional entities, defined as average ICCs. Sets of identical ICCs were compared between groups by two-tailed paired t -tests, corrected for multiple comparisons using the Holm-Sidak method. A threshold of $p < 0.05$ was considered significant for the rejection of the null hypothesis.

Root mean square error and effect sizes: A simulation analysis was conducted to analyze appropriate cohort size and data robustness. A random number generator was used to reduce the cohort sizes by one mouse at a time, and a new ICC matrix was calculated for each cohort. For each sample size of P301S and matching sample size of WT controls, root mean square error (RMSE) was calculated ($\text{RMSE} = \sqrt{(\sum(\text{ICC}_{\text{P301S}} - \text{ICC}_{\text{WT}})^2 / n_{\text{ICC}})}$). Subsequently, the sample size-dependent effect size was calculated for individual regions using Cohen's d .

Inter-Scanner comparison: For the scanner comparison, Pearson's correlation coefficients (R) were calculated from the SUVR data of μ PET and μ PET/MR, respectively. These were used as index for the ICC from each VOI pair. The ICCs were plotted in heat maps and correlated with each other. A linear regression analysis and a paired t -test between the ICCs of both scanners were performed to assess quantitative agreement. In a subanalysis, the correlation between the intra-neocortical connections, as the most representative region, was also performed.

3. Results

3.1. SUVR scaling is more sensitive for the detection of MC differences between P301S and WT mice when compared to SUV

We used a large cohort of P301S and corresponding WT mice to run a simulation analysis to determine the effect of the sample size on MC results.

Smaller RMSE as a function of increased sample size was obtained for ICCs from SUV analysis (mean RMSE between $n = 10$ – 20 : P301S = 0.02 ± 0.00 , WT = 0.03 ± 0.01) when compared to ICCs derived from SUVR analysis (mean RMSE between $n = 10$ – 20 : P301S = 0.16 ± 0.03 , WT = 0.13 ± 0.01). For both approaches, RMSE was below 0.25 for a cohort size ≥ 12 mice (Fig. 2A).

ICCs derived from SUVR analysis delivered robust effect sizes for the contrast of MC quantification between P301S and WT mice when ≥ 12 mice were considered. Effect sizes for the P301S versus WT comparison of ICCs derived from SUV analysis were inferior when compared to ICCs derived from SUVR analysis, regardless of the sample size (Cohen's d [CTX-CTX]: AVG[SUVR] = 0.40; AVG[SUV] = 0.06; $p < 0.0001$; Fig. 2B). Overall, this analysis indicated that SUVR serve as a more sensitive read-out for MC alterations in P301S mice vs. WT mice.

3.2. ^{18}F FDG SUVR and metabolic connectivity in awake and anesthetized mice are comparable

Previous studies have observed a reduction of cortical ^{18}F FDG uptake in anesthetized rats, compared to awake animals at the time of ^{18}F FDG injection (Shimoji et al., 2004). Such change in glucose uptake could lead to alterations of the metabolic pattern, which may lead to deviations in metabolic connectivity. For this purpose, we compared ^{18}F FDG- μ PET scans of WT mice after tracer injection in awake and anesthesia conditions.

Global mean normalized regional ^{18}F FDG uptake was similar between awake injected mice and mice injected under isoflurane anesthesia in most of the studied VOIs (Fig. 3A and B). A reduced ^{18}F FDG uptake was observed in the piriform cortex (SUVR[Awake] = 1.04 ± 0.07 ; SUVR[Isoflurane] = 0.86 ± 0.06 ; $p < 0.0001$) in the anesthetized mice. In contrast, the hypothalamus (SUVR[Awake] = 0.94 ± 0.1 ; SUVR[Isoflurane] = 1.09 ± 0.04 ; $p < 0.001$) and the amygdala (SUVR[Awake] = 0.73 ± 0.09 ; SUVR[Isoflurane] = 0.82 ± 0.05 ; $p < 0.01$) showed significantly increased ^{18}F FDG uptake in anesthesia condition (Fig. 3A). The correlation matrices show similar network patterns in awake and anesthesia conditions (Fig. 3C) and a strong overall correlation between the ICCs of the two matrices ($R = 0.77$; Fig. 3D). Direct

quantitative comparison of ICCs revealed no significant differences between both conditions (Supplemental Fig. 5)

3.3. Metabolic connectivity shows robust results for FDG-PET data derived from different scanners

For a reproducibility analysis, we performed the calculation of ICCs for APPPS1 β -amyloid and age-matched WT mice, with images acquired on two different μ PET scanners (Siemens Inveon DPET; Mediso μ PET/MRI) (Fig. 4). Based on SUVR data of both scanners, connectivity matrices showed a strong quantitative agreement when correlating all ICC for both APPPS1 mice and WT mice (R [APPPS1, all] = 0.61, $p < 0.0001$; R [WT, all] = 0.62, $p < 0.0001$) (Supplemental Fig. 6) as well as in a sub-analysis of only intra-neocortical connections (R [APPPS1, CTX-CTX] = 0.67, $p = 0.0001$; R [WT, CTX-CTX] = 0.53, $p = 0.0041$) (Fig. 4B). In the quantitative evaluation of intra-neocortical ICCs, no significant differences between μ PET and μ PET/MRI were evident for APPPS1 (ICC[CTX-CTX, μ PET] = 0.31 ± 0.32 ; ICC[CTX-CTX, μ PET/MR] = 0.29 ± 0.40 ; $p = 0.90$) or WT (ICC[CTX-CTX, μ PET] = 0.41 ± 0.24 ; ICC[CTX-CTX, μ PET/MR] = 0.42 ± 0.27 ; $p = 0.93$) (Fig. 4C).

3.4. ICCs indicate significant metabolic connectivity loss in β -amyloid and tau mouse models

PS2APP mice showed no significant difference compared to WT for intra-neocortical connections (ICC[CTX-CTX, PS2APP] = 0.57 ± 0.20 ; ICC[CTX-CTX, WT] = 0.54 ± 0.23 ; $p = 0.5$) (Fig. 5). Among regions of the spatial learning network, a loss of connections in PS2APP mice was found in the hippocampus (ICC[HIP, PS2APP] = 0.33 ± 0.21 ; ICC[HIP, WT] = 0.40 ± 0.19 ; $p = 0.001$) and the amygdala (ICC[AMY, PS2APP] = 0.35 ± 0.22 ; ICC[AMY, WT] = 0.53 ± 0.22 ; $p < 0.0001$). ICCs of brainstem connections did not indicate significant differences between this β -amyloid model and WT controls (ICC[BST, PS2APP] = 0.45 ± 0.23 ; ICC[BST, WT] = 0.42 ± 0.22 ; $p = 0.5$).

ICC Analysis in the APPPS1 model demonstrated no significant alterations in any network connections compared to WT controls besides from inter-cortical connections (ICC[SUBCTX-CTX, APPPS1] = 0.29 ± 0.19 ; ICC[SUBCTX-CTX, WT] = 0.36 ± 0.21 ; $p = 0.004$).

In P301S mice, ICCs for intra-neocortical connections showed a significantly lower connectivity compared to age and sex matched WT mice (ICC[CTX-CTX, P301S] = 0.43 ± 0.30 ; ICC[CTX-CTX, WT] = 0.54 ± 0.23 ; $p = 0.0012$). Among regions of the spatial learning network, there was a significant connectivity loss for hippocampal (ICC[HIP, P301S] = 0.31 ± 0.21 ; ICC[HIP, WT] = 0.40 ± 0.19 ; $p < 0.0001$) and amygdaloidal (ICC[AMY, P301S] = 0.46 ± 0.26 ; ICC[AMY, WT] = 0.57

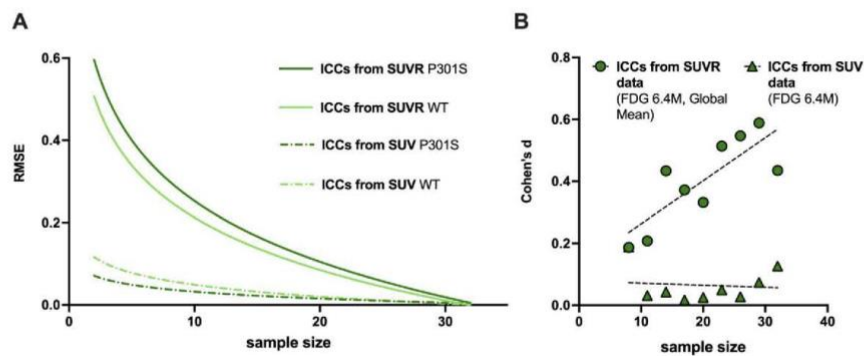


Fig. 2. A Root mean square error (RMSE) for ICCs derived from SUV and SUVR readouts according to sample size in P301S and WT controls. B Effect sizes (Cohen's d) in intra-neocortical connections (CTX-CTX) between P301S and WT controls for ICCs derived from SUV and SUVR readouts according to sample size.

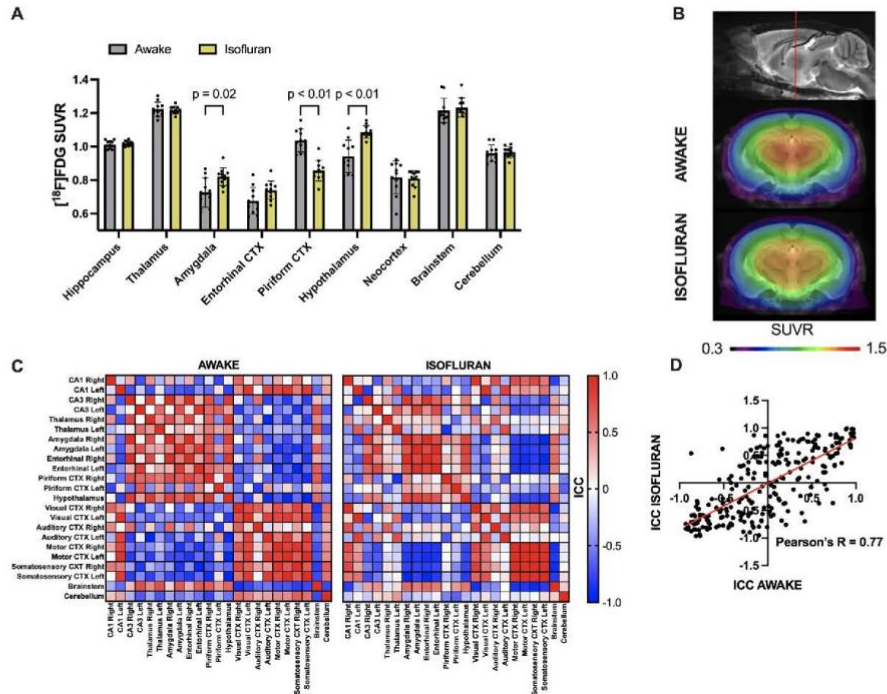


Fig. 3. A Global mean normalized [¹⁸F]FDG SUVR in the subgroups of awake and anesthetized wild-type mice; **p* < 0.05; ***p* < 0.01; ****p* < 0.001; *****p* < 0.0001. B Group average images for wild-type mice injected awake and during anesthesia with isoflurane (global mean normalized). C Correlation matrix showing ICCs for all 23 analyzed brain regions in mice injected awake and during anesthesia. D Correlation plot between ICCs for all 23 analyzed brain regions in mice injected awake and during anesthesia.

± 0.19; *p* = 0.018) connections. Contrary to the amyloid models, connections of the brainstem did reveal a severe attenuation in P301S mice (ICC[BST, P301S] = 0.25 ± 0.14; ICC[BST, WT] = 0.42 ± 0.22; *p* = 0.002).

3.5. FDG-PET metabolic connectivity indicates better agreement with behavioral testing when compared to regional FDG uptake

Given the observed robust reductions of FDG-μPET MC in AD models, we questioned whether MC alterations may better resemble behavioral testing in AD mouse models when compared to common SUVR quantification of regional FDG uptake (Fig. 6). Escape latency in MWM was used as a surrogate of cognitive performance and velocity in MWM was used as a surrogate of the motor function.

VOI-based analysis of FDG-uptake in the area of motor function showed significant hypermetabolism in the PS2APP and APPPS1 model compared to WT (SUVR[MOT-CTX, PS2APP] = 0.98 ± 0.05; SUVR[MOT-CTX, WT] = 0.87 ± 0.09; *p* < 0.0001 / SUVR[MOT-CTX, APPPS1] = 0.94 ± 0.06; SUVR[MOT-CTX, WT] = 0.89 ± 0.06; *p* < 0.0001). The tau model P301S revealed no significant difference in FDG-uptake of the motor cortex (SUVR[MOT-CTX, P301S] = 0.83 ± 0.09; SUVR[MOT-CTX, WT] = 0.84 ± 0.10; *p* = 0.5).

In contrast, MC analysis of connections between motor and remaining cortical VOIs revealed a significant loss of motor connections in P301S (ICCs[MOT-CTX, P301S] = 0.29 ± 0.23; ICCs[MOT-CTX, WT] = 0.45 ± 0.17; *p* = 0.04). However, no significant motor network alterations were observed in both mouse models of amyloidosis (ICCs

[MOT-CTX, PS2APP] = 0.51 ± 0.2; ICCs[MOT-CTX, WT] = 0.55 ± 0.25; *p* = 0.61 / ICCs[MOT-CTX, APPPS1] = 0.22 ± 0.16; ICCs[MOT-CTX, WT] = 0.34 ± 0.2; *p* = 0.1). An overview in differences in correlation matrices of all transgenic mouse models is provided in **Supplemental Fig. 7**. MC-based analysis was consistent with behavioral testing, where no significant velocity reduction was detected in PS2APP and APPPS1 mice (Velocity[AVG, PS2APP] = 20 cm/s ± 2 cm/s; Velocity[AVG, WT] = 21 cm/s ± 2 cm/s; *p* = 0.35 / Velocity[AVG, APPPS1] = 19 cm/s ± 4 cm/s; Velocity[AVG, WT] = 19 cm/s ± 1 cm/s; *p* = 0.63). A significant loss of motor function was measured in P301S mice (Velocity[AVG, P301S] = 15 cm/s ± 4 cm/s; Velocity[AVG, WT] = 21 cm/s ± 2 cm/s; *p* < 0.0001).

In brain regions associated with spatial learning, conventional VOI-based analysis of FDG-uptake showed no significant alterations in glucose metabolism in PS2APP and P301S mice (SUVR[HIP, PS2APP] = 1.00 ± 0.05; SUVR[HIP, WT] = 1.01 ± 0.07; *p* = 0.16 / SUVR[HIP, P301S] = 1.00 ± 0.05; SUVR[HIP, WT] = 1.01 ± 0.06; *p* = 0.15), but significant hypermetabolism in the β-amyloid model APPPS1 (SUVR[HIP, APPPS1] = 1.00 ± 0.07; SUVR[HIP, WT] = 0.98 ± 0.04; *p* = 0.03).

MC analysis based on ICCs of intra-subcortical connections detected significant connectivity loss in the PS2APP model (ICC[SUBCTX-SUBCTX, PS2APP] = 0.32 ± 0.25; ICC[SUBCTX-SUBCTX, WT] = 0.41 ± 0.25, *p* = 0.013) as well as in the P301S model (ICC[SUBCTX-SUBCTX, P301S] = 0.33 ± 0.23; ICC[SUBCTX-SUBCTX, WT] = 0.41 ± 0.23; *p* = 0.005; **Supplemental Fig. 7**). Thus, in the PS2APP and P301S models MC was in line with findings in behavioral testing, suggesting a loss of

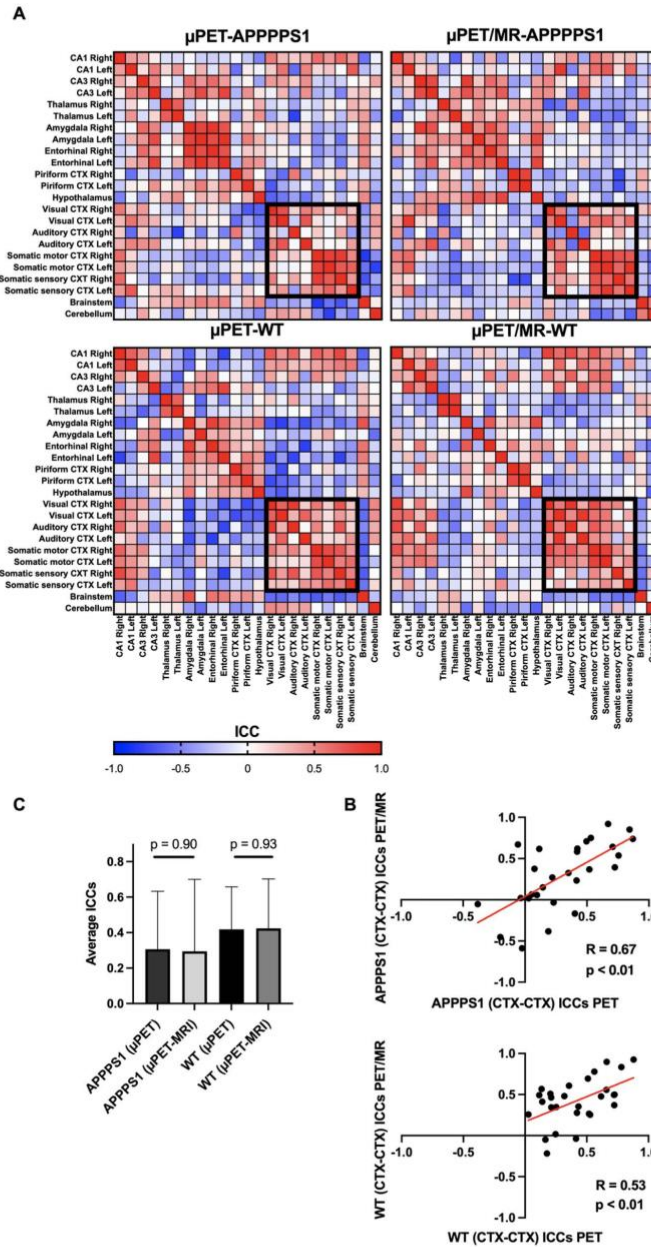


Fig. 4. Metabolic connectivity reproducibility analysis between dedicated μ PET and μ PET/MR scanners for APPPS1 and wild-type (WT) controls. **A** Correlation matrix of ICCs for all 23 VOIs and intra-neocortical connection (CTX-CTX) highlighted by the black frame. **B** Correlation of intra-neocortical ICCs (CTX-CTX) between μ PET with μ PET/MR, in APPPS1 and WT respectively. **C** Comparison of intra-neocortical ICCs between both scanners for APPPS1 and WT mice.

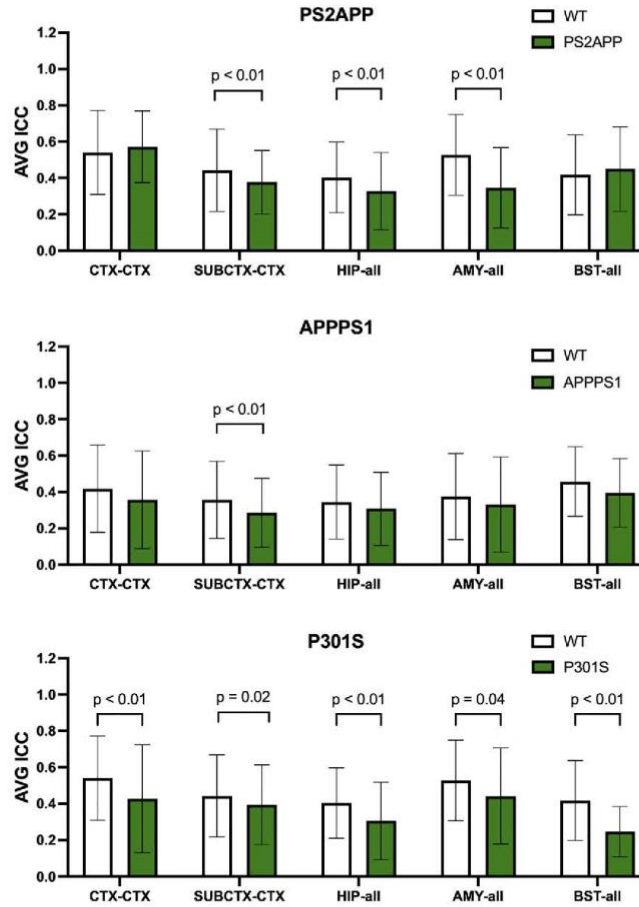


Fig. 5. Comparison of average ICC (AVG ICC) from μ PET SUVR data in different transgenic (TG) mouse models versus corresponding wild-type (WT) controls in intra-neocortical (CTX-CTX), inter-cortical (SUBCTX-CTX), hippocampal (HIP-all), amygdaloidal (AMY-all) and brainstem (BST-all) connections; Multiple paired t tests corrected for multiple comparisons using the Holm-Šidák method (only comparisons with $p < 0.05$ are displayed).

spatial learning in MWM (Latency[AVG, PS2APP] = $22 s \pm 12 s$; Latency [AVG, WT] = $12 s \pm 10 s$; $p = 0.01$ / Latency[AVG, P301S] = $37 s \pm 20 s$; Latency[AVG, WT] = $12 s \pm 10 s$; $p < 0.001$). In the APPPS1 model no significant alterations of MC were observed (ICC[SUBCTX-SUBCTX, APPPS1] = 0.31 ± 0.25 ; ICC[SUBCTX-SUBCTX, WT] = 0.33 ± 0.21 , $p = 0.56$), while significant loss of spatial memory (Latency[AVG, APPPS1] = $42 s \pm 21 s$; Latency[AVG, WT] = $22 s \pm 12 s$; $p = 0.046$) could be monitored.

4. Discussion

In this study, we performed a systematical analysis of MC in transgenic mouse models of neurodegenerative diseases using $[^{18}F]$ FDG- μ PET. In Alzheimer's research, functional neuroimaging methods are of growing interest, as they allow the investigation of interacting brain regions and thus interregional network alterations. Among them, FDG-PET-based metabolic connectivity is increasingly used (Yakushev et al., 2017). Besides monitoring pathology-specific neuronal network

alterations and thus a more targeted evaluation of diagnostic and predictive value, utilization of MC in research of neurodegeneration also may enable assessment of functional changes in the brain during therapeutic intervention.

The informative value of MC has been proven in different clinical research studies, e.g. in a study demonstrating that the loss of connections, particularly to the posterior cingulate cortex (PCC), a region where hypometabolism is commonly associated with AD, precedes synaptic degeneration (Morbelli et al., 2012) and therefore proving a predictive value of MC on synaptic network alterations. Further hypometabolism in the PCC, as well as a decrease in metabolic correlation between PCC and the hippocampus, proved to be common to all AD subtypes, suggesting a functional decline in this connection as a core characteristic of AD (Herholz et al., 2018). Additionally, MC enables the analysis of specific neuronal networks, such as the dopaminergic mesocorticolimbic pathway on the issues of depression-typical network alterations in AD (Iaccarino et al., 2020).

Compared to clinical studies of humans, the usage of β -amyloid and

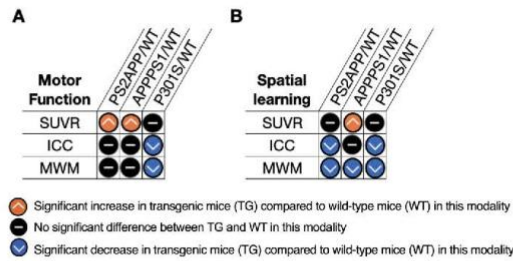


Fig. 6. Summary of significant differences ($p > 0.05$) between different transgene (TG) mouse models and matching wild-type (WT) for [18 F]FDG-PET SUVR analysis, metabolic connectivity (MC) analysis and behavioral analysis (MWM). A Motor functions (SUVR uptake in motor cortex VOIs; MC average ICC in motor cortex connections, MWM velocity). B Spatial learning (SUVR uptake in hippocampal VOIs; MC average ICC in intra-subcortical connections, MWM escape latency).

tau mouse models allows for a more focused and individual analysis of pathological hallmarks of AD. However, MC has not widely been used for the investigation of neurodegeneration in transgenic mouse models of neurodegenerative diseases yet. MC has been established for the investigation of vestibular compensation in the rat brain after unilateral labyrinthectomy (Grosch et al., 2021), and in another rodent model, MC has been used to illustrate the neuroenergetic contribution of astrocytes in FDG- μ PET of rat brains (Zimmer et al., 2017). In this study, we performed a systematical analysis of MC in β -amyloid and tau mouse models and thereby demonstrated the strengths and limitations of MC.

Most importantly, for all three investigated mouse models, the alterations in MC matched the phenotype in behavioral testing. The P301S tau model showed a robust MC decrease in networks associated with motor function as well as a significant loss in MC in spatial learning networks, which were in line with deficits in motor function and spatial learning. Contrary, a common SUVR-based FDG- μ PET analysis was not sensitive enough to detect significant alterations of glucose uptake in these brain regions at the investigated age of 6.4 months in the cohort. In our previous study in tau P301S mice, we observed that early microglial inflammation was correlated with reduced cortical and hippocampal glucose uptake at the late stage (Eckenweber et al., 2020), regionally matching the seed regions of MC deficits. Tau-related impairments of glucose uptake and MC are also in line with a human AD study suggesting that elevated early tau is connected to decreased metabolism and reduced synaptic activity (Adams et al., 2019). In humans, tau spread through brain networks overlaps with a large range of functional networks. In contrast, the human β -amyloid network is characterized by a spatial pattern that shares large overlap with the default mode network (Sala et al., 2023). Correspondingly, our analysis of the tau mouse model showed a participation of all functional network units, reflected by the decrease in ICC whereas in β -amyloidosis models a decrease of cortical-subcortical connections can be found.

Interestingly, in both β -amyloidosis models PS2APP and APPPS1 where glial activation is linked to elevated relative glucose metabolism (Brendel et al., 2016; Xiang et al., 2021), MC showed likewise more coherent results with the MWM phenotype than VOI-based analyses. Conventional VOI-based analysis proved not sensitive or even showed contradictory results on network impairments for these models. According to our previous findings, we attribute this to increased microglial inflammation and thus increased glucose consumption in the β -amyloidosis mouse models, which must be considered in FDG-PET studies (Eckenweber et al., 2020). In APPPS1, amyloid-plaques appear in the cortex at 6 weeks of age and in the hippocampus at 3–4 months of age (Radde et al., 2006), much earlier than in PS2APP animals in which plaques are found at 6 months of age and a high plaque load is found in

the hippocampus at 10 months of age (Weidensteiner et al., 2009; Ozmen et al., 2009). In PS2APP microglial activation is age-dependent and correlates positively with the amyloid load (Brendel et al., 2016). Also in APPPS1, studies indicate, that microglial activation increases with aging and aggregates particularly within and around $A\beta_{42}$ -positive plaques in the brain (Cao et al., 2021). Differences in the spatial arrangement and in the severity of microglial inflammation can be assumed between the two models, which also lead to differences in glucose metabolism.

In PS2APP mice, MC proved to be superior to a conventional analysis by showing clear network impairments in spatial learning regions, which cannot be monitored by a conventional VOI-based analysis. Moreover, in this model, MC served as a sensitive predictor for change in behavioral outcomes in MWM. In APPPS1 mice FDG- μ PET data indicated a significant increase in hippocampal regions in the conventional VOI-based analysis, being completely contradictory to the significant loss of spatial learning functions we detected in the MWM at approximately 15 months of age, also confirmed by other behavioral studies (Webster et al., 2014). In contrast, using MC a minor decrease in hippocampal networks could be found. Although not significant this was still in better accordance with the findings of the behavioral testing, suggesting MC is less prone to microglial-inflammation-related change in FDG uptake. Furthermore, MC proved to be a more suitable predictor for motor functions and corresponding velocity in APPPS1 mice.

Regarding methodological aspects of the study, we considered SUVR scaling to be superior to an SUV scaling approach for the assessment of MC. Primarily measuring global heterogeneity an SUV-based scaling tends to be the less sensitive read-out of both. Large differences in regional cerebral uptake in individual mice lead to low basal correlations between different brain regions and thus consistently small effect sizes all derived from the utilization of SUV scaled data. Using a simulation analysis with a random number generator to evaluate the required sample size for the calculation of MC showed that SUVR scaling is the more stable and suitable readout. Effect sizes of SUVR scaled MC in intra-neocortical connections increased with each additional mouse and a sample size of approximately 12 mice was necessary to obtain significant effect sizes with a Cohen's d over 0.2 at a well acceptable RMSE < 0.2 . By performing a comparison of two different μ PET scanners we could demonstrate scanner independent reproducibility of our data. Connectivity matrices showed similar patterns for both scanners, indicating data source independent applicability of MC for analysis of FDG- μ PET scans.

In previous studies a difference in [18 F]FDG uptake and regional distribution pattern between awake and isoflurane-anaesthetized rats was observed (Shinoji et al., 2004). In fact, differences in arterial blood flow and consecutive tracer distribution as well as cerebral glucose utilization can be argued. However, a specific study on [18 F]FDG uptake in mice, showed similar values of whole brain [18 F]FDG uptake in awake mice compared to isoflurane-anesthetized mice, supporting the routine use of isoflurane anesthesia in preclinical imaging studies (Bascunana et al., 2019). Likewise, we observed only minor impact of FDG injection during isoflurane anesthesia compared to awake injection in a head-to-head comparison. Regarding MC analyses, highly similar network connectivity between both conditions was observed. Therefore, we consider MC analyses of FDG-PET data in mice that was acquired after injection during isoflurane anesthesia to be valid and transferable to the awake state, which also supports the 3R principle of animal welfare.

Limitations that arose with the study of APPPS1 mice in the scanner comparison between μ PET and μ PET/MR, included a sample size disparity, due to different individual animals used in the scanner comparison, minor age differences between the groups (average 0.6 months for APPPS1 and 0.9 months for WT) as well as day-dependent difference in the test conditions which aggravated comparability as well as statistical accuracy. Additionally, the differences in the average images (Supplemental Fig. 3), ICCs (Fig. 4A and B), and R-values

(Supplemental Fig. 6) between the two scanners can be possibly explained by such inter-scanner differences as the reconstruction methods (μ PET: OSEM3D/MAP; μ PET/MR: Tera-Tomo), the images used for the attenuation correction (μ PET: transmission scan; μ PET/MR: MR scan), the spatial resolution (μ PET: 1.5–3.0 mm FWHM in the radial direction and 1.5–1.8 mm FWHM in the tangential direction; μ PET/MR: 1.50–2.01 mm FWHM and 1.32–1.65 mm, respectively; both reported for a point source and 2D filtered backprojection reconstruction), and the peak sensitivity (μ PET: 11.1 %; μ PET/MR: 8.4 %) (Visser et al., 2009; Nagy et al., 2013). Additional cross-scanner harmonization can be performed in the future to reduce the impact of these differences. However, in summary, we already observed a satisfactory agreement of MC read-outs derived from FDG-PET imaging of both machines, which likely represents a real-life scenario for pooling or comparing multi-center data.

Another limitation was the optimal VOI size for the calculation of MC in the mouse models used in the study. We did not apply VOIs for potential functional relevant subregions of several brain structures (i.e. thalamic nuclei) since the limited spatial resolution in μ PET leads to an increase in statistical error with a smaller VOI size (Visser et al., 2009). Also, a potential proportionally larger spill in of bone uptake and stronger partial volume effects as well as increased cross-contamination of surrounding tissue due to atrophy might be a negative aspect of the usage of smaller cortical VOIs. Therefore, subsequent studies are desirable to determine the optimal VOI size for MC in mouse models. One more concern regarding MC in AD mouse models is the fact that MC is calculated at group level and therefore no conclusions can be drawn about individual mice. However in mouse models most important observations such as therapy effects of drugs are commonly made at group level. As preclinical usage of MC is sparse and to date no AD mouse studies have focused on monitoring of therapeutic effects using MC further research should be carried out in this promising field. Even though promising results were reported in this work, additional studies are needed to ensure the reproducibility of the applied methodology.

5. Conclusion

Our study proves that MC serves as a valid tool for the investigation of specific neuronal network changes in transgenic β -amyloid and tau mouse models. Compared with a conventional VOI-based μ PET analysis MC shows higher agreement with results of behavioral testing in MWM as well as better detection of change of interregional glucose metabolism in different β -amyloid and tau mouse models. Functional connectivity studies in specific mouse models of neurodegenerative diseases could contribute to further insight into the link between pathology and brain function. Further MC may contribute to the validation of biomarkers and evaluation of disease-modifying therapeutics in AD.

Ethics statement

All animal experiments complied with the ARRIVE guidelines and were carried out in accordance with the U.K. Animals (Scientific Procedures) Act, 1986 and associated guidelines, EU Directive 2010/63/EU for animal experiments.

Disclosure

No potential conflicts of interest are reported for this study.

CRedit authorship contribution statement

François Ruch: Formal analysis, Writing – original draft, Investigation, Validation, Visualization, Methodology. **Johannes Gnörich:** Formal analysis, Investigation, Writing – review & editing. **Karin Wind:** Formal analysis, Investigation, Writing – review & editing. **Mara Köhler:** Formal analysis, Investigation, Writing – review & editing.

Artem Zatcepin: Investigation, Writing – review & editing. **Thomas Wiedemann:** Investigation, Writing – review & editing. **Franz-Joseph Gildehaus:** Investigation, Resources, Writing – review & editing. **Simon Lindner:** Investigation, Writing – review & editing. **Guido Boening:** Investigation, Resources, Writing – review & editing. **Barbara von Ungern-Sternberg:** Investigation, Writing – review & editing. **Leonie Beyer:** Conceptualization, Resources, Writing – review & editing. **Jochen Herms:** Conceptualization, Resources, Writing – review & editing. **Peter Bartenstein:** Conceptualization, Resources, Writing – review & editing. **Matthias Brendel:** Conceptualization, Formal analysis, Supervision, Writing – original draft, Funding acquisition, Writing – review & editing, Project administration. **Florian Eckenweber:** Conceptualization, Formal analysis, Supervision, Writing – original draft, Writing – review & editing, Project administration.

Declaration of competing interest

LB is an employee of Novartis. MB received speaker honoraria from GE healthcare, Roche and Life Molecular Imaging and is an advisor of Life Molecular Imaging. All other authors do not report a conflict of interest.

Data availability

Imaging data are available in nifti format and can be transferred per request by the corresponding author. Behavioral data and statistical analysis are available in table format on Mendeley Data. Statistics and Graphs are available per request as GraphPad Prism Data.

Acknowledgments

Synergy: M.B. was funded by the Deutsche Forschungsgemeinschaft (DFG) under Germany's Excellence Strategy within the framework of the Munich Cluster for Systems Neurology (EXC 2145 SyNergy – ID 390857198).

Supplementary materials

Supplementary material associated with this article can be found, in the online version, at [doi:10.1016/j.neuroimage.2024.120513](https://doi.org/10.1016/j.neuroimage.2024.120513).

References

- Adams, J.H., Lockhart, S.N., Li, L., Jagust, W.J., 2019. Relationships between tau and glucose metabolism reflect Alzheimer's disease pathology in cognitively normal older adults. *Cereb. Cortex* 29 (5), 1997–2009.
- Allen, B., Ingram, E., Takao, M., Smith, M.J., Jakes, R., Virdee, K., et al., 2002. Abundant tau filaments and nonapoptotic neurodegeneration in transgenic mice expressing human P301S tau protein. *J. Neurosci.* 22 (21), 9340–9351.
- Barnes, J., Bartlett, J.W., van de Pol, L.A., Loy, C.T., Scabill, R.L., Frost, C., et al., 2009. A meta-analysis of hippocampal atrophy rates in Alzheimer's disease. *Neurobiol. Aging* 30 (11), 1711–1723.
- Bascurana, P., Thackeray, J.T., Bankstahl, M., Bengel, F.M., Bankstahl, J.P., 2019. Anesthesia and preconditioning induced changes in mouse brain [¹⁸F] FDG uptake and kinetics. *Mol. Imaging Biol.* 21 (6), 1089–1096.
- Brendel, M., Probst, F., Jaworska, A., Overhoff, F., Korzhova, V., Albert, N.L., et al., 2016. Glial activation and glucose metabolism in a transgenic amyloid mouse model: a triple-tracer PET study. *J. Nucl. Med.* 57 (6), 954–960.
- Brendel, M., Focke, C., Blume, T., Peters, F., Deussing, M., Probst, F., et al., 2017. Time courses of cortical glucose metabolism and microglial activity across the life span of wild-type mice: a PET study. *J. Nucl. Med.* 58 (12), 1984–1990.
- Brendel, M., Deussing, M., Blume, T., Kaiser, L., Probst, F., Overhoff, F., et al., 2019. Late-stage Anle138b treatment ameliorates tau pathology and metabolic decline in a mouse model of human Alzheimer's disease tau. *Alzheimers Res. Ther.* 11 (1), 67.
- Cao, S., Fisher, D.W., Rodriguez, G., Yu, T., Dong, H., 2021. Comparisons of neuroinflammation, microglial activation, and degeneration of the locus coeruleus-norepinephrine system in APP/PS1 and aging mice. *J. Neuroinflamm.* 18 (1), 10.
- Eckenweber, F., Medina-Luque, J., Blume, T., Sacher, C., Biechel, G., Wind, K., et al., 2020. Longitudinal TSPO expression in tau transgenic P301S mice predicts increased tau accumulation and deteriorated spatial learning. *J. Neuroinflamm.* 17 (1), 208.


- Glover, G.H., 2011. Overview of functional magnetic resonance imaging. *Neurosurg. Clin. N. Am.* 22 (2), 133–139 vii.
- Grosch, M., Lindner, M., Barntstein, P., Brandt, T., Dieterich, M., Ziegler, S., et al., 2021. Dynamic whole-brain metabolic connectivity during vestibular compensation in the rat. *NeuroImage* 226, 117568.
- Guedj, E., Varrone, A., Bodlaard, R., Albert, M.L., Barthel, H., van Berckel, B., et al., 2021. EANM procedure guidelines for brain PET imaging using [(18)F]FDG, version 3. *Eur. J. Nucl. Med. Mol. Imaging*.
- Herholz, K., Haense, C., Gerhard, A., Jones, M., Anton-Rodriguez, J., Segobin, S., et al., 2018. Metabolic regional and network changes in Alzheimer's disease subtypes. *J. Cereb. Blood Flow Metab.* 38 (10), 1796–1806.
- Iaccarino, L., Sala, A., Caminiti, S.P., Presotto, L., Perani, D., 2020. Alzheimer's disease neuroimaging I. *In vivo* MRI structural and PET metabolic connectivity study of dopamine pathways in Alzheimer's disease. *J. Alzheimers Dis.* 75 (3), 1003–1016.
- Jack, C.R., Bennett, D.A., Blennow, K., Carrillo, M.C., Feldman, H.H., Frisoni, G.B., et al., 2016. A/T/N: an unbiased descriptive classification scheme for Alzheimer disease biomarkers. *Neurology* 87 (5), 539–547.
- Judenhofer, M.S., Wehl, H.F., Newport, D.F., Catania, C., Siegel, S.B., Becker, M., et al., 2008. Simultaneous PET-MRI: a new approach for functional and morphological imaging. *Nat. Med.* 14 (4), 459–465.
- Ma, Y., Hof, P.R., Grant, S.C., Blackband, S.J., Bennett, R., Slate, L., et al., 2005. A three-dimensional digital atlas database of the adult C57BL/6J mouse brain by magnetic resonance microscopy. *Neuroscience* 135 (4), 1203–1215.
- Morbili, S., Drzezga, A., Perneczky, R., Frisoni, G.B., Caroli, A., van Berckel, B.N., et al., 2012. Resting metabolic connectivity in prodromal Alzheimer's disease. A European Alzheimer disease consortium (EADC) project. *Neurobiol. Aging* 33 (11), 2533–2550.
- Morbili, S., Garibotto, V., Van De Giessen, E., Arbizu, J., Chetelat, G., Drzezga, A., et al., 2015. A cochrane review on brain [(1)(8)F]FDG PET in dementia: limitations and future perspectives. *Eur. J. Nucl. Med. Mol. Imaging* 42 (10), 1487–1491.
- Nagy, K., Toth, M., Major, P., Patay, G., Egri, G., Haggkvist, J., et al., 2013. Performance evaluation of the small-animal nanoScan PET/MRI system. *J. Nucl. Med.* 54 (10), 1825–1832.
- Overhoff, F., Brendel, M., Jaworska, A., Kozhova, V., Delker, A., Probst, F., et al., 2016. Automated spatial brain normalization and hindbrain white matter reference tissue give improved [(18)F]-florbetaben PET quantitation in Alzheimer's model mice. *Front. Neurosci.* 10, 45.
- Ozmen, I., Albentz, A., Czech, C., Jacobsen, H., 2009. Expression of transgenic APP mRNA is the key determinant for beta-amyloid deposition in PS2APP transgenic mice. *Neurodegener. Dis.* 6 (1–2), 29–36.
- Radde, R., Bolmont, T., Kaeser, S.A., Coomaraswamy, J., Lindau, D., Stoltze, L., et al., 2006. Abeta42-driven cerebral amyloidosis in transgenic mice reveals early and robust pathology. *EMBO Rep.* 7 (9), 940–946.
- Sacher, C., Blume, T., Beyer, L., Peters, F., Eckenweber, F., Sgobio, C., et al., 2019. Longitudinal PET monitoring of amyloidosis and microglial activation in a second-generation amyloid-beta mouse model. *J. Nucl. Med.* 60 (12), 1787–1793.
- Sala, A., Izarraga, A., Caminiti, S.P., Calhoun, V.D., Eickhoff, S.B., Habeck, C., et al., 2023. Brain connectomics: time for a molecular imaging perspective? *Trends Cogn. Sci.* 27 (4), 353–366.
- Shimoji, K., Ravasi, L., Schmidt, K., Soto-Montenegro, M.L., Esaki, T., Seidel, J., et al., 2004. Measurement of cerebral glucose metabolic rates in the anesthetized rat by dynamic scanning with 18F-FDG, the ATLAS small animal PET scanner, and arterial blood sampling. *J. Nucl. Med.* 45 (4), 665–672.
- Smailagic, N., Vacante, M., Hyde, C., Martin, S., Ukoumunne, O., Sachpekidis, C., 2015. [(1)(8)F]FDG PET for the early diagnosis of Alzheimer's disease dementia and other dementias in people with mild cognitive impairment (MCI). *Cochrane Database Syst. Rev.* 1, CD010632.
- Visser, E.P., Disselhorst, J.A., Bron, M., Laverman, P., Gotthardt, M., Oyen, W.J., et al., 2009. Spatial resolution and sensitivity of the Inveon small-animal PET scanner. *J. Nucl. Med.* 50 (1), 139–147.
- Webster, S.J., Bachstetter, A.D., Nelson, P.T., Schmitt, F.A., Van Eldik, L.J., 2014. Using mice to model Alzheimer's dementia: an overview of the clinical disease and the preclinical behavioral changes in 10 mouse models. *Front. Genet.* 5, 88.
- Weidensteiner, C., Metzger, F., Bruns, A., Bohrmann, B., Kuenneke, B., von Kienlin, M., 2009. Cortical hypoperfusion in the B6.PS2APP mouse model for Alzheimer's disease: comprehensive phenotyping of vascular and tissular parameters by MRI. *Magn. Reson. Med.* 62 (1), 35–45.
- Xiang, X., Wind, K., Wiedemann, T., Blume, T., Shi, Y., Briel, N., et al., 2021. Microglial activation states drive glucose uptake and FDG-PET alterations in neurodegenerative diseases. *Sci. Transl. Med.* 13 (615), eabe5640.
- Yakushev, I., Drzezga, A., Habeck, C., 2017. Metabolic connectivity: methods and applications. *Curr. Opin. Neurol.* 30 (6), 677–685.
- Zimmer, E.R., Parent, M.J., Souza, D.G., Leuzy, A., Lecrux, C., Kim, H.I., et al., 2017. [(18)F]FDG PET signal is driven by astroglial glutamate transport. *Nat. Neurosci.* 20 (3), 393–395.

RESEARCH

Open Access

Glial activation is moderated by sex in response to amyloidosis but not to tau pathology in mouse models of neurodegenerative diseases



Gloria Biechele¹, Nicolai Franzmeier², Tanja Blume^{1,3}, Michael Ewers^{2,3}, Jose Medina Luque³, Florian Eckenweber¹, Christian Sacher¹, Leonie Beyer¹, Francois Ruch-Rubinstein¹, Simon Lindner¹, Franz-Josef Gildehaus¹, Barbara von Ungern-Sternberg¹, Paul Cumming^{4,5}, Peter Bartenstein^{1,7}, Axel Rominger^{1,4}, Günter U. Höglinger^{2,8,9}, Jochen Herms^{2,7,6} and Matthias Brendel^{1,7*} 

Abstract

Background: In vivo assessment of neuroinflammation by 18-kDa translocator protein positron-emission-tomography (TSPO-PET) ligands receives growing interest in preclinical and clinical research of neurodegenerative disorders. Higher TSPO-PET binding as a surrogate for microglial activation in females has been reported for cognitively normal humans, but such effects have not yet been evaluated in rodent models of neurodegeneration and their controls. Thus, we aimed to investigate the impact of sex on microglial activation in amyloid and tau mouse models and wild-type controls.

Methods: TSPO-PET (¹⁸F-GE-180) data of C57Bl/6 (wild-type), *App*^{NL^GF} (β-amyloid model), and P301S (tau model) mice was assessed longitudinally between 2 and 12 months of age. The *App*^{NL^GF} group also underwent longitudinal β-amyloid-PET imaging (Aβ-PET; ¹⁸F-florbetaben). PET results were confirmed and validated by immunohistochemical investigation of microglial (Iba-1, CD68), astrocytic (GFAP), and tau (AT8) markers. Findings in cerebral cortex were compared by sex using linear mixed models for PET data and analysis of variance for immunohistochemistry.

Results: Wild-type mice showed an increased TSPO-PET signal over time (female +23%, male +4%), with a significant sex × age interaction ($T = -4.171, p < 0.001$). The Aβ model *App*^{NL^GF} mice also showed a significant sex × age interaction ($T = -2.953, p = 0.0048$), where cortical TSPO-PET values increased by 31% in female *App*^{NL^GF} mice, versus only 6% in the male mice group from 2.5 to 10 months of age. Immunohistochemistry for the microglial markers Iba-1 and CD68 confirmed the TSPO-PET findings in male and female mice aged 10 months. Aβ-PET in the same *App*^{NL^GF} mice indicated no significant sex × age interaction ($T = 0.425, p = 0.673$). The P301S tau model showed strong cortical increases of TSPO-PET from 2 to 8.5 months of age (female + 32%, male + 36%), without any significant sex × age interaction ($T = -0.671, p = 0.504$), and no sex differences in Iba-1, CD68, or AT8 immunohistochemistry.

(Continued on next page)

* Correspondence: matthias.brendel@med.uni-muenchen.de

¹Department of Nuclear Medicine, University Hospital of Munich, LMU Munich, Marchioninstraße 15, 81377 Munich, Germany

²Department of Neurology, Hannover Medical School, Hannover, Germany

Full list of author information is available at the end of the article



© The Author(s). 2020 **Open Access** This article is licensed under a Creative Commons Attribution 4.0 International License, which permits use, sharing, adaptation, distribution and reproduction in any medium or format, as long as you give appropriate credit to the original author(s) and the source, provide a link to the Creative Commons licence, and indicate if changes were made. The images or other third party material in this article are included in the article's Creative Commons licence, unless indicated otherwise in a credit line to the material. If material is not included in the article's Creative Commons licence and your intended use is not permitted by statutory regulation or exceeds the permitted use, you will need to obtain permission directly from the copyright holder. To view a copy of this licence, visit <http://creativecommons.org/licenses/by/4.0/>. The Creative Commons Public Domain Dedication waiver (<http://creativecommons.org/publicdomain/zero/1.0/>) applies to the data made available in this article, unless otherwise stated in a credit line to the data.

(Continued from previous page)

Conclusion: Female mice indicate sex-dependent microglia activation in aging and in response to amyloidosis but not in response to tau pathology. This calls for consideration of sex difference in TSPO-PET studies of microglial activation in mouse models of neurodegeneration and by extension in human studies.

Keywords: Sex, Microglia, TSPO, Amyloid, Tau

Introduction

Alzheimer's disease (AD) is the most prevalent neurodegenerative disease in societies with aging populations [1]. The neuropathology of AD is characterized by the histological triad of accumulation of extracellular amyloid- β peptide (A β) plaques, fibrillary tau aggregates within neurons, and the activation of neuroinflammatory pathways mediated by microglia and astrocytes [2–6]. Importantly, the assessment of glial activation by 18-kDa translocator protein (TSPO) positron emission tomography (TSPO-PET) has received growing interest in the last decade [7], which has spurred the development of a wide range of tracers for human studies [8]. Molecular imaging for stratification and monitoring of glial activation could become crucial for target engagement and response assessment of immunomodulatory therapies [9].

Human clinical data indicate that men and women exhibit sex differences in the neuropathological and symptomatic progression of AD [10]. The lifetime risk of later developing AD for 65-year-old females is twice that of men of the same age (12% vs. 6.3%, respectively) [11]. Women also show faster progression from mild cognitive impairment to AD dementia when compared to men [12]. There is growing evidence that sex differences in neuroinflammation pathways including microglia could play a crucial role in driving the sex differences observed in AD [13]. Nonetheless, the few reports on sex differences in TSPO expression have mainly focused on astrocytes in culture. For example, cultured astrocytes derived from female mouse pups showed stronger increases in TSPO mRNA expression upon exposure to bacterial lipopolysaccharide challenge than cultured astrocytes derived from male littermates [14]. Notably, glial cells express receptors for estrogens and androgens, suggesting the potential for modulation of neuroinflammatory responses by sex steroid hormones [15–17]. Furthermore, a key function attributed to TSPO in microglia is cholesterol transport within the mitochondria [18], which implies downstream effects on the synthesis and metabolism of sex steroid hormones.

A recent human study in cognitively healthy individuals revealed significant sex differences of ^{11}C -PBR28 binding in brain, with women showing a higher TSPO-PET signal [17]. However, although TSPO-PET is increasingly used for investigation in vivo of microglial activation in mouse models of AD [19–22], preclinical

studies have not previously considered possible sex effects on TSPO-PET findings.

Given this background, we aimed to investigate sex differences in the TSPO-PET signal in wild-type mice as well as in mouse models of A β and tau pathology. We tested if the observed effects are independent from potential sex differences in protein aggregation in these models. Finally, we aimed to elucidate if our effects are specific to TSPO-PET binding or if they can be validated by immunostaining for microglia.

Material and methods

Animals and study design

All experiments were performed in compliance with the National Guidelines for Animal Protection, Germany, and with the approval of the regional animal committee (Regierung Oberbayern), with oversight by a veterinarian. Mice were housed in a temperature- and humidity-controlled environment with a 12-h light-dark cycle and with free access to food (Sniff, Soest, Germany) and water. Males and females were housed separately in the same animal facility, with cages of equal size and comparable handling. A larger sample of female mice was a priori included in the longitudinal studies listed below due to the higher frequency of aggressive behavior among male cage mates, which can cause space issues when they need to be separated. Cage mates were kept together in small cohorts when entering the imaging facility and no mice had to be separated during longitudinal imaging. All mice with longitudinal imaging data were included in the analysis as stated below. A detailed overview on the sample size of the mouse cohort is provided in Table 1.

All PET raw data is derived previous in-house studies conducted using the same tomograph and with identical acquisition parameters. The raw data were reprocessed to obtain maximal agreement of spatial and activity normalization between studies. We included data from descriptive datasets or control groups of therapy/genotype studies:

- *C57BL/6*: Historical cross-sectional ^{18}F -GE-180 data from 126 scans of wild-type *C57BL/6* mice aged 2–13 months were reanalyzed. Iba-1 staining was performed in four wild-type mice of each sex at 12–14 months of age. In total, 86 of the 126 (68%) TSPO-

Table 1 Sample sizes of the mouse cohorts across PET and histo- and immunohistochemistry modalities

Genotype		2–3 M		4–5 M		6–7 M		8–11 M		12–14 M	
Sex		Male	Female	Male	Female	Male	Female	Male	Female	Male	Female
C57BL/6	TSPO-PET	16	31	9	18	2	5	5	27	4	9
	Iba-1									4	4
<i>App^{NL-G-F}</i>	TSPO-PET	6	6	6	15	6	15	6	15		
	A β -PET	6	6	6	15	6	15	6	15		
	Iba-1							4	5		
	CD68							4	4		
	Methoxy-x04							4	5		
	GFAP							4	4		
P301S	TSPO-PET	19	33	18	32	15	27	6	6		
	Iba-1							7	7		
	CD68							7	7		
	AT8							7	7		

PET scans of C57BL/6 mice were imaged in parallel with *App^{NL-G-F}* and P301S mouse models, whereas the remaining 40 mice (32%) were imaged within the same time-period (2016–2020) but not in parallel with *App^{NL-G-F}* and P301S mice included in the current study.

- *App^{NL-G-F}(App^{NL-G-F/NL-G-F})*: The knock-in mouse model *App^{NL-G-F}* carries a mutant amyloid precursor protein (APP) gene encoding the humanized A β sequence (G601R, F606Y, and R609H) with three pathogenic mutations, namely Swedish (KM595/596NL), Beyreuther/Iberian (I641F), and Arctic (E618G). Homozygotic *App^{NL-G-F}* mice progressively exhibit widespread cerebral A β accumulation from 2 months of age [23, 24]. Longitudinal ¹⁸F-GE-180 data from 75 serial scans of homozygotic *App^{NL-G-F}* mice imaged at four different ages (2.5, 5.0, 7.5, and 10 months) from previous [25, 26] and unpublished studies were reprocessed. Six mice of each sex were imaged longitudinally at all four time-points whereas nine females entered PET imaging starting from 5.0 months of age. Only mice with successful imaging until 10 months of age were included. The average cage occupancy (*n* per cage) was 2.1 for females and 1.5 for males. All these mice had a contemporaneous ¹⁸F-florbetaben A β -PET scan, which was reprocessed and analyzed analogously. Iba-1, CD68, GFAP, and methoxy-X04 staining in four to five *App^{NL-G-F}* mice of each sex at 11 months of age.
- *P301S*: P301S mice express the human 0N4R tau isoform with the P301S mutation in exon 10 of MAPT gene, which is under control of the murine thy1 promoter on a C57BL/6 background [27, 28]. This model develops aggregates of hyperphosphorylated tau mainly in the brainstem,

with onset starting at 2–3 months of age. Tau filaments in these mice appear mostly as half-twisted ribbons, with a lesser abundance of larger paired helical tau filaments resembling those seen in human AD patients. The behavioral phenotype of P301S mice manifests as learning deficits from 2–3 months of age, and onset of motor impairment at 4 months, leading to early death before 12 months of age. Longitudinal ¹⁸F-GE-180 data from 156 serial scans of P301S mice imaged at up to four different time-points (2, 4, 6, and 8 months) from a previous [21] and an unpublished study were reprocessed. Six mice of each sex were imaged longitudinally at all four time-points whereas 27 female and 13 male mice were imaged from 2 to 6 months of age. Failed imaging sessions at follow-up time-points were excluded. The average cage occupancy (*n* per cage) was 2.6 for females and 1.9 for males. Iba-1, CD68, and AT8 staining had been performed in seven homozygotic P301S mice of each sex at 7–8 months of age.

PET imaging

PET data acquisition, reconstruction, and post-processing

For all PET procedures, including radiochemistry, acquisition and pre-processing, we used an established and standardized protocol [19, 29]. In brief, ¹⁸F-GE-180 TSPO-PET recordings (average dose 12.3 \pm 2.2 MBq) with an emission window of 60–90 min after injection were obtained to measure glial activation. ¹⁸F-florbetaben A β -PET recordings (average dose 11.8 \pm 1.9 MBq) with an emission window of 30–60 min after injection were performed for assessment of fibrillar A β accumulation. Anesthesia was induced with 3.0% isoflurane delivered via a mask at 3.5 L/min, with maintenance of

anesthesia by 1.5% isoflurane during the imaging time window.

PET image analysis

We performed all PET data analyses using PMOD (version 3.5; PMOD technologies). Normalization of TSPO-PET emission images was performed by standardized uptake value ratios (SUVr) using previously established reference tissues in the WT (white matter), *App*^{NL-G-F} (periaqueductal grey), and P301S (nucleus accumbens) mice [19, 25, 29, 30]. Two bilateral volumes of interest placed in the frontal cortex (comprising 15 mm³ each) served for calculation of target-to-reference SUVr. We chose frontal cortex for quantification of TSPO-PET signal based on earlier findings in C57BL/6, *App*^{NL-G-F}, and P301S mice [21, 25, 30], and due to the documented presence of neuropathology in *App*^{NL-G-F} and P301S mice, along with the requirement for a sufficiently large standard volume of interest (VOI).

Immunohistochemistry

Iba-1, CD68, methoxy-X04, and AT8 immuno- and histochemical stainings were performed as described previously [21, 25]. In brief, we performed a standard free-floating immunofluorescence protocol cortex and brainstem areas matching the PET brain regions. As previously described, perfusion fixed 50- μ m-thick brain sections were rinsed either overnight or for 48 h in PBS with 0.2% Triton X-100 containing one of the following primary antibodies: rabbit monoclonal Iba-1 (1:500, Wako: 19-19741), rat monoclonal CD68 (1:500, Bio-Rad: MCA1857), and mouse monoclonal phospho-Tau (1:500, Thermo Fisher: MN1020). After washing in PBS, sections were then incubated in a combination of three secondary antibodies (Alexa 488 goat anti-rabbit, Alexa 594 goat anti-mouse, and Alexa 647 goat anti-rat IgG). Following this step, A β fibrils were stained for 25 min upon addition of methoxy-X04 (10 μ g/mL in 50% ethanol) at room temperature, followed by washing in buffer (4 times ten min each).

For GFAP staining, free-floating sections were blocked with Normal Goat serum (5%) in PBS + 0.3% Triton X-100 for 1 h at room temperature. We obtained immunohistochemical labelling of astrocytes using the antibody anti-GFAP (Synaptic Systems) 1:500 in 1% NGS blocking solution overnight at 4 °C and the Alexa Fluor 555 secondary antibody anti-rabbit (Invitrogen) 1:500 in 1% NGS blocking solution for 3 h at room temperature. The unbound dye was removed by three washing steps with PBS, and the slices were then mounted on microscope slides with fluorescent mounting medium (Dako, Germany).

We performed quantitation in ImageJ (<https://imagej.nih.gov/ij/>) with images obtained from a confocal microscope (LSM 780 Axio invers). For each marker, we

calculated the percentage coverage of positive staining in a cortical region matching the PET VOI.

Statistics

In wild-type mice, we first assessed whether there was an age-dependent increase in TSPO-PET signal, using a linear mixed model with age at scanning as a predictor of TSPO-PET controlling for sex (fixed effect) as well as for random slope and intercept. Next, we tested for sex differences in the age dependence of TSPO-PET results by additionally including a sex \times age interaction as a predictor.

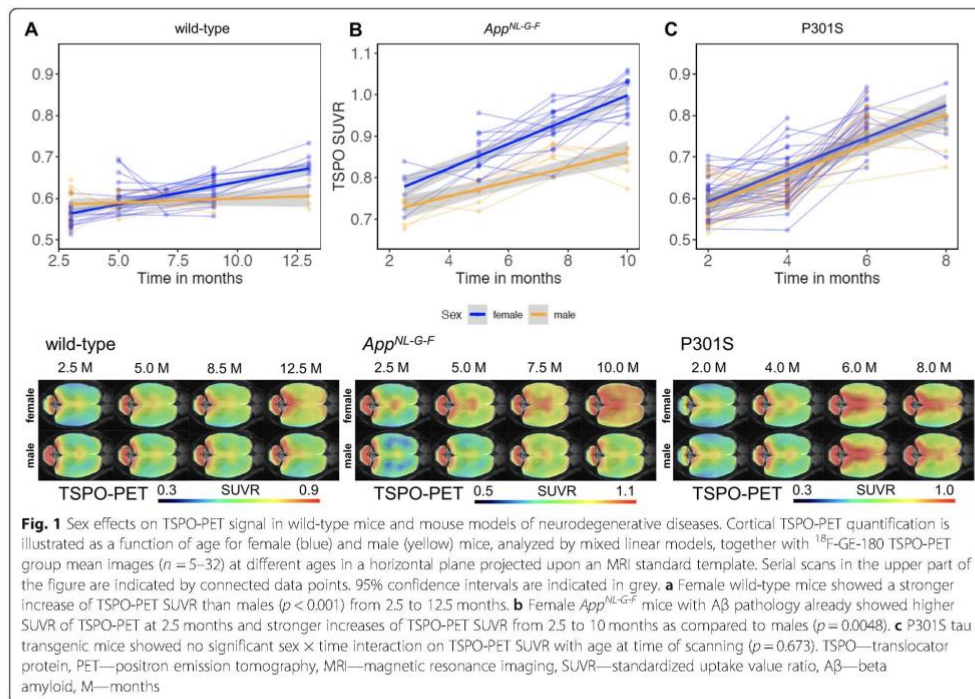
We applied equivalent models in the *App*^{NL-G-F} mice both for TSPO-PET and A β -PET, and likewise in the P301S tau transgenic mice for TSPO-PET, to determine whether sex moderated the age-dependent PET increases. When assessing the sex by age interaction effect on the increases in TSPO-PET binding in the *App*^{NL-G-F} mice, we additionally controlled the models for individual concomitant A β -PET levels to isolate sex-specific effects on the TSPO-PET increases from confound due to the primary fibrillar A β pathology.

Effects of sex on histo- and immunohistochemistry area-% readouts were tested by unpaired Student's *t* test, and effect sizes were calculated as Cohen's *d*. Statistical analyses were performed in R using the lme4 package for linear mixed models. For all models, we applied an alpha threshold of 0.05 for considering effects to be statistically significant.

Results

Stronger elevation of the cortical TSPO-PET signal in females is reproducible in rodents

Our first objective was to investigate if recent human findings of higher TSPO-PET signal in cognitively healthy females when compared to males [17] also hold true for healthy wild-type mice. Therefore, we availed ourselves of our large μ PET database to make a cross-sectional comparison of ¹⁸F-GE-180 TSPO-PET scans by sex. Wild-type mice showed increasing TSPO-PET SUVr in cortex with age ($T = 8.915$, $b/SE = 0.009/0.001$, $p < 0.001$, Cohen's $d = 1.608$), in line with our earlier report on this phenomenon [30]. Furthermore, we found a significant age \times sex interaction ($T = -4.171$, $b/SE = -0.009/0.002$, $p < 0.001$, Cohen's $d = 0.755$) in these animals, controlling for slope (age) and random intercept, indicating that female mice showed more pronounced TSPO-PET SUVr increases than did male mice (Fig. 1a). Immunohistochemistry confirmed higher Iba-1 quantification in female wild-type mice at 12–14 months of age when compared to males ($3.23 \pm 0.09\%$ vs. $2.97 \pm 0.10\%$, $p = 0.010$, Cohen's $d = 1.87$; Fig. 2a). In summary, we confirmed our hypothesis that (as seen in cognitively intact humans) female wild-type mice would show greater



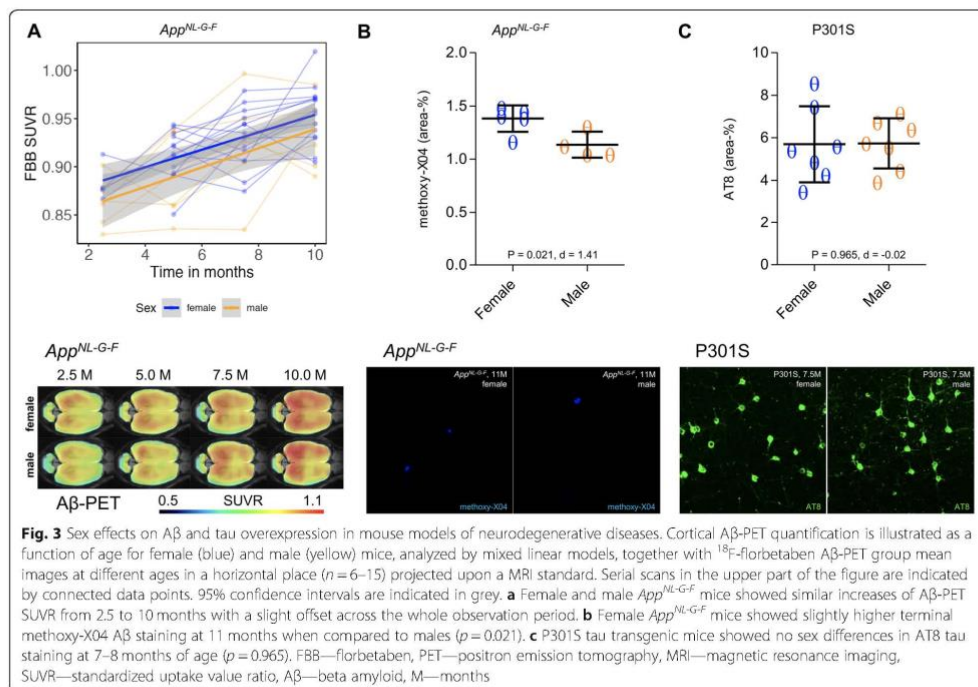
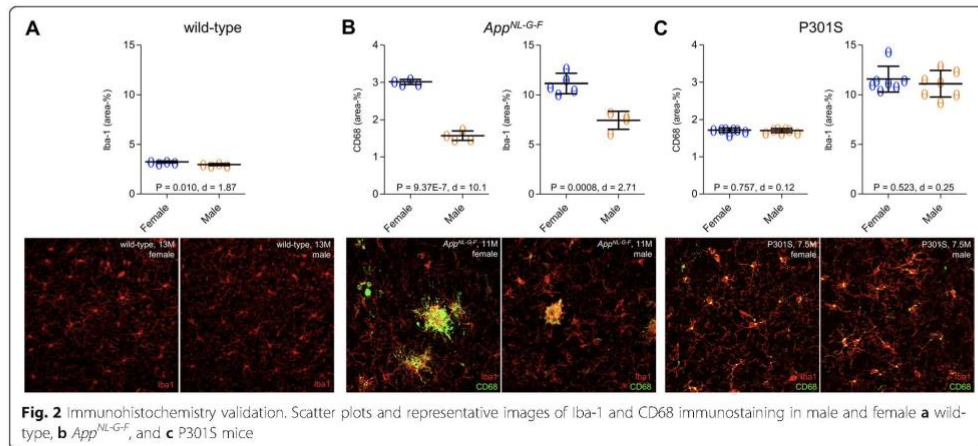
age-dependent increases in TSPO-PET binding, which was evident by diverging slopes of female and male mice starting from 6 to 7 months of age.

Sex-specific TSPO-PET increase in the presence of A β pathology

Next, we tested whether female *App*^{NL-G-F} mice showed greater longitudinal increases in microglial activation, using TSPO-PET as a proxy. There was a pronounced TSPO-PET increase in the cortex of *App*^{NL-G-F} mice with age when considering both female and male mice ($T = 11.831$, $b/SE = 0.024/0.002$, $p < 0.0001$, Cohen's $d = 5.893$, linear mixed model, adjusted for sex, random slope, and intercept). We then proceeded to test for a sex \times age interaction for TSPO-PET SUVR, controlling for random slope (i.e., age at scanning) and intercept. As hypothesized, we found a significant sex \times age interaction for TSPO-PET SUVR ($T = -2.953$, $b/SE = -0.011/0.004$, $p = 0.0048$, Cohen's $d = 0.827$, Fig. 1b), where the female *App*^{NL-G-F} mice showed a greater increase in TSPO-PET SUVR with age than did male mice.

To account for potential sex differences in fibrillar A β aggregation, we tested whether *App*^{NL-G-F} mice showed sex differences in A β -PET. Using longitudinal ^{18}F -

florbetaben-PET data in the same mice, we tested the sex \times age interaction on ^{18}F -florbetaben-PET SUVR, using linear mixed models controlling for random slope (i.e., age) and intercept. There was no significant sex \times age interaction on ^{18}F -florbetaben-PET SUVRs ($T = 0.425$, $b/SE = 0.001/0.003$, $p = 0.673$, Cohen's $d = 0.141$, Fig. 3a). Thus, we conclude that the longitudinal increases of fibrillar A β aggregation in cortex are comparable between male and female *App*^{NL-G-F} mice (main effect of age on ^{18}F -florbetaben-PET SUVR, controlling for sex, random slope, and intercept: $T = 6.048$, $b/SE = 0.009/0.002$, $p < 0.0001$, Cohen's $d = 1.872$). More importantly, the aforementioned sex effect on TSPO-PET remained consistent when controlling for ^{18}F -florbetaben-PET SUVR at each time-point ($T = -2.926$, $b/SE = -0.011/0.0038$, $p = 0.0051$, Cohen's $d = 0.820$), suggesting that sex differences in TSPO-PET SUVR are not driven by sex-specific differences in fibrillar A β burden. Immunohistochemistry at the terminal time-point confirmed the observations in vivo, showing higher expression of activated microglial markers in the female mice compared to males (Iba-1: $11.14 \pm 1.02\%$ vs. $7.44 \pm 0.91\%$, $p = 0.0008$, Cohen's $d = 2.71$; CD68: $3.01 \pm 0.06\%$ vs. $1.57 \pm 0.13\%$, $p = 1\text{E-}6$, Cohen's $d = 10.13$) (Fig. 2b).



Methoxy-X04 histology indicated slightly higher fibrillar A β levels in *App*^{NL-G-F} females at the terminal time-point ($1.38 \pm 0.12\%$ vs. $1.14 \pm 0.12\%$, $p = 0.021$, Cohen's $d = 1.41$, Fig. 3b). GFAP immunohistochemistry showed slightly higher levels of reactive astrocytes in *App*^{NL-G-F} females at the terminal time-point ($7.23 \pm 1.00\%$ vs. $5.60 \pm 0.28\%$, $p = 0.020$, Cohen's $d = 1.58$, Fig. 4).

In summary, we find a striking effect of sex on the age-dependent increase in cortical TSPO-PET signal in A β -transgenic mice, in the absence of notable sex differences in fibrillar A β pathology to ¹⁸F-florbetaben-PET SUVR, and with only slightly higher fibrillar A β to histology at the terminal time-point. This indicates that the sex difference in microglial activation is not readily attributable to sex differences of fibrillar A β pathology.

TSPO-PET increases in response to tau pathology are not moderated by sex

Next, we tested whether sex-specific increases of the TSPO-PET signal were specifically related to cerebral A β accumulation, or rather a more general function of AD-like brain pathology. To this end, we assessed longitudinal TSPO-PET in P301S tau transgenic mice, finding the expected longitudinal increases in TSPO-PET SUVR with age ($T = 15.77$, $b/SE = 0.038/0.002$, $p < 0.0001$, Cohen's $d = 2.987$). There was, however, no significant sex \times age interaction with TSPO-PET SUVR, controlling for slope (i.e., age) and random intercept ($T = -0.671$, $b/SE = -0.003/0.005$, $p = 0.504$, Cohen's $d = 0.128$, Fig. 1c). Thus, the TSPO-PET SUVR increases in response to 4-repeat isoform tau pathology did not differ between male and female P301S mice. Terminal immunohistochemical analysis likewise did not indicate any significant sex differences in microglial markers (Iba-1, $11.56 \pm 1.29\%$ vs. $11.10 \pm 1.33\%$, $p = 0.523$, Cohen's $d = 0.25$; CD68, $1.72 \pm 0.06\%$ vs. $1.71 \pm 0.05\%$, $p = 0.757$, Cohen's $d = 0.12$; Fig. 2c) or AT8-positive tau accumulation ($5.69 \pm 1.79\%$ vs. $5.73 \pm 1.18\%$, $p = 0.965$, Cohen's $d = -0.02$; Fig. 3c) in P301S mice aged 7–8 months.

Discussion

This is the first investigation aiming to elucidate sex differences in microglial activation in aging wild-type mice and mouse models of AD-like pathologies. Our data show a sex-specific effect on the cortical TSPO-PET signal and immunohistochemical markers of microgliosis in wild-type mice, with a greater age-dependent increase in female mice, thus in line with human TSPO-PET data in cognitively healthy men and women. Notably, we also observed a strong sex-specific effect on TSPO-PET signal during accumulation of A β pathology, indicating higher TSPO-PET binding in female *App*^{NL-G-F} mice than in males. Contemporaneous A β -PET from the same mice allowed us to adjust TSPO-PET results for possible confounding effects due to sex differences in the progression of fibrillar A β pathology. In contrast, P301S mice did not indicate sex differences in TSPO-PET signal increases in response to their accumulation of tau pathology. Terminal histo- and immunohistochemical analyses of phosphorylated tau, A β , and microglial markers confirmed all of the main PET findings.

Similar to a recent multi-center TSPO-PET in cognitively healthy men and women [17], we observed a strong effect of sex on the cortical TSPO-PET signal in a cross-sectional cohort of wild-type mice, indicating progressively higher TSPO-PET signal in cortex of females as compared to males. Importantly, we used data from mice housed under standard conditions, and with a completely matched TSPO-PET protocol, thus minimizing variance from methodological and environmental factors. This is critically important, given our compilation of data from various studies.

The human TSPO-PET study showed a more distinctly higher grey matter signal in younger women, which declined with increasing age of the subjects [17]. In contrast, our wild-type mouse data showed a sex difference in TSPO-PET favoring the females, which became more prominent with increasing age. However, we note that our tracking of TSPO-PET extended to only to 13 months of age, which is perhaps comparable to

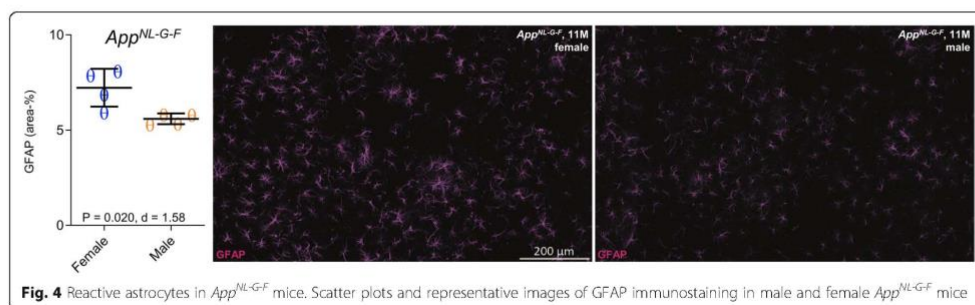


Fig. 4 Reactive astrocytes in *App*^{NL-G-F} mice. Scatter plots and representative images of GFAP immunostaining in male and female *App*^{NL-G-F} mice

middle age in humans [31]. Therefore, sex differences in TSPO-PET may follow differing time-courses in healthy mice and humans in relation to their vastly different lifespans. Our histo- and immunohistochemical validations of the in vivo TSPO-PET results present a distinct advantage of our preclinical study. Thus, we unambiguously establish the congruence of TSPO-PET findings with greater elevation of the microglia marker Iba-1 in aged female wild-type mice when compared to males. This result also supports the claims made in the human study cited above that increasing TSPO-PET binding with healthy aging is attributable to microglial activation, i.e., neuroinflammation. The large variability of human TSPO-PET binding in healthy individuals [17] and the allelic dependence of most TSPO tracers [8] predict a need for substantial group sizes to detect sex interactions with TSPO-PET signal in neurodegenerative diseases like AD. Our present use of inbred mouse lineages may have tended to reduce variance in the various endpoints, and our use of transgenic mouse models with overexpression of A β or hyperphosphorylated tau allows the isolation of effects of different protein aggregates on the interaction between sex and TSPO-PET expression. While preclinical AD patients can show A β -positivity and tau-negativity [32], there is lingering uncertainty about the threshold of disease progression for detection of tau in cerebrospinal fluid or tau-PET assessments [33]. However, our investigation reveals a sex-specific effect on TSPO-PET increases during accumulation of A β pathology in *App^{NL-G-F}* mice, with an interaction of a magnitude similar to that seen in aging wild-type mice. The progression of A β pathology is more rapid in female AD-model mice than in males [34]. A primary accumulation of fibrillar A β triggers a secondary neuroinflammation mediated by activated microglia [35]. Preliminary results had indicated sex differences in A β accumulation in *App^{NL-G-F}* mice, albeit with onset in the interval between 12 and 18 months [23], thus occurring after the present observation period. We did not observe sex differences of the A β -PET increase in *App^{NL-G-F}* mice and inclusion of A β -PET results in the linear mixed model did not alter the sex difference in TSPO-PET. Methoxy-X04 staining indicated moderately higher fibrillar A β pathology in female *App^{NL-G-F}* mice compared to male *App^{NL-G-F}* mice, which may reflect greater sensitivity of the histological staining [20], or the preponderant weighting of the A β -PET signal to fibrillar A β and its insensitivity to soluble A β proportions. Thus, we cannot exclude the possibility that the effect of sex on TSPO-PET in *App^{NL-G-F}* mice may be influenced by sex differences in the biochemical nature of the A β pathology. While the main attribution of the TSPO-PET signal is to activate microglia, there is also a contribution from pro-inflammatory astrocytes [36]. We note that the

proportion of astroglial versus microglial contributions to TSPO-PET signals might differ between male and female mice and our immunohistochemistry data showed sex differences for both CD68 reactivity and GFAP reactivity in *App^{NL-G-F}* mice. A direct correlation analyses between TSPO-PET and immunohistochemistry in larger cohorts of male and female *App^{NL-G-F}* mice could better substantiate the cellular origin of the TSPO-PET signal.

Surprisingly, we were unable to detect corresponding sex-specific effects on longitudinal TSPO-PET increases in the P301S tau mouse model. Negative PET findings are supported by the absence of sex differences in Iba-1 and CD68 immunohistochemistry, and by the equal levels of hyperphosphorylated AT8-positive tau in female and male P301S mice at 7 months of age. Although there were significant sex differences in microglial microRNA expression model mice [37], our present in vivo findings do not indicate any sex difference in the TSPO-PET binding with aging of P301S mice. Indeed, these tauopathy model mice did not manifest the sex effect seen in wild-type mice, perhaps due to masking by effects of strong tau pathology in aging P301S mice. We also note that PET imaging paradigms give a macroscopic view of neuroinflammation components in mouse brain as compared to immunohistochemistry or in situ hybridization methods. However, we emphasize the translational relevance of neuroinflammation PET biomarkers [6]. Thus, the synthesis of our combined findings comprise strong evidence for a sex-specific effect on the TSPO-PET signal in aging wild-type mice, and the association between microglia activation with A β accumulation in transgenic mice, without corresponding association with tauopathy in P301S mice. Present observations are hypothesis generating for studies of microglial activation by manipulation of sex hormones, i.e., by ovariectomy or orchidectomy [10]. Furthermore, cross-breeding of A β and tauopathy mouse models with TSPO knock-out mice [38] could mechanistically help elucidate the effect of sex differences of TSPO on functionally related pathways such as cholesterol synthesis. We note the present imbalance of numbers of male and female mice, which arises from retrospective design of this study.

There is growing evidence that tau pathology follows accumulation of A β in AD patients [39]. Recent data showed that NLRP3 inflammasome activation triggers tau pathology [40], and importantly, there is evidence that women present a higher level of tau pathology even at the preclinical stage of AD [41]. This stands in contrast to present finding of absent sex differences in tauopathy in the P301S model mice, which lack A β pathology. Thus, enhanced microglial activation in response to A β could constitute the key factor resulting

elevated in tau pathology in female AD patients. TSPO-PET in conjunction with tau- and/or A β -PET in cohorts of AD and primary tauopathy patients (i.e., progressive supranuclear palsy or corticobasal degeneration) would translate our present findings into the study of human disease.

Conclusions

Sex-specific effects on the age-dependent increase in cortical TSPO-PET signal are present in wild-type mice and in mouse models of neurodegenerative diseases. Sex moderates the cortical microgliosis in response to amyloidosis but not to tau pathology in transgenic mice. Strict controlling for sex is required for TSPO-PET studies of microglial activation in mouse models of neurodegenerative diseases and requires attention in corresponding studies in human disease.

Abbreviations

AB: Beta amyloid; AD: Alzheimer's disease; ANOVA: Analysis of variance; APP: Amyloid precursor protein; B/SE: Main and interaction effects; IHC: Immunohistochemistry; MRI: Magnetic resonance imaging; PET: Positron emission tomography; M: Months; MAPT: Microtubule-associated protein tau; MCI: Mild cognitive impairment; SPM: Statistical parametric mapping; SUV: Standardized uptake value; SUVr: SUV ratio; TSPO: Translocator protein; VOIs: Volumes of interest; WT: Wild-type

Acknowledgements

We thank Karin Bormann-Giglmaier and Diana Mahlstedt for excellent technical assistance. *App*^{tg} mice were provided by RIKEN BRC through the National Bio-Resource Project of the MEXT, Japan. GE Healthcare manufactured the ¹⁸F-GE-180 cassettes, which were made available through an early-access agreement. Florbetaben precursor was kindly provided by Life Molecular Imaging.

Authors' contributions

GB, FE, CS, and FR performed the majority of PET experiments. NF and ME performed the linear mixed models analysis. TB and JML performed immunohistochemistry staining. GB, FE, CS, LB, FR, and MB analyzed and quantified the data. PB, AR, and MB performed interpretation of the PET data. SL and FG performed and improved radiochemistry. GB rendered expert IT support. NF, ME, PB, AR, GUH, JH, and MB contributed to the conception and design of the study and interpreted the combined findings. GB, MB, and PC wrote the manuscript. BU supervised the study as a veterinarian. All authors participated in the generation of the original data, added important intellectual content to the manuscript and provided critical assessment of the current manuscript. All authors read and approved the final manuscript.

Funding

The study was financially supported by the SyNergy Cluster (J.H., P.B., C.H., and A.R.) and by the Deutsche Forschungsgemeinschaft (DFG) by a dedicated PET imaging grant to M.B. and A.R. (BR4580/1-1 & RO5194/1-1). G.H. is supported by the German Federal Ministry of Education and Research (01EK1605A HitTau), the NOMIS foundation (FTLD project). Open Access funding enabled and organized by Projekt DEAL.

Availability of data and materials

The datasets used and/or analyzed during the current study are available from the corresponding author upon reasonable request.

Ethics approval and consent to participate

All experiments were carried out in compliance with the National Guidelines for Animal Protection, Germany, and following the guidelines of the EU Directive 2010/63/EU. Experiments were approved by the regional Animal

Care Committee of the Government of Oberbayern (Regierung Oberbayern) and were overseen by a veterinarian.

Consent for publication

Not applicable.

Competing interests

G.U.H. received research support from GE Healthcare and NeuroPore; has ongoing research collaborations with Orion and Prothena; serves as a consultant for AbbVie, AlzProtect, Asceneuron, Biogen, Biohaven, Lundbeck, Novartis, Roche, Sanofi, and UCB; received honoraria for scientific presentations from AbbVie, Biogen, Roche, Teva, UCB, and Zamboni; and holds a patent on PERK Activation for the Treatment of Neurodegenerative Diseases (PCT/EP2015/068734). M.B. received speaking honoraria from Life Molecular Imaging and GE healthcare. M.B. is an advisor of Life Molecular Imaging. All other authors report no conflicts of interest.

Author details

¹Department of Nuclear Medicine, University Hospital of Munich, LMU Munich, Marchioninstraße 15, 81377 Munich, Germany. ²Institute for Stroke and Dementia Research, University Hospital of Munich, LMU Munich, Munich, Germany. ³DZNE - German Center for Neurodegenerative Diseases, Munich, Germany. ⁴Department of Nuclear Medicine, Inselspital, University Hospital Bern, Bern, Switzerland. ⁵School of Psychology and Counselling, Queensland University of Technology, Brisbane, Australia. ⁶Munich Cluster for Systems Neurology (SyNergy), Munich, Germany. ⁷Department of Neurology, Hannover Medical School, Hannover, Germany. ⁸Department of Neurology, Technical University Munich, Munich, Germany. ⁹Center of Neuropathology and Prion Research, University of Munich, Munich, Germany.

Received: 20 July 2020 Accepted: 25 November 2020

Published online: 14 December 2020

References

- Ziegler-Graham K, Brookmeyer R, Johnson E, Arighi HM. Worldwide variation in the doubling time of Alzheimer's disease incidence rates. *Alzheimers Dement*. 2008;4:316–23.
- Braak H, Braak E. Demonstration of amyloid deposits and neurofibrillary changes in whole brain sections. *Brain Pathol*. 1991;1:213–6.
- Hyman BT, Phelps CH, Beach TG, Bigio EH, Cairns NJ, Camillo MC, Dickson DW, Duyckaerts C, Frosch MP, Masliah E, et al. National Institute on Aging-Alzheimer's Association guidelines for the neuropathologic assessment of Alzheimer's disease. *Alzheimers Dement*. 2012;8:1–13.
- Serrano-Pozo A, Frosch MP, Masliah E, Hyman BT. Neuropathological alterations in Alzheimer disease. *Cold Spring Harb Perspect Med*. 2011;1:a006189.
- Querfurth HW, LaFerla FM. Alzheimer's disease. *N Engl J Med*. 2010;362:329–44.
- Heneka MT, Carson MJ, Khoury JE, Landreth GE, Brosseron F, Feinstein DL, Jacobs AH, Wyss-Coray T, Vitorica J, Ransohoff RM, et al. Neuroinflammation in Alzheimer's disease. *Lancet Neurol*. 2015;14:388–405.
- Stefaniak J, O'Brien J. Imaging of neuroinflammation in dementia: a review. *J Neurol Neurosurg Psychiatry*. 2016;87:21–8.
- Cumming P, Burgher B, Patkar O, Breakspear M, Vasdev N, Thomas P, Liu GJ, Banati R. Sifting through the surfeit of neuroinflammation tracers. *J Cereb Blood Flow Metab*. 2018;38:204–24.
- Werry EL, Bright FM, Piguet O, Ittner LM, Halliday GM, Hodges JR, Kiernan MC, Loy CT, Kril JJ, Kassou M. Recent developments in TSPO PET imaging as a biomarker of neuroinflammation in neurodegenerative disorders. *Int J Mol Sci*. 2019;20:3161.
- Pilke CJ. Sex and the development of Alzheimer's disease. *J Neurosci Res*. 2017;95:671–80.
- Podcasy JL, Epperson CN. Considering sex and gender in Alzheimer disease and other dementias. *Dialogues Clin Neurosci*. 2016;18:437–46.
- Lin KA, Choudhury KR, Rathakrishnan BG, Marks DM, Petrella JR, Doraiswamy PM. Alzheimer's Disease Neuroimaging I: Marked gender differences in progression of mild cognitive impairment over 8 years. *Alzheimers Dement (N Y)*. 2015;1:103–10.
- Kodama L, Gan L. Do microglial sex differences contribute to sex differences in neurodegenerative diseases? *Trends Mol Med*. 2019;25:741–9.

14. Santos-Galindo M, Acaz-Fonseca E, Bellini MJ, Garcia-Segura LM. Sex differences in the inflammatory response of primary astrocytes to lipopolysaccharide. *Biol Sex Differ*. 2011;2:7.
15. Nissen JC. Microglial function across the spectrum of age and gender. *Int J Mol Sci*. 2017;18:561.
16. Uchoa MF, Moser VA, Pike CJ. Interactions between inflammation, sex steroids, and Alzheimer's disease risk factors. *Front Neuroendocrinol*. 2016; 43:60–82.
17. Tulsiku J, Plaven-Sigay P, Gaiser EC, Airas L, Al-Abdulrasul H, Bruck A, Carson RE, Chen MK, Cosgrove KP, Ekblad L, et al. Effects of age, BMI and sex on the glial cell marker TSPO - a multicentre [(11)C]PBR28 HRRT PET study. *Eur J Nucl Med Mol Imaging*. 2019;46:2329–38.
18. Garcia-Segura LM, Melcangi RC. Steroids and glial cell function. *Glia*. 2006;54: 485–98.
19. Brendel M, Probst F, Jaworska A, Overhoff F, Korzhova V, Albert NL, Beck R, Lindner S, Gildehaus FJ, Baumann K, et al. Glial activation and glucose metabolism in a transgenic amyloid mouse model: a triple-tracer PET study. *J Nucl Med*. 2016;57:954–60.
20. Parhizkar S, Arzberger T, Brendel M, Kleinberger G, Deussing M, Focke C, Nuscher B, Xiong M, Ghasemigharagoz A, Katzmarski N, et al. Loss of TREM2 function increases amyloid seeding but reduces plaque-associated ApoE. *Nat Neurosci*. 2019;22:191–204.
21. Eckenweber F, Medina-Luque J, Blume T, Sacher C, Biechele G, Wind K, Deussing M, Briel N, Lindner S, Boening G, et al. Longitudinal TSPO expression in tau transgenic P301S mice predicts increased tau accumulation and deteriorated spatial learning. *J Neuroinflammation*. 2020;17:208.
22. Blume T, Focke C, Peters F, Deussing M, Albert NL, Lindner S, Gildehaus FJ, von Ungern-Stemberg B, Ozmen L, Baumann K, et al. Microglial response to increasing amyloid load saturates with aging: a longitudinal dual tracer in vivo muPET-study. *J Neuroinflammation*. 2018;15:307.
23. Masuda A, Kobayashi Y, Kogo N, Saito T, Saito TC, Itohara S. Cognitive deficits in single App knock-in mouse models. *Neurobiol Learn Mem*. 2016; 135:73–82.
24. Saito T, Matsuba Y, Mihira N, Takano J, Nilsson P, Itohara S, Iwata N, Saito TC. Single App knock-in mouse models of Alzheimer's disease. *Nat Neurosci*. 2014;17:661–3.
25. Sacher C, Blume T, Beyer L, Peters F, Eckenweber F, Sgobio C, Deussing M, Albert NL, Unterrainer M, Lindner S, et al. Longitudinal PET monitoring of amyloidosis and microglial activation in a second-generation amyloid-beta mouse model. *J Nucl Med*. 2019;60:1787–93.
26. Sacher C, Blume T, Beyer L, Biechele G, Sauerbeck J, Eckenweber F, Deussing M, Focke C, Parhizkar S, Lindner S, et al. Asymmetry of fibrillar plaque burden in amyloid mouse models. *J Nucl Med*. 2020;61:1825–31.
27. Allen B, Ingram E, Takao M, Smith MJ, Jakes R, Virdee K, Yoshida H, Holzer M, Craxton M, Emson PC, et al. Abundant tau filaments and nonapoptotic neurodegeneration in transgenic mice expressing human P301S tau protein. *J Neurosci*. 2002;22:9340–51.
28. Xu H, Rosler TW, Carlsson T, de Andrade A, Bruch J, Hollerhage M, Oertel WH, Hoglinger GU. Memory deficits correlate with tau and spine pathology in P301S MAPT transgenic mice. *Neuropathol Appl Neurobiol*. 2014;40:833–43.
29. Overhoff F, Brendel M, Jaworska A, Korzhova V, Delker A, Probst F, Focke C, Gildehaus FJ, Carlsen J, Baumann K, et al. Automated spatial brain normalization and hindbrain white matter reference tissue give improved [(18)F]-florbetaben PET quantitation in Alzheimer's model mice. *Front Neurosci*. 2016;10:45.
30. Brendel M, Focke C, Blume T, Peters F, Deussing M, Probst F, Jaworska A, Overhoff F, Albert N, Lindner S, et al. Time courses of cortical glucose metabolism and microglial activity across the life span of wild-type mice: a PET study. *J Nucl Med*. 2017;58:1984–90.
31. Flurkey K, Currer JM, Harrison D. Mouse models in aging research. In *The mouse in biomedical research*. Elsevier; 2007:3:637–72.
32. Kosciak RL, Betthausen TJ, Jonaitis EM, Allison SL, Clark LR, Hermann BP, Cody KA, Engle JW, Barnhart TE, Stone CK, et al. Amyloid duration is associated with preclinical cognitive decline and tau PET. *Alzheimers Dement* (Amst). 2020;12:e12007.
33. Jack CR Jr, Bennett DA, Blennow K, Carrillo MC, Dunn B, Haeberlein SB, Holtzman DM, Jagust W, Jessen F, Karlawish J, et al. NIA-AA research framework toward a biological definition of Alzheimer's disease. *Alzheimers Dement*. 2018;14:535–62.
34. Carroll JC, Rosario ER, Kreimer S, Villamagna A, Gentschein E, Stanczyk FZ, Pike CJ. Sex differences in β -amyloid accumulation in 3xTg-AD mice: role of neonatal sex steroid hormone exposure. *Brain research*. 2010;1366:233–45.
35. Monasor LS, Müller SA, Colombo A, König J, Roth S, Liesz A, Berghofer A, Saito T, Saito TC, Hems J, et al. Fibrillar A β triggers microglial proteome alterations and dysfunction in Alzheimer mouse models. *eLife*. 2020;9: e54083.
36. Pannell M, Economopoulos V, Wilson TC, Kersemans V, Isenegger PG, Larkin JR, Smart S, Gilchrist S, Gouverneur V, Sibson NR. Imaging of translocator protein upregulation is selective for pro-inflammatory polarized astrocytes and microglia. *Glia*. 2020;68:280–97.
37. Kodama L, Guzman E, Etcheagaray JI, Li Y, Sayed FA, Zhou L, Zhou Y, Zhan L, Le D, Udeochu JC, et al. Microglial microRNAs mediate sex-specific responses to tau pathology. *Nat Neurosci*. 2020;23:167–71.
38. Barron AM, Ji B, Kito S, Suhara T, Higuchi M. Steroidogenic abnormalities in translocator protein knockout mice and significance in the aging male. *Biochem J*. 2018;475:75–85.
39. Bloom GS. Amyloid-beta and tau: the trigger and bullet in Alzheimer disease pathogenesis. *JAMA Neurol*. 2014;71:505–8.
40. Ising C, Venegas C, Zhang S, Scheiblich H, Schmidt SV, Vieira-Saecker A, Schwartz S, Albaset S, McManus RM, Tejera D, et al. NLRP3 inflammasome activation drives tau pathology. *Nature*. 2019;575:669–73.
41. Buckley RF, Mornino EC, Rabin JS, Hohman TJ, Landau S, Hanseeuw BJ, Jacobs HL, Papp KV, Amarglio RE, Properzi MJ, et al. Sex differences in the association of global amyloid and regional tau deposition measured by positron emission tomography in clinically normal older adults. *JAMA Neurol*. 2019;76:542–51.

Publisher's Note

Springer Nature remains neutral with regard to jurisdictional claims in published maps and institutional affiliations.

Ready to submit your research? Choose BMC and benefit from:

- fast, convenient online submission
- thorough peer review by experienced researchers in your field
- rapid publication on acceptance
- support for research data, including large and complex data types
- gold Open Access which fosters wider collaboration and increased citations
- maximum visibility for your research: over 100M website views per year

At BMC, research is always in progress.

Learn more blomedcentral.com/submissions



IX Danksagung

An erster Stelle möchte ich meinem Doktorvater, Herrn Prof. Dr. med. Matthias Brendel, meinen aufrichtigen Dank aussprechen – sowohl für die Bereitstellung dieses äußerst faszinierenden Forschungsthemas als auch für seine kontinuierliche Unterstützung, Motivation und bemerkenswerte Erreichbarkeit bei Fragen und Bedenken.

Meinem Betreuer, Herrn Dr. med. Florian Eckenweber, danke ich herzlich für seine herausragende Betreuung und Einarbeitung. Zudem möchte ich meinen Vorgängern und Mitdoktoranden, Dr. med. Gloria Biechele und Thomas Wiedemann, für ihre Anleitung und Unterstützung bei der Durchführung sowie Auswertung von Kleintier-PET-Scans danken. Ebenso gebührt Karin Bormann-Giglmaier mein Dank für ihre routinierte Kompetenz und die angenehme Zusammenarbeit bei der Durchführung der Experimente.

Schließlich gebührt meinen Eltern, Agnes Rubinstein und Dr. med. Matthias Ollwig, sowie meiner Freundin, Luisa, ein besonderer Dank für ihre durchgehende Ermutigung und moralische Unterstützung während der Erstellung dieser Dissertation. Ihre Förderung und ihr Beitrag zu meinem Werdegang sind mir von unschätzbarem Wert.

Publikationen:

- Palleis C, Sauerbeck J, Beyer L, et al. In Vivo Assessment of Neuroinflammation in 4-Repeat Tauopathies. *Mov Disord*. 2021
- Biechele G, Franzmeier N, Blume T, et al. Glial activation is moderated by sex in response to amyloidosis but not to tau pathology in mouse models of neurodegenerative diseases. *J Neuroinflammation*. 2020
- Gnörich J, Reifschneider A, Wind K, et al. Depletion and activation of microglia impact metabolic connectivity of the mouse brain. *J Neuroinflammation*. 2023
- Kunze LH, Ruch F, Biechele G, et al. Long-Term Pioglitazone Treatment Has No Significant Impact on Microglial Activation and Tau Pathology in P301S Mice. *Int J Mol Sci*. 2023
- Ruch F, Gnörich J, Wind K, et al. Validity and value of metabolic connectivity in mouse models of β -amyloid and tauopathy. *Neuroimage*. 2024